

# Photophysical Studies of Amyloid Aggregation

Mariana Manuela Salgado da Costa Amaro

A thesis presented in partial fulfillment  
of the requirements for the degree of  
Doctor of Philosophy



Department of Physics  
University of Strathclyde

December 2011

This thesis is the result of the author's original research. It has been composed by the author and has not been previously submitted for examination which has lead to the award of a degree.

The copyright of this thesis belongs to the author under the terms of the United Kingdom Copyright Acts as qualified by University of Strathclyde Regulation 3.50. Due acknowledgment must always be made for the use of any material contained in, or derived from, this thesis.

Signed:

Date:

# Acknowledgments

I would like to thank my supervisor Dr. Olaf Rolinski and my second supervisor Professor David Birch for all the help, guidance and support they offered over the course of my studies. I am also grateful to Graham Hungerford and all members of the Photophysics group, and those who have been a part of "the office", for all have helped me in many ways throughout these three years.

I must also thank my friends and my family, without whom all would have been less pleasant. Finally, a special thank you to Craig for every single moment.

# Abstract

Fluorescent techniques are amongst the methods used to study the self assembly of proteins into oligomers, however, most of the reports in literature use extrinsic fluorophores to obtain information on the peptide system. The goal of this thesis is to demonstrate how the intrinsic Tyrosine fluorescence of the  $\beta$ -amyloid peptide can be used to monitor its own aggregation with, therefore, minimal interference on the peptide's native structure, its biochemistry and its spontaneous process of aggregation.

Firstly, it is shown that the fluorescence of amino acid Tyrosine, naturally present in wild type  $\beta$ -amyloid, responds to the spontaneous aggregation of the peptide. This is achieved by performing time-correlated single-photon counting experiments during the process of the peptide's aggregation into amyloid fibrils. Through comparison with the well established Thioflavin T assay is also demonstrated that Tyrosine decay responds to changes caused by peptide aggregation well before the appearance of the characteristic  $\beta$ -sheet structures present in the fibrils.

Then the use of  $\beta$ -amyloid's intrinsic Tyrosine amino acid as a sensor for the pre-fibrillar stages of aggregation is further tested and researched through a series of experiments with different initial  $\beta$ -amyloid concentrations. Patterns of consistent behaviour are found confirming that Tyrosine can act as a sensor for the formation of oligomers and kinetic information about the oligomerisation process is retrieved.

Using this approach a comparison between the oligomerisation kinetics of the two most common variants of  $\beta$ -amyloid is performed. In the process

of studying Tyrosine response to the peptide aggregation the accuracy of the discrete exponential decay model used to describe the decays is debated. A model-free analysis is used to study Tyrosine decay photophysics in the  $\beta$ -amyloid peptides throughout the process of aggregation. It is found that Tyrosine decay is a composition of four discrete decay components suggesting the existence of four rotameric forms of the amino acid in the  $\beta$ -amyloid peptides. The findings are further corroborated by molecular dynamic simulations, breaking with the traditional model of three rotameric forms for the fluorescent amino acids in protein chains.

Finally, the sensing method is used to study the influence of external fluorophores, both associating and covalently bound, on the process of oligomerisation.

# List of Publications

The following publications have been derived from work presented in this thesis:

1. Olaf J. Rolinski, Mariana Amaro, David J. S. Birch, "Early stages of amyloid aggregation detected by intrinsic fluorescence", *Biosensors and Bioelectronics*, 25 (2010) 2249-2252
2. Mariana Amaro, David J. S. Birch, Olaf J. Rolinski, "Beta-Amyloid oligomerisation monitored by intrinsic tyrosine fluorescence", *Physical Chemistry Chemical Physics*, 13 (2011) 6434-6441

# Contents

<b>1</b>	<b>Introduction</b>	<b>1</b>
<b>2</b>	<b>Amyloidoses</b>	<b>5</b>
2.1	Introduction . . . . .	5
2.2	Neurodegenerative amyloidoses . . . . .	8
2.2.1	The case of Alzheimer's disease and the $\beta$ -amyloid peptide . . . . .	10
2.3	Amyloid formation . . . . .	14
2.4	Methods in oligomer studies . . . . .	18
<b>3</b>	<b>Fluorescence Theory and Methods</b>	<b>23</b>
3.1	Introduction . . . . .	23
3.2	Fluorescence . . . . .	24
3.3	Time-resolved measurements . . . . .	28
3.3.1	Time-correlated Single-photon Counting . . . . .	29
3.3.2	Data analysis . . . . .	30
3.3.3	Decay associated spectra . . . . .	37
3.4	Protein fluorescence . . . . .	38
3.4.1	Tyrosine fluorescence . . . . .	40
<b>4</b>	<b>Tyrosine sensitivity to early stages of <math>A\beta_{40}</math> aggregation</b>	<b>45</b>
4.1	Introduction . . . . .	45
4.2	Thioflavin T . . . . .	46
4.3	Methodology . . . . .	47

4.4	Results and discussion . . . . .	48
4.5	Conclusions . . . . .	53
<b>5</b>	<b>Examination of Tyrosine response to <math>A\beta_{40}</math> oligomerisation</b>	<b>54</b>
5.1	Introduction . . . . .	54
5.2	Methodology . . . . .	55
5.3	Results and discussion . . . . .	57
5.3.1	Effect of initial monomer concentration . . . . .	57
5.3.2	Evolution of fluorescence response with peptide aggregation . . . . .	60
5.4	Conclusions . . . . .	70
<b>6</b>	<b>Discrete and continuous lifetime analysis of Tyrosine fluorescence decay during <math>A\beta_{40}</math> and <math>A\beta_{42}</math> oligomerisation</b>	<b>72</b>
6.1	Introduction . . . . .	72
6.2	Methodology . . . . .	73
6.3	Results and Discussion . . . . .	73
6.3.1	Three-exponential model . . . . .	73
6.3.2	Model-free lifetime distributions . . . . .	77
6.3.3	Molecular dynamic simulations . . . . .	85
6.4	Conclusions . . . . .	88
<b>7</b>	<b>Oligomerisation of dye-labelled <math>A\beta_{40}</math></b>	<b>91</b>
7.1	Introduction . . . . .	91
7.2	Methodology . . . . .	91
7.3	Results and Discussion . . . . .	92
7.3.1	DEAC labelled $A\beta_{40}$ . . . . .	93
7.3.2	HLF labelled $A\beta_{40}$ . . . . .	97
7.3.3	HLF labelled $A\beta_{40}$ + ThT . . . . .	101
7.4	Conclusions . . . . .	105
<b>8</b>	<b>Conclusions</b>	<b>107</b>

# List of Abbreviation/Acronyms

$A\beta$	$\beta$ -amyloid peptide
$A\beta_{40}$	40 amino acid long $\beta$ -amyloid peptide variant
$A\beta_{42}$	42 amino acid long $\beta$ -amyloid peptide variant
AD	Alzheimer's disease
AFM	Atomic force microscopy
APP	$\beta$ -amyloid precursor protein
CD	Circular dichroism
DAS	Decay associated spectra
DEAC	7-diethylaminocoumarin-3-carbonyl
FCS	Fluorescence correlation spectroscopy
FWHM	Full width at half maximum
FRET	Förster resonance energy transfer
HEPES	N-(2-Hydroxyethyl)piperazine-N'-(2-ethanesulfonic acid)
HFIP	Hexafluoroisopropanol
HLF	Hilyte Fluor 488
MCA	Multi-channel analyser
MD	Molecular dynamics
MEM	Maximum entropy method
NAYA	N-acetyltyrosinamide
NMR	Nuclear magnetic resonance
NLLS	Non-linear least squares
SANS	Small angle neutron scattering
SAXS	Small angle X-Ray scattering

SEM	Scanning electron microscopy
STEM	Scanning tunneling electron microscopy
TAC	Time-to-amplitude converter
TEM	Transmission electron microscopy
ThT	Thioflavin T
TICT	Twisted intramolecular charge transfer
Trp	Tryptophan
TSCPC	Time-correlated single-photon counting
Tyr	Tyrosine

# Chapter 1

## Introduction

Amyloidosis is a term for a vast group of more than twenty diseases that share a common feature, the deposition in organs and tissues of proteins in the form of fibrillar structures named amyloid fibrils. Each kind of amyloidosis is caused by the deposition of a specific protein as fibrils. In this group are included some of the most debilitating conditions in modern society. There is no cure for amyloidosis and the pathogenic role of amyloid deposition is still not fully understood.

Amyloid deposition can be systemic or localised, when deposition is localised in the brain it results in neurodegenerative diseases. Alzheimer's disease, the most common form of neurodegenerative disorders, is an amyloidosis which is thought to be caused by the deposition of the  $\beta$ -amyloid peptide. As most of the amyloidosis diseases, Alzheimer's disease is age-related. As human lifespan increases it is expected that the incidence of this type of diseases will increase substantially, therefore the need for new approaches and drug design will be even more important in the future.

According to Alzheimer's Disease International's 2010 World Alzheimer Report it is estimated that there were 35.6 million people living with dementia worldwide in 2010, a value expected to increase to 65.7 million by 2030 and with it an estimated 85% increase of the costs to society. There is great need to find ways to prevent Alzheimer's disease, delay onset or retard its

progress. An effective treatment that delayed the disease onset by 5 years in average would reduce the cost to society by nearly 50% [1].

The enhancement of knowledge about the mechanism of protein aggregation, amyloid fibril growth and degradation should help to design more effective therapeutics not only for the case of Alzheimer's disease but for all amyloidoses. All types of amyloid fibrils are variations on a common structure, new discoveries made from one specific protein may well have a very general character. Still to this day the full mechanism of amyloid aggregation is not known and techniques providing more detailed monitoring of the process at a molecular level would be of considerable benefit in developing intervention therapies. In particular, very little is known about the early stages of the aggregation where the normal and soluble peptides are converted into soluble oligomers and insoluble amyloid fibrils. These early stages have special importance namely in the neurodegenerative amyloidosis, such as Alzheimer's disease, since it is now believed that the soluble oligomers originated in such periods are the entities that spark neuronal dysfunction and cell death [2,3].

Besides the invaluable understanding of the relationship between protein misfolding, aggregation and disease there is also other significance for this type of work. In the most fundamental view, the ability to understand and control the aggregation process would help understand more about proteins and their properties and in a more technological view produce and use amyloid fibrils as functional biocompatible nanomaterials [4].

In order to build up an information network that can be used as a scaffold to reach the so necessary and desired therapies for amyloidoses, many research groups are using fluorescence techniques. These have become one of the fundamental methods to study systems with micro heterogeneities in biophysics, biochemistry, biotechnology and material sciences. Fluorescence techniques are highly sensitive and respond to events occurring in the surroundings of a fluorophore within Ångstrom scales. These precious features

of fluorescence allied with the ability to perform time and spacial resolved measurements make it possible to obtain information on structural parameters and on the dynamics of fast phenomenon. All over the world fluorescence is being used to investigate the amyloid formation process, however most researchers mainly resort to the use of the extrinsic fluorophores.

Extrinsic fluorophores can be linked to proteins or used as associating probes in order to obtain information on the amyloid protein and its aggregation process. The main problem is that these external tags might disturb the biomolecule and/or the actual process of aggregation one pretends to monitor, thus resulting in biased conclusions. To avoid such inconvenients while still benefiting from the all the advantages of using fluorescence techniques one can make use of the fluorescence of the protein itself. The main problem with such approach is the complexity of the fluorescence response. Such complexity can make the retrieval of information from the fluorescence signal an overwhelming task.

The direct contribution to the field of the most "epidemic" form of dementia, Alzheimer's disease, and the possible translation of knowledge towards the understanding of other amyloidosis are two of the reasons why this thesis focuses on the  $\beta$ -amyloid protein. The other reason is more practical,  $\beta$ -amyloid is a relatively small protein that contains only one Tyrosine (Tyr). This fact makes the  $\beta$ -amyloid a simpler system when compared to bigger and more complex proteins with different numbers of different types of fluorescent amino acids. The existence of multiple fluorescent amino acids (even if of the same type) in different positions of a proteic chain increases significantly the complexity of the fluorescence data collected through experiment. The fact that each amino acid is exposed to a different microenvironment creates a multitude of different overlapping fluorescent responses which translates into complex data interpretation. Therefore, from a photophysical point of view, the  $\beta$ -amyloid is an excellent object for amyloid aggregation studies using intrinsic fluorescence due to the possibility of selectively exciting and

monitoring the only Tyr present in its structure.

It will be demonstrated in this thesis how it is possible to monitor the early stages of  $\beta$ -amyloid aggregation non-invasively. Using time-resolved spectroscopy of Tyr, naturally present in the  $\beta$ -amyloid protein, a window to study the amyloid oligomerisation is open. With the extended knowledge derived from this work a baseline can be drawn and the method applied to study the formation of early oligomers in different conditions, which perhaps might bring the discovery of better therapies one step closer to reality. In this work it is also shown how the addition of extrinsic fluorophores can modify the protein's aggregation behaviour, thus even more heightening the advantages of using the intrinsic fluorescence of  $\beta$ -amyloid when aiming to study the peptide-to-peptide molecular interactions that result in the formation of the small cytotoxic oligomers.

# Chapter 2

## Amyloidoses

### 2.1 Introduction

Proteins are very important molecular elements in any living organism. These macromolecules are abundant in all cells and all parts of cells. They occur in many different types and their range of sizes is vast going from relatively small peptides to gigantic polymers. This great structural diversity is translated into the large variety of biological roles that proteins play (immune function, structural purposes, transportation, muscle contraction, catalytic activity, etc.) [5].

Under suitable conditions of solvent and temperature each protein adopts spontaneously a unique structure - the native state [6]. It is in this state that the protein is biologically active and serves its purpose. In their native state proteins do not have a rigid structure and, in fact, structural movements are very important for the function of many proteins. There are small movements of protein atoms but also larger conformational changes between different functional states [7].

Proteins are also in constant dynamic equilibrium and even after a successful folding process leading to the native state, unfolding in the cellular environment may take place [8]. If a protein fails to fold correctly or to remain correctly folded it will not be biologically active. The misfolded protein

will inevitably expose to the cell environment parts of its structure that in the native state are protected and buried inside the properly folded structure of the protein. Because of this the misfolded protein should be degraded as it can give rise to malfunctions. It can interact inappropriately with other cellular components causing loss of cell viability, cell death and disease. There is for a fact an increasing number of diseases linked to this phenomenon, these are broadly called "protein misfolding" or "protein conformational" diseases [4].

A range of strategical control systems have been developed by living organisms during evolution to deal with the problem of protein misfolding. In fact, a third of synthesized proteins can be immediately destroyed by these due to incorrect folding [5, 9]. However, proteins may escape the quality-control tests and evade the cellular mechanisms that protect against misfolding.

Misfolded proteins have a tendency to aggregate and many diseases are now recognized to be caused by protein aggregation. A large number of these can be grouped and described as amyloidoses. This group includes many of the most debilitating conditions in modern society, for example Alzheimer's disease (AD), type II diabetes, Creutzfeldt-Jakob disease, Parkinson's disease, etc [4]. The common link between them all is the deposition of the protein aggregates as amyloid fibrils in tissue. It should be noted although, that protein misfolding does not necessarily lead to amyloidosis and can cause serious diseases through different mechanisms, as it is the case of cystic fibrosis and cancer.

The term amyloid (starch-like) was introduced by Rudolph Virchow in 1854 when he reported that an iodine stain used to identify starch gave positive results on masses found in brain tissue. Later it was discovered that these waxy deposits, also reported found in other tissues from as early as the year of 1639, contained no carbohydrates but were proteic in nature, nonetheless they continued to be denominated amyloid.

Amyloidosis	Main Peptide/Protein component in amyloid deposits
Alzheimer's disease	$\beta$ -amyloid peptide
Amyotrophic lateral sclerosis	Superoxide dismutase 1
Atrial amyloidosis	Atrial natriuretic factor
Familial amyloid polyneuropathy III	Apolipoprotein AI fragments
Finnish hereditary systemic amyloidosis	Gelsolin
Haemodialysis-related amyloidosis	$\beta_2$ -microglobulin
Huntington's disease	Huntingtin
Injection-localised amyloidosis	Insulin
Parkinson's disease	$\alpha$ -synuclein
Primary sistemic amyloidosis	Ig light chains
Spinocerebellar ataxias	ataxins

**Table 2.1:** Sample of most common amyloidosis and proteins or peptides involve in the disease.

In 1971 Benditt and Glenner independently found through the new technique of amino acid sequence analysis that amyloid deposits were composed of one main protein and were not a bundle of different proteins as was thought before. Others followed this new research pathway leading to the recognition that for each disease associated with amyloid deposits there was a unique and distinct protein as the main amyloid component [10, 11]. Each amyloidosis is therefore related to the misfolding and aggregation of a specific protein. These proteins have no similarities in size, structure, composition or location within the cell (in table 2.1 are shown some of the most common amyloidosis and the proteins involved in each disease). However, in all cases the proteins aggregate to form stable and insoluble amyloid fibrils, with similar properties and appearance, that are not cleared from the body and deposit in tissue.

The mature amyloid fibrils found in the amyloid deposits are typically several micrometers long, relatively straight and unbranched. They have diameters in the order of 6 to 16 nanometers and are composed of two up to six protofibrils of diameter between 30 to 40 Ångstrom (Å). These protofibrils are twisted around each other to form the "rope-like" structure of the amyloid fibril (figure 2.1). X-ray studies show a characteristic diffraction pattern with

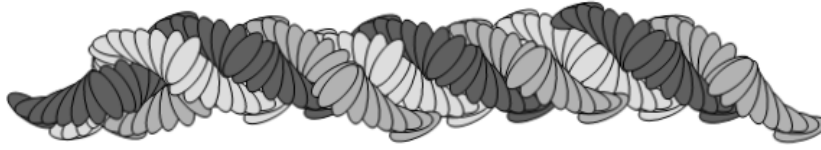


**Figure 2.1:** Representative cartoon of a mature amyloid fibril composed of three protofibrils (colored in different shades of grey).

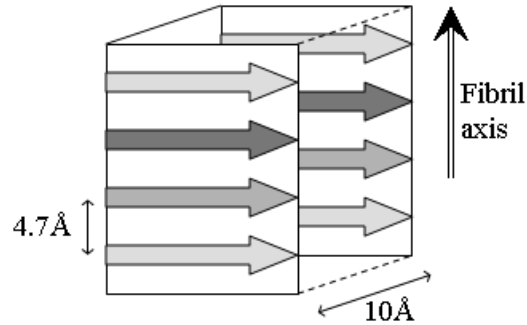


**Figure 2.2:** Drawing of the cross- $\beta$ -sheet structural motif.

a meridional reflection at  $\approx 4.7\text{\AA}$  and an equatorial reflection at  $\approx 10\text{\AA}$ . The pattern is explained by protofibrils rich in  $\beta$ -sheet structures arranged in a characteristic cross- $\beta$  pattern (figure 2.2). In this particular arrangement the  $\beta$ -sheet strands run perpendicular to the fibril axis [12–15].

## 2.2 Neurodegenerative amyloidoses

Neurodegenerative disorders are characterized by a selective and symmetrical loss of neurons, they are chronic and progressive. The loss of brain function ultimately leads to dementia and as it progresses the person affected with the disease will ultimately become completely dependent on others for nursing care.

When amyloid deposition occurs in the brain the disease is termed neurodegenerative amyloidosis because it leads to neuron death and dementia. Although amyloidosis is defined as the extracellular deposition of the amyloid fibrils, Parkinson's and Huntington's diseases which involve intracellular

deposition of fibrils can most of the times be found in this category. This is also the case of prion diseases because they resemble neurodegenerative amyloidoses but in this case it is the presence of amyloid fibrils that has not yet been established [11].

AD, the most common of all neurodegenerative disorders (50 – 60% of all diagnosed dementias, according to Alzheimer’s Disease International), is characterized by the formation of senile plaques (amyloid containing aggregates), neurofibrillary tangles (aggregates of tau protein) and neuronal loss in the hippocampus, entorhinal cortex and areas of the neocortex. Parkinson’s (the second most common neurodegenerative disease) is characterized by the intracellular deposition of Lewy bodies (amyloid containing aggregates) predominantly in the melanin containing neurons of the substantia nigra leading to their death and shortage of dopamine. Huntington’s disease is also characterized by the intracellular deposition of amyloid aggregates, in this case of the Huntingtin protein, causing severe neuronal loss in the neostriatum and cerebral cortex [1, 6].

How amyloidoses cause cell death in the particular case of the neurodegenerative diseases still evades our knowledge. Due to the similarities of the diseases one common mechanism of toxicity seems reasonable however the possibility of different mechanisms for different diseases is also feasible and at this point which option is the correct one is still an unknown. Until this day there is an open discussion about what is the actual cause of disease and the mechanisms that lead to neuron death.

Nowadays the plaques of aggregated amyloid fibrils are not considered to be the pathogenic factor but are viewed as a reservoir of inactive species. The entities that are now believed to spark neuronal dysfunction and cell death are the smaller soluble protein aggregates termed oligomers [2,3]. In this new century increasing evidence has been found to support the idea that oligomers are more neurotoxic than mature fibrils however, the mechanism through which oligomers promote cell death is still to be found. Nimmrich et al. [16]

suggest that the oligomers interference with synaptic activity could be due to direct interaction with synaptic proteins and that this recurrent synaptic failure could initiate a pathological cascade. Others suggest that oligomers can disrupt membranes and create pores through which an abnormal flow of ions can occur leading to loss of cell viability [17]. Many other hypothesis are being researched [18] and there is still much to be done in this field.

### **2.2.1 The case of Alzheimer's disease and the $\beta$ -amyloid peptide**

In 1906 Alois Alzheimer reported for the first time the clinical symptoms and the morphology of a disease that would later become known as AD. Alzheimer was the first to report the finding of senile plaques in brain tissue and to link these with the phenotype of the disease [19]. Even though known for more than a century there is still no cure for AD, or any other amyloidosis. However, 27 years ago a new era started on the research of AD that might bring one closer to the discovery of effective therapeutics. This was the time when the  $\beta$ -amyloid ( $A\beta$ ) peptide was first sequenced and identified in the senile plaques [20].

Senile plaques are spherically shaped lesions that contain extracellular deposits of  $A\beta$  abundantly in the form of amyloid fibrils. Degenerating axons, dendrites, activated microglia and astrocytes are also found within senile plaques or in their close surroundings. The two classical lesions of AD (senile plaques and neurofibrillary tangles) can occur independently. Neurofibrillary tangles (intraneuronal bundles of helically wound filaments of aggregated tau protein) occur in a number of uncommon neurodegenerative diseases but in which no  $A\beta$  deposits and senile plaques are found. Even severe neurofibrillary tangle formation does not lead to senile plaques formation, therefore it is believed that their formation succeeds  $A\beta$  deposition and is one of the responses by cells to the accumulation of  $A\beta$ . This is one of the arguments supporting the "amyloid hypothesis", brought to light in the early nineties by Selkoe, Hardy and Higgins. Then the amyloid hypothesis basically

consisted in the proposition that the neurodegeneration in AD is caused by the deposition of  $A\beta$  as plaques in the brain tissue. In such hypothesis,  $A\beta$  deposition would be the primary pathogenic event and all other processes would be a consequence of it [20, 21].

Although controversial the amyloid hypothesis is still researched [22] and has suffered some changes along the years as more information was gathered. Currently it is believed that the oligomers are the most important entities that lead to a cascade of neurotoxic effects and the amyloid hypothesis is now sometimes referred to as the "oligomeric amyloid hypothesis" or the "amyloid cascade hypothesis".

### **$\beta$ -amyloid peptide**

$A\beta$  peptide is a cleavage product of the  $\beta$ -amyloid precursor protein (APP).  $A\beta$  can be found in the plasma and cerebrospinal fluid of healthy humans and other mammals, being the  $A\beta_{40}$  form (40 amino acid long) the most common. According to the amyloid hypothesis the increased production or reduced clearance of  $A\beta$  peptides, and consequent increase of its concentration, will result in its aggregation and deposition leading to AD [23, 24].

APP is a type I transmembrane protein of up to 770 amino acids in its longer form with a large extracellular domain, a single transmembrane region and a small intracellular part [25]. It is expressed in many cells throughout the body but it's in the neurons where it is more concentrated. APP has a relatively short half-life at the plasma membrane ( $\approx 10$  min) where it is cleaved by at least three proteinases (enzymes that cleave peptide bonds inside protein chains [26]) named  $\alpha$ -,  $\beta$ - and  $\gamma$ -secretases [24].

APP processing (figure 2.3) starts with cleavage by the  $\alpha$ -secretase enzyme and results in shedding a big part of the protein into the extracellular space as a soluble fragment termed sAPP $\alpha$ . The remaining protein fragment is then cleaved by the  $\gamma$ -secretase enzyme which releases a small peptide (p3) into the extracellular space and the remaining protein fragment into the intracellular domain (figure 2.3a). However, APP's proteolysis can occur

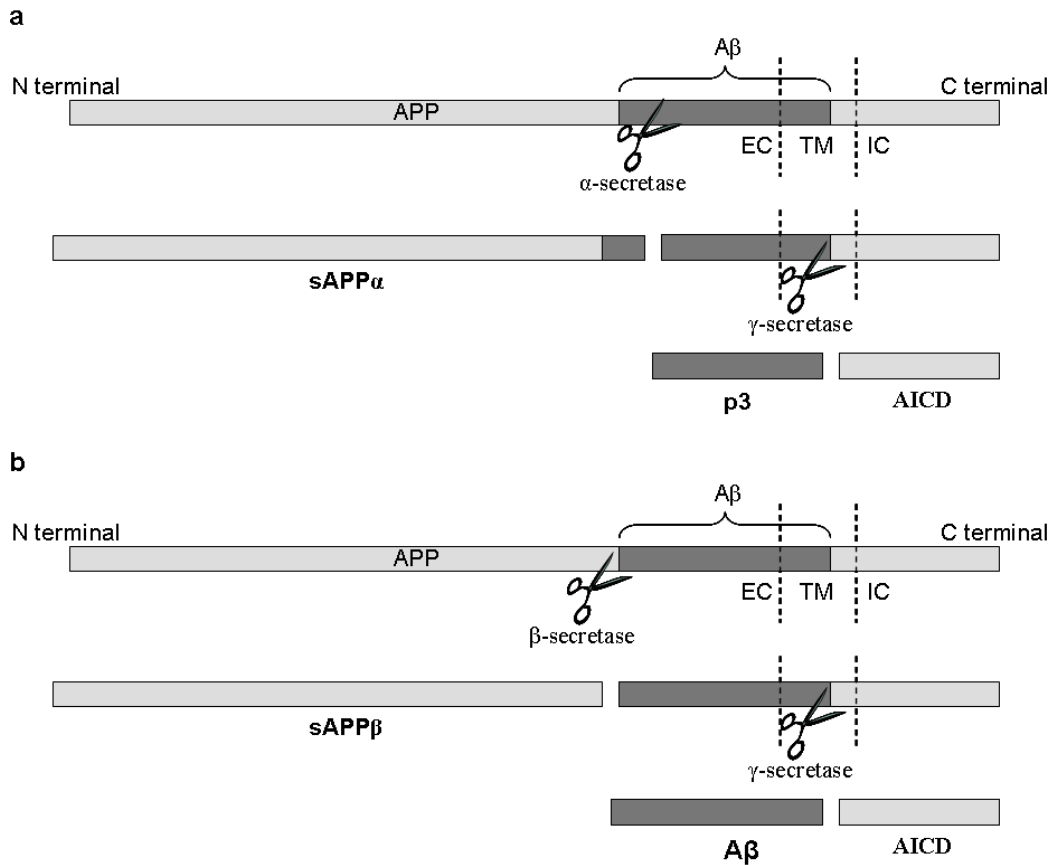


**Figure 2.3:** Simplified schematic diagrams of APP proteolysis (not to scale). A $\beta$  peptide is highlighted in dark grey. a) processing by  $\alpha$ - and  $\gamma$ -secretases, resulting in the release of sAPP $\alpha$  and p3 into the extracellular space and AICD into the cytoplasm. b) processing by  $\beta$ - and  $\gamma$ -secretases, resulting in the release of sAPP $\beta$  and A $\beta$  into the extracellular space and AICD into the cytoplasm. EC: extracellular domain; TM: transmembrane domain; IC: intracellular domain; AICD: APP intracellular domain fragment.

through an alternative pathway leading to  $A\beta$  formation - in healthy brains this is a quantitatively less important cleavage pathway (figure 2.3b). In this case the proteolysis does not start with a  $\alpha$ -secretase but with a  $\beta$ -secretase enzyme. The  $\beta$ -secretase activity releases a slightly smaller part of the APP into the extracellular domain named sAPP $\beta$  fragment. The remaining membrane bound fragment of APP has the same fate as the fragment left behind by the  $\alpha$ -secretase. Important to notice is that now when the fragment is cleaved by the  $\gamma$ -secretase the peptide released into the extracellular space is not the p3 but the  $A\beta$  peptide [23–25, 27].

$A\beta$  peptide is a 38 to 42 amino acid long residue, the 40 and 42 long species -  $A\beta_{40}$  and  $A\beta_{42}$  respectively - are most common being the  $A\beta_{40}$  the most abundantly produced [2, 28]. The  $A\beta_{42}$  differs from  $A\beta_{40}$  only at the C-terminus where two additional apolar amino acids (isoleucine and alanine) are present at the end of the sequence.  $A\beta$  is part of the extracellular and transmembrane domain of the APP, this results on  $A\beta$  having an amphipathic nature. The 12/14 amino acids of the C-terminal sequence, belonging to the transmembrane part of the APP, are almost exclusively non-polar and hydrophobic (figure 2.4). The remaining N-terminal sequence of 28 amino acids, included in the extracellular domain of APP, is overall polar and hydrophilic [26, 28]. The hydrophobic C-terminal sequence seems to play a determinant role in the spontaneous aggregation of the peptides and it has been shown that  $A\beta_{42}$  peptides, with their two extra amino acids, aggregate into amyloid fibrils more rapidly than the  $A\beta_{40}$  form [29–31].

It is well understood that the hydrophobic effect is particularly important for protein stability. Most hydrophobic amino acid residues are arranged in the interior of a protein's structure in its native conformation, while polar amino acids are mainly found on the surface [26]. However, the self assembly of the proteins into amyloids is not solely driven by hydrophobic effects but also steric effects and the propensity of protein chains to form hydrogen bonds and the concomitant  $\beta$ -sheet motifs [32, 33].



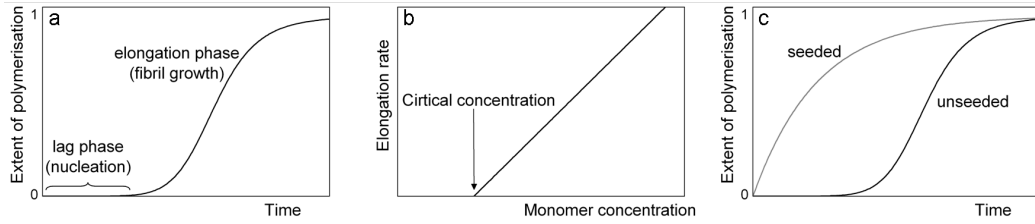


**Figure 2.5:** Kinetic characteristics of a nucleation dependent polymerisation: a) lag phase; b) critical concentration; c) seeding removes lag phase.

mation of the fibrillar end product (see figure 2.5a). The lag time is due to the nucleation phase and is concentration dependent. As the initial concentration of monomers becomes smaller the lag period becomes larger and this gives rise to another characteristic of this type of mechanism of aggregation: the existence of a critical concentration below which no polymerization will occur (figure 2.5b). The last characteristic feature of this mechanism is the abolishment of the lag phase by seeding (figure 2.5c). Adding pre-formed nuclei (seeds) therefore changes the kinetic profile of fibril formation [14,39].

Several reasonable approximations can be made to model and study the complex kinetics of fibril formation. The sigmoidal shaped curves are usually fitted to logistic functions, for example, one commonly used form of the logistic function is

$$Y = y_1 + \frac{y_2}{1 + \exp^{-(t-t_0)k_f}} \quad (2.1)$$

where the lag time is given by  $t_0 - 2/k_f$  and the apparent rate for fibril growth is  $k_f$  [40].

As a comparison, a nucleation independent mechanism does not present separate nucleation and elongation (fibril growth) phases. This type of polymerization reaction has a similar kinetic profile to the elongation phase of a seeded nucleation dependent polymerization. In the kinetic profile no lag phase is seen and the rate of fibril formation is fastest at the initial stages and then the rate decreases as the polymerization proceeds towards the equilib-

rium. In this type of aggregation mechanism there is no critical concentration since there is no dependence on the formation of nuclei [14, 39].

The kinetic profiles can be approximated and treated as pseudo-first-order (or reversible first-order) chemical reactions and modeled according to equation (2.2), which is commonly known in the biological sciences as a monomolecular growth function [41, 42].

$$Y = y_1 - y_2 \exp(-k_g t) \quad (2.2)$$

where  $k_g$  is the apparent growth rate constant.

Putting aside all the differences between models and focusing on the similarities, a general simple description of the process of aggregation can be done (figure 2.6): initially the monomers in solution (misfolded or natively unfolded as is the case of  $A\beta$ ) coalesce to form amorphous oligomers and these later undergo a process of reorganization or conformational change giving rise to molecularly organized oligomers containing  $\beta$ -sheets (sometimes termed protofilaments [43]). These associate with each other and/or monomers (through end-to-end or/and lateral associations) evolving into protofibrils which continue to further associate yielding the final mature amyloid fibrils. A more elaborate description is hard to perform because still up to this day there is no agreement on the detailed process of fibril formation [14].

The growing evidence that the structures which promote cell death are the oligomers formed in the initial stages (lag phase) of the fibrillisation process as lead to an increasing number of research being done on these species. Research groups from different disciplines have shifted the focus of research from the study and characterization of the mature fibrils to the study and characterization of oligomers. However, studying the early stages of aggregation leading to oligomer formation, or oligomerisation, has proved challenging. It is difficult to experimentally monitor and describe the beginnings of aggregation due to the very small, heterogeneous and transient species that

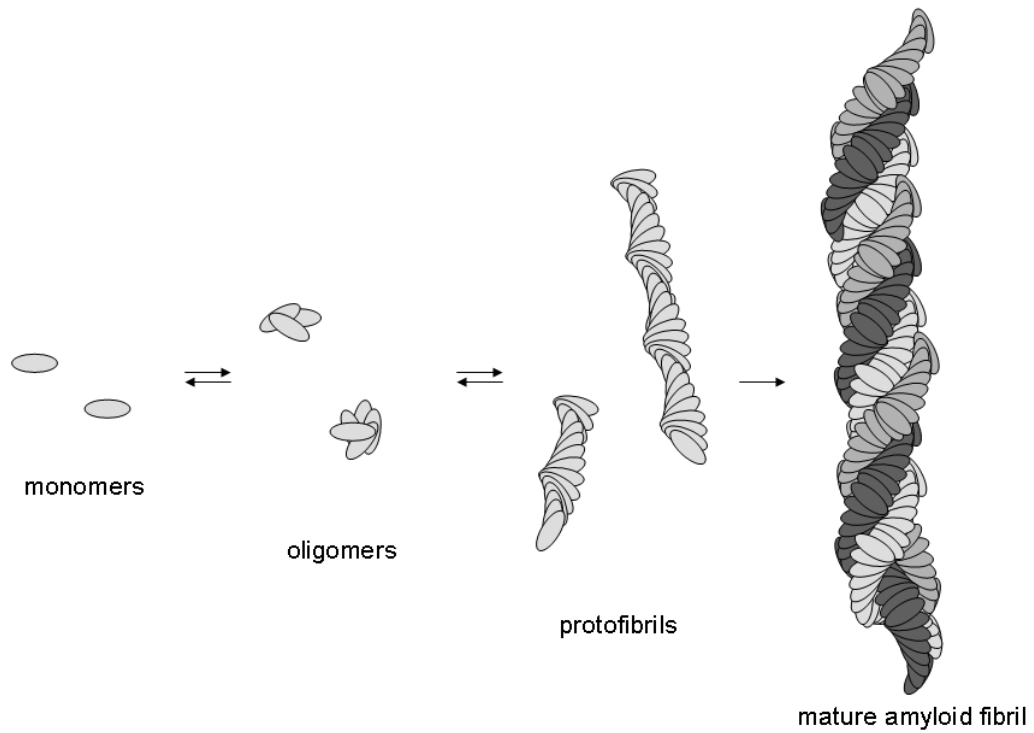


**Figure 2.6:** Simplified cartoon of aggregation. Unfolded or misfolded protein monomers coalesce to form oligomeric structures. These grow in size and complexity originating protofibrils. The process then continues through end-to-end or/and lateral associations to form mature amyloid fibrils.

are involved [39, 44].

## 2.4 Methods in oligomer studies

Current therapies for amyloidoses only ameliorate the disease symptoms and do not treat the disease itself, therefore the search for a therapy that can slow down or even halt the progress of the disease is of major importance.

Most amyloidoses are age-related and as the human population continues to live longer the need for effective therapies becomes even more urgent. Our current knowledge is tremendously incomplete but allows us to take steps towards a treatment for neurodegenerative amyloidoses in particular and all amyloidoses in general. In the particular case of AD, the discovery of the cytotoxic effect of oligomers reveals a way forward to discovery of treatment. Finding a factor that dis-assembles, neutralises or inhibits the formation of oligomers could lead to the development of an effective therapy.

While it is a long step from the laboratory bench to the establishment of a cure, current information tells us to seek intervention at the earliest stages of oligomerisation in order to prevent the formation of the cytotoxic entities. There is thus great need to study the oligomers and the process of oligomerisation. Better characterization should enable a more effective development of strategies on the road to a better therapeutics. For this, the ability to detect and monitor small oligomeric species is crucial. Many techniques are currently being used to achieve such goal.

In the realm of structural characterization contributions to build our understanding come from both direct and indirect methods. Commonly used direct methods include electron microscopy (EM) (be it transmission EM (TEM), scanning EM (SEM), scanning tunneling EM (STEM), or Cryo-EM), atomic force microscopy (AFM), small angle neutron or X-Ray scattering (SANS or SAXS), nuclear magnetic resonance spectroscopy (NMR) and X-Ray diffraction. Circular dichroism (CD), Raman and infrared spectroscopy

are typical indirect methods used to study secondary structure and monitor conformational changes, namely the formation of  $\beta$ -sheets [45].

Electron microscopy has the obvious advantage of being a direct method that allows visualisation of amyloid fibrils. TEM and SEM only allow low- to medium-resolution (down to nanometer) characterisation but Cryo-EM, on the other hand, permits higher resolution (sub-nanometer) and reconstruction of the data has been used successfully to reveal structural features such as the helical pitch of fibrils [46], number and dimension of protofilaments within fibrils [12] and even visualise annular protofibrils [47].

The advantage of STEM and AFM over Cryo-EM is that they provide 2D profiles of single particles as opposed to the averaging and reconstruction methods often used in Cryo-EM. AFM has also been used in time-resolved fashion to obtain information on the process of oligomer formation [48]. However, both techniques are nonetheless still low-resolution methods.

A common disadvantage of all the direct methods mentioned above is the extensive surface contact between the samples and their physical support. Surfaces have been shown to play a significant role in amyloid aggregation and its kinetics [49] and also in the fibril morphology [50]. SANS or SAXS and NMR can be applied to solutions of amyloid proteins and, therefore, have the advantage of minimized surface effects.

Small Angle Scattering allows one to gather direct structural information, such as size, shape and volume and construct low-resolution models of the molecules [51]. It can be successfully used to study heterogeneous solutions, for example Bernardó et al. [52] have structurally characterized dimers and monomers in equilibrium, but the study of naturally flexible proteins (as is the case of the  $A\beta$  peptide) proves to be more challenging [53].

On the high-resolution end of the spectrum are NMR and X-ray diffraction, with which it is possible to obtain structural information with atomic resolution. Some recent examples of the detailed information it is possible to obtain with these techniques are the molecular arrangement of the  $\beta$ -sheets structure of fibrils [54], solvent protection patterns [55] and conformational

changes of protein domains [56]. A disadvantage of X-ray diffraction is the requirement of protein crystallization and, due to that, it cannot be used to study transient species that exist in the aggregating systems. All methods have, obviously, advantages and limitations but it is their combined use that allows the current understanding of amyloid proteins.

Spectroscopic techniques are probably the most used methods to study oligomer formation in real time. The above referred CD, Raman and infrared spectroscopy can be used in a time resolved fashion to provide kinetic data about the aggregation process. For example, Koppaka and Axelsen [36] have shown through infrared spectroscopy that oxidatively damaged phospholipid membranes accelerate the accumulation of A $\beta$  peptide and promote  $\beta$ -sheet formation. On the other hand, these methods focus on secondary-structure changes and do not provide a complete view of oligomerisation since the aggregation into small oligomers does not necessarily promote significant structural changes from random-coil or  $\alpha$ -helices [14].

In the area of oligomer monitorisation fluorescence spectroscopy shows off its strengths. Because of its high sensitivity and the ability to use low protein concentration, fluorescence techniques are widely used to study the oligomerisation process. All dimensions of fluorescence are being explored to build up knowledge in the amyloid field. However, not all approaches are suitable to study oligomers. This is, for example, the case of the widely used associating dye Thioflavin T (ThT) because the dye's response seems to be specific to  $\beta$ -sheet containing structures and therefore is not sensitive to the presence of the smaller oligomeric species.

A few successful examples of current fluorescent techniques used to study oligomers are anisotropy, Förster resonance energy transfer (FRET) and fluorescence correlation spectroscopy (FCS). FCS allows to determine the size of molecules based on their diffusion. Nath, et al. [57] have shown that estimating the coefficient diffusion of dimers is possible but the heterogeneity of the sample and the averaging of the data do not allow indisputable results. In

the same report it was shown the possibility of following the kinetics of early aggregation by monitoring the decreasing number of monomeric species.

FCS has good sensitivity to detect the dynamics of monomers or large oligomers but is not as adequate to study conformational changes of monomers or small oligomer formation. Fluorescence cross-correlation spectroscopy is better suited for the latter purposes and FRET for the former. As an example, Kim and Lee [58] have used FRET to investigate  $A\beta_{11-25}$  fragments during their oligomerisation having found a multi-step process of conformational changes during the peptides self-assembly. The information on distances between the donor-acceptor pairs involved in the energy transfer can help not only to understand the organization and structure of the biomolecules, but can also be used to detect formation of oligomers even though it does not allow to determine the sizes of the aggregates [59].

In time-resolved anisotropy, the possibility of using a small ratio of tagged-to-untagged proteins is an advantage, it reduces the influence of the probe on the biomolecule and its aggregation, and also reduces the cost of the experiment. The size of proteins can be estimated through time-resolved fluorescence anisotropy from the apparent rotation of bound fluorescent dyes. However, it is impossible to obtain information on the rotational correlation times, and therefore estimate the size of the particles, if these are longer than three to five times the lifetime of the fluorescent probe. This means that for large proteins, or complexes, bigger than approximately 50 kDa the fluorescent probe must have a decay time in the order of tens of nanoseconds [60]. Even with such limitations it is still possible to retrieve useful information from anisotropy experiments, for example, an increase in residual anisotropy over time can be correlated to the formation of increasingly larger structures [61,62].

The mentioned techniques are chosen according to the problem in study and all provide useful information regarding early aggregation stages but there is, however, one common blatant disadvantage of these methods which

is the use of labelling. The vast majority of reports found in the literature make use of external tags. The addition of extrinsic fluorophores has the potential to not only disturb the structure of the protein in study but also the actual process of oligomerisation, producing results that are not the best representation of the real system when the fluorescent tag is not present. This is not an ideal situation when one is looking for accurate descriptions of oligomers and the oligomerisation phenomenon in order to create effective drugs that can lead to therapeutic progress.

Using the intrinsic fluorescence of proteins abolishes this problem and gives one a unique non-invasive window to study the protein and its aggregation process. Intrinsic protein fluorescence is viewed as an extremely complex phenomenon and until the 1980's it was used in a more qualitative rather than quantitative way due precisely to its complexity [63]. Since then interest built up around protein fluorescence and with advances in technology (fluorescence instrumentation and data analysis, and also biochemical engineering) many advances have been made in the field and intrinsic protein fluorescence is now better understood. With our current knowledge and technology status, intrinsic protein fluorescence can indeed be a generator of useful information and the phenomenon's complexity can be thought off as a richer source of information.

# Chapter 3

## Fluorescence Theory and Methods

### 3.1 Introduction

Fluorescence as a sensing technology is used across many disciplinary fields. Improvements in instrumentation lead to the widespread use of fluorescence methods as tools for researching the structure and dynamics, at a molecular level, of inert or living systems. This successful and extensive use of fluorescence techniques is due to their high sensitivity and the ability of obtaining temporal as well as spatial information, allied with the fact that the fluorescence response is specified by the microenvironment surrounding the fluorophore within nanometer scale. The possibility of obtaining information on structural parameters and on the dynamics of fast phenomenon have made fluorescence a main research tool in biophysics, biochemistry and material sciences [64].

The intrinsic fluorescence of proteins is nowadays often used in biotechnology. From the four main classes of molecules in biochemistry (saccharides, proteins, lipids and nucleic acids) only proteins and nucleic acids display significant fluorescence. However, the intrinsic fluorescence of nucleic acids (DNA, for instance) is too weak to be useful. This makes proteins rather

unique in the sense of the usefulness of their intrinsic fluorescence and this is often explored in the biophysical and biochemical sciences [65].

Fluorescence can be affected by environmental parameters such as polarity, pH, viscosity, temperature, hydrogen bonds, etc., and the interaction between the fluorescent molecule and its "nanoenvironment" can be explored to provide information on a wide range of molecular processes. The phenomenon of fluorescence carries in itself various dimensions of information (quantum yield, lifetime, spectral shape, polarisation,...) that can be assessed with different instrumentation. These dimensions and their dependence with the environment surrounding the emitting species allow multiple views into a problem and the creation of a network of information at a molecular level. Continuous advances in fluorescence technology diminish the cost and complexity of instrumentation and for all this fluorescence spectroscopy will no doubt continue to contribute to advances in biology, biotechnology and nanotechnology [64, 65].

## 3.2 Fluorescence

When molecules are excited by absorption of photons they can discard or use the excess energy in a number of ways, including dissipation as heat and emission of photons. The latter gives rise to the phenomenon of luminescence which can be divided in two categories: fluorescence and phosphorescence. Distinction between fluorescence and phosphorescence is based on their mechanisms. In fluorescence the transition that originates the creation of a photon is done between two states of the same spin multiplicity, while in phosphorescence the transition occurs between states of different spin multiplicity [64–66].

The events proceeding electronic excitation by photon absorption will be depicted and explained using a Jablonski diagram illustrated in figure 3.1. The singlet electronic states denoted  $S_0$ ,  $S_1$ ,  $S_2$  correspond to the fundamental (or ground), first and second electronic states respectively. The first triplet

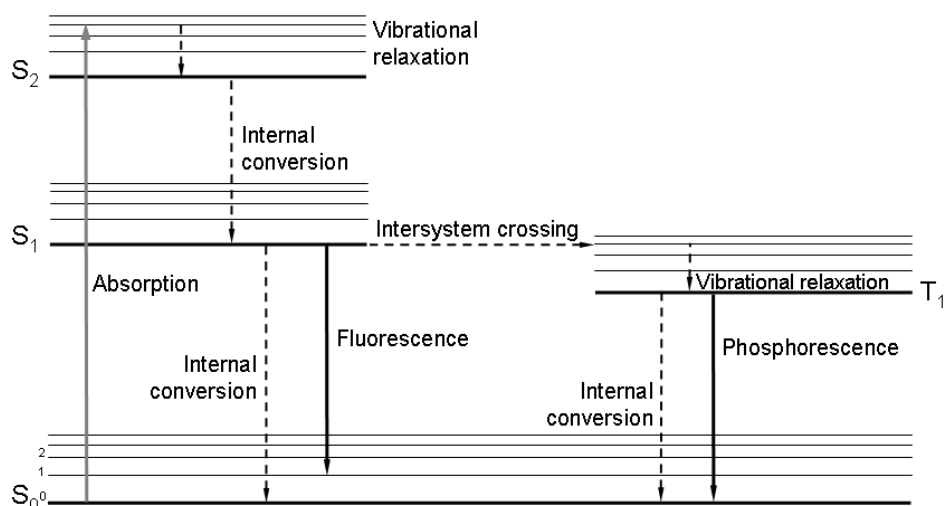


**Figure 3.1:** Jablonski energy diagram illustrating photon absorption and consequent possible relaxation pathways. Events involving the absorption or emission of photons are represented by straight arrows, other non-radiative de-excitation pathways are represented by dashed arrows.

state,  $T_1$ , is also represented. Associated with each electronic state are vibrational energy levels identified by the numbers 0, 1, 2,.... Transitions between states which involve absorption or emission of photons are represented by straight arrows.

At room temperature the majority of molecules are in the lowest vibrational energy level of  $S_0$ , absorption of a photon excites a molecule and brings it to one of the vibrational levels of the higher energy electronic states ( $S_1$ ,  $S_2$ ,..., depending on the photon energy) in a very fast process that takes approximately  $10^{-15}$  seconds. When the molecule is excited to a higher energy state than the lowest vibrational level of the first electronic state the molecule will relax to the lower level of  $S_1$  typically within  $10^{-12}$  s or less. This is achieved by vibrational relaxation resulting from intermolecular collisions and by internal conversion, a non-radiative transition between electronic states of the same spin multiplicity.

Once in the  $S_1$  state internal conversion to  $S_0$  is less efficient due to the higher energy gap between electronic states. The molecule then persists in the  $S_1$  state and if the lifetime of this excited state is long enough (typically in

the order of  $10^{-8}$  s) spontaneous emission can occur generating a photon and the fluorescence phenomenon. Another competitive de-excitation pathway is intersystem crossing to the triplet state from which emission of photons can also be observed giving rise to phosphorescence.

Once in the triplet state transition to the fundamental state is spin forbidden, therefore the molecule remains for longer in  $T_1$  eventually decaying to the  $S_0$  level, thus resulting in the fact that phosphorescence is a phenomenon that can occur on time scales from microseconds up to minutes. The rate constants of depopulation of the excited  $S_1$  states will be denoted in this thesis as follows:  $k_F$ , deactivation with emission of fluorescence;  $k_{IC}$ , internal conversion;  $k_{ISC}$ , intersystem crossing.

Not depicted in this Jablonski diagram are intermolecular processes that can competitively also depopulate the  $S_1$  state and relax the molecules to the fundamental level. These so called quenching processes include, amongst others, dynamic and static quenching, electron transfer, proton transfer and Förster energy transfer. Due to the multiplicity of competitive non-radiative depopulation pathways it is sometimes convenient to define a non-radiative rate constant,  $k_{NR}$ , that is the sum of all non-radiative pathways of de-excitation from the  $S_1$  state.

Consider a solution of fluorescent molecules and a  $\delta$ -pulse of light that creates a population of fluorophores in the excited state, whose concentration is  $[N_0]$ . The excited molecules can decay either radiatively or non-radiatively and the rate of their disappearance can be expressed as

$$-\frac{d[N](t)}{dt} = (k_F + k_{NR})[N](t) \quad (3.1)$$

Integration of equation (3.1) results in the function  $[N](t)$  which describes the evolution of the excited molecules concentration in time, i.e.,

$$[N](t) = [N_0]exp^{-(k_F+k_{NR})t} \quad (3.2)$$

or

$$[N](t) = [N_0]exp^{(-t/\tau)} \quad (3.3)$$

where  $\tau$  is

$$\tau = \frac{1}{k_F + k_{NR}} \quad (3.4)$$

The constant  $\tau$  is the characteristic decay time or average excited state lifetime and is calculated as the time taken for the fluorescence intensity to drop to  $1/e$  of its initial value.

The fluorescence intensity at time  $t$  after excitation  $I(t)$  is proportional to the concentration of molecules still excited at that time  $[N](t)$ , therefore the variation of  $I(t)$  can be described by the following decay law:

$$I(t) = I_0exp^{(-t/\tau)} \quad (3.5)$$

where  $I_0$  is the fluorescence intensity immediately after excitation.

The lifetime and the quantum yield of a fluorophore are likely its most important characteristics. The fluorescence lifetime determines the time available for the fluorophore to interact with its environment and therefore determines the time frame for observation of dynamic phenomena and the information one can obtain. The excited state lifetime depends on the radiative and non-radiative depopulation rates according to equation (3.4)

The quantum yield,  $\Phi$ , is the number of photons emitted relatively to the number of photons absorbed and therefore is a sort of measurement of how efficient is the process of generation of fluorescence photons. The quantum yield is obviously influenced by the rates of depopulation of the excited state. It is intuitive that if the rate of the non-radiative processes is much

smaller than the rate of fluorescence then the excited state will be mainly depopulated by emission of fluorescence. The quantum yield in such case will be close to unity as the number of emitted photons is closely matched to the number of absorbed photons [64–66]. The relationship between quantum yield and the depopulation rates of the excited state is given by equation (3.6).

$$\Phi = \frac{k_F}{k_F + k_{NR}} \quad (3.6)$$

### 3.3 Time-resolved measurements

There are two grand categories of fluorescence measurements one can perform, steady-state or time-resolved measurements. Steady-state measurements are averages over the intensity decay of the nanosecond scale phenomenon that is fluorescence. A lot of information is therefore lost in the time averaging of steady-state measurements.

Much of the molecular information present in the fluorescence emission is only accessible through time-resolved measurements. For example, it is possible to obtain the precise shape of anisotropy decays or determine through the intensity decays if quenching processes are due to static or dynamic quenching. With time-resolved spectroscopy one can obtain more detailed information about the rates and kinetics of intra or intermolecular processes, obtain information on structural parameters as well as on the dynamics of fast phenomenon [65].

In time-resolved measurements, time-domain techniques record the intensity of the fluorescent signal as a function of time after excitation with a pulse of light. The most common method used in time-domain measurements is the Time-Correlated Single-Photon Counting (TCSPC). TCSPC allows high time resolution and a near-ideal efficiency, has high sensitivity

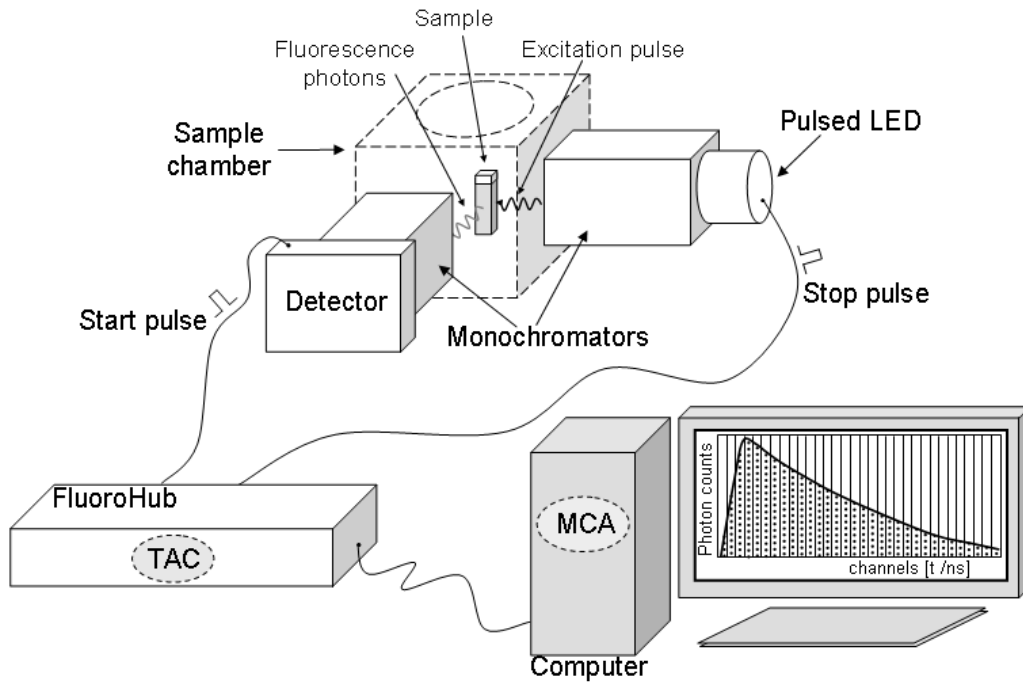


**Figure 3.2:** Schematic diagram of the single-photon counting instrument operating in reverse start-stop mode used in this work.

and well defined statistics [64, 65, 67].

### 3.3.1 Time-correlated Single-photon Counting

The TCSPC technique has its foundations on the principle that, after excitation with a pulse of light, the probability of detecting a single photon at time  $t$  is proportional to the fluorescence intensity at that given time. Hence, recording and timing a large number of photons that follow after a large number of excitation pulses allows to reconstruct the fluorescence decay curve [64]. Figure 3.2 illustrates the layout of the TCSPC instrument operating on the reverse start-stop mode that was used for the work presented in this thesis.

In TCSPC measurements a low power, high repetition rate light source is used to excite a sample and the time delay between excitation and detection of an emitted photon is recorded and stored in a multichannel analyser

(MCA) memory. The time interval between excitation and detection of a photon is measured with a Time-to-Amplitude converter (TAC). The TAC generates an output that is proportional to the time interval between a start and a stop pulse. The start pulse switches the current on and starts the charging of a capacitor within the TAC whose voltage increases linearly with time. The stop pulse turns the current off and the final voltage represents the time between the two pulses. This voltage is then converted and allocated to a proportional channel number in the MCA as a single event. Repeating the cycle allows the construction of an histogram of photon versus "time between excitation and detection" which represents the intensity decay profile. In a reverse mode TCSPC the TAC is started when a photon is detected and the next excitation pulse from the light source is the stop signal [67, 68].

The time-resolved measurements presented in this thesis were performed in the reverse mode on a IBH Fluorocube fluorescence lifetime system (Horiba Jobin Yvon IBH Ltd., Glasgow, UK) equipped with both excitation and emission monochromators. The FluoroHub and data acquisition were controlled by the DataStation software from Horiba Jobin Yvon IBH Ltd. An AlGaIn version of a pulsed light emitting diode was used at 279 nm in order to excite Tyr directly [69]. The optical pulse duration was  $\approx 600$  ps (FWHM) and repetition rate 1 MHz.

### 3.3.2 Data analysis

The measured decay  $M(t)$  obtained with the TCSPC technique is not the intensity decay of the fluorophore,  $I(t)$ . The  $I(t)$  response function of the fluorophore is what would be observed with  $\delta$ -function excitation and a  $\delta$ -function instrument response (figure 3.3a). This is not achieved technically and the detected  $M(t)$  is the convolution of the real impulse response function  $I(t)$  with the instrumental prompt response  $P(t)$ ,

$$M(t) = P(t) \otimes I(t) \tag{3.7}$$

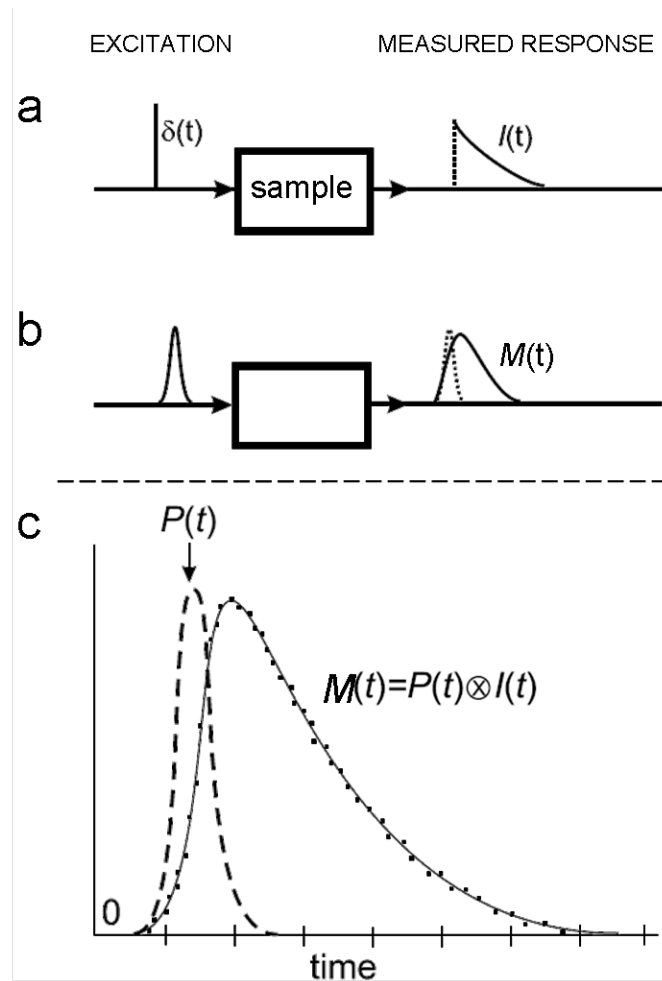


**Figure 3.3:** Diagram of the principle of time-resolved pulse fluorescence spectroscopy, adapted from [64]. a) representation of the ideal measured TCSPC data of a sample's fluorescence response to a  $\delta$ -pulse excitation, with  $\delta$ -function instrument response; b) representation of the actual measured TCSPC data of the same sample when excited with a short-pulse of light; c) magnified representation of the TCSPC experiment data output, where the measured instrumental prompt response  $P(t)$  and measured decay  $M(t)$  are identified.

A schematic depiction can be seen in diagrams b and c of figure 3.3.

The instrument response function contains not only the pulse shape of the light source but also characteristics of the detector and timing electronics, such as the transit time spread, temporal dispersion and timing jitter. However, the  $P(t)$  function can be measured and represents the shortest time profile that can be detected. This is achieved by using a zero lifetime sample, i.e. a dilute scattering suspension, and recording the instrumental response [64, 65, 67, 68].

### Nonlinear Least Squares Method

Many methods can be used to solve the problem of deconvolution and curve fitting, the most widely used is based on nonlinear least squares (NLLS). The objective of the NLLS method is to test if a given mathematical model, describing the intensity decay law, is consistent with the retrieved data and to obtain the parameter values of such model that provide the best match to the recorded data and therefore have the highest probability of being correct [64, 65, 68].

The NLLS method principle lies on the minimization of the mismatch between real data and calculated data. The mathematical model for  $I(t)$  is convolved with  $P(t)$  and a calculated version of the measured decay,  $M_c(t)$ , is obtained. The mismatch between the calculated data and the real data is given by

$$\chi^2 = \sum_{i=1}^N \left[ \frac{M(t_i) - M_c(t_i)}{\sqrt{M(t_i)}} \right]^2 \quad (3.8)$$

where  $N$  is the number of data points. Dividing  $\chi^2$  by the number of degrees of freedom  $\nu$  results in the normalized (or reduced) chi-square  $\chi_r^2$  (equation (3.9)) that is independent of  $N$  and whose value should be close 1 for a good

agreement between the calculated and the real data, i.e., for a good fit.

$$\chi_r^2 = \frac{1}{v} \sum_{i=1}^N \left[ \frac{M(t_i) - M_c(t_i)}{\sqrt{M(t_i)}} \right]^2 \quad (3.9)$$

with

$$v = N - p \quad (3.10)$$

where  $p$  is the number of fitted parameters.

A minimization algorithm searches for the parameters of  $I(t)$  that produce the best fit, performing the reconvolution of  $I(t)$  with  $P(t)$  at each iteration. If for a fit of a certain model the  $\chi_r^2$  values obtained are below 0.8 or above 1.2 the model should be rejected as it is unlikely that such deviations are produced by random errors. For this reason  $\chi_r^2$  is often termed the "goodness-of-fit parameter", one can use it to help determine if a certain model acceptably describes the obtained data [64, 65].

The data presented in this thesis has been analysed using the DAS6 data analysis package (Horiba Jobin Yvon IBH Ltd., Glasgow, UK). The software was used for reconvolution analyses of multi-exponential models using the NLLS method. The decay models  $I(t)$  were chosen to fit the data on the basis of the best  $\chi_r^2$  values and visual inspection of the random distributions of weighted residuals.

The multi-exponential model constructs the intensity decay as a sum of individual single exponential decays and is given by

$$I(t) = \sum_{i=1}^n \alpha_i \exp(-t/\tau_i) \quad (3.11)$$

where  $\tau_i$  are the lifetimes of each individual decay component  $i$  and  $\alpha_i$  are the

corresponding pre-exponential factors. The fractional contributions of each lifetime component  $f_i$  to the overall intensity can be calculated as:

$$f_i = \frac{\alpha_i \tau_i}{\sum_{k=1}^n \alpha_k \tau_k} \quad (3.12)$$

### Maximum Entropy Method

As mentioned previously, intrinsic protein fluorescence is considered one of the most complex areas of biochemical fluorescence because of the photo-physical behaviour of the fluorescent amino acids. In fact, it has been found many times over the years that the fluorescent decay of biomolecules can be even more complex than multi-exponential and in reality display a non-exponential behaviour. In such cases, analysis using lifetimes distributions instead of the discrete multi-exponential approach yields more realistic and accurate descriptions of the fluorescence phenomenon.

When working with intrinsic protein fluorescence it is useful to determine if the fluorescence response indeed consists of discrete exponential decays or alternatively is a continuous distribution of lifetime components. Due to the complex nature of protein fluorescence the assumption of a model for the fluorescence decay can be sometimes restrictive and cause loss of information therefore the best approach is to analyse the data without making any assumptions about the decay function.

The maximum entropy method (MEM) allows the analysis of data without *a priori* assumptions about the shape of the decay components. In the case of a non-exponential decay MEM can recover the shape of the lifetime distribution more realistically, as opposed to other lifetime distribution methods that assume the decay as a composition of Gaussian or Lorentzian profiles which is not necessarily accurate. MEM can also reveal if a decay is composed of discrete components that can, in fact, be regarded as discrete

single exponential decays.

MEM considers the fluorescence decay as a distribution of exponential components whose pre-exponential factors are  $g(\tau)$ . The fluorescence impulse response function  $I(t)$  is rationalized as

$$I(t) = \int g(\tau) \exp(-t/\tau) d\tau \quad (3.13)$$

the objective being to retrieve the probability distribution of decay times  $g(\tau)$  from the available time-resolved decay data.

To recover  $g(\tau)$ , the Laplace transform is applied to equation (3.7) resulting in

$$m(t) = p(t) \times i(t) \quad (3.14)$$

Convolution is Laplace transformed into multiplication and one can obtain the Laplace transform of the decay function  $i(t)$  without big difficulties. However, to recover  $g(\tau)$  inverting the Laplace transform is necessary and this is an ill posed problem due to the fact that the  $M(t)$  and  $P(t)$  data are noisy and incomplete. This creates a large group of multiple solutions allowed for  $g(\tau)$ . Within such set of retrieved results some can be disregarded as physically and statistically unacceptable, the problem is then transposed into choosing the best description amongst the remaining feasible group of solutions for  $g(\tau)$  [64, 70, 71].

The great advance provided by information theory lies in the discovery that there is a unique, unambiguous criterion for the "amount of uncertainty" represented by a discrete probability distribution (...) It is now evident how to solve our problem; in making inferences on the basis of partial information we must use that probability distribution which has maximum entropy [uncer-

tainty] subject to whatever is known. This is the only unbiased assignment we can make. (Jaynes 1957, p.622)

The choice of the preferred solution can be achieved by maximising the "uncertainty" associated to a certain  $g(\tau)$  distribution. The principle of maximum entropy (entropy and uncertainty are used as synonyms in this context) states that from a set of distributions that fit the data one should always choose the one with the highest entropy because it is the most unbiased, the most reasonable or least prejudiced, and the most likely to be correct [72]. To calculate such "uncertainty" factor MEM uses the Shannon-Jaynes entropy as it has been proved to be the function that introduces less artifacts and gives the least correlated solutions. The function is defined as

$$S = \int_0^{\infty} \left[ g(\tau) - m_0(\tau) - g(\tau) \log \frac{g(\tau)}{m_0(\tau)} \right] d\tau \quad (3.15)$$

where  $m_0(\tau)$  is an assumed starting model. If there is no prior knowledge about the system and the values of the  $g(\tau)$  for each  $\tau$  are unknown then  $m_0(\tau)$  is a flat distribution where each  $g(\tau)$  has the same initial probability [64, 73].

The Pulse5 software (MaxEnt Solutions Limited/Maximum Entropy Data Consultants Ltd, Cambridge, UK) was used for the data analysis exposed in this thesis. The program is an optimization algorithm designed to maximise the Shannon-Jaynes entropy subject to chi-square constraints on the data. Technically, the software considers  $I(t)$  as a sum over a finite number of components  $n$ , equally spaced in a logarithmic scale, therefore equation (3.13) is transformed into

$$I(t) = \sum_{j=1}^n g(\tau_j) \exp(-t/\tau_j) \quad (3.16)$$

where  $n=200$  and each  $n^{th}$  lifetime component has a  $g(\tau_j)$  probability of

contributing to the fluorescence response function.

The  $g(\tau_j)$  lifetime distribution retrieved with the MEM software is then normalized according to

$$g_N(\tau_j) = \frac{\tau_j g(\tau_j)}{\sum_{k=1}^n \tau_k g(\tau_k)} \quad (3.17)$$

In the  $g_N(\tau)$  distribution, the amplitude of each component is its fractional contribution  $\phi$  to the overall fluorescent decay. The sum over all the  $n^{\text{th}}$   $g_N(\tau_j)$  components that create a determined  $i$  peak profile is  $\phi_i$  (equation (3.18)) and is the MEM equivalent of the fractional contributions  $f_i$  obtained through the NLLS method presented previously.

$$\phi_i = \sum g_N(\tau_j) \quad (3.18)$$

### 3.3.3 Decay associated spectra

The complexity of the fluorescence emission of biomolecules can be seen in their fluorescence decay and is also imprinted in the fluorophore's emission spectrum.

The heterogeneity or complexity of the photophysics behind emission can be due for example to excited state reactions or ground state heterogeneity as in the case of, e.g., identical emitting species existing in different microenvironments or different fluorophores with overlapping emission spectra. The fluorescence intensity can then be expressed as a function of both time and wavelength  $I(t, \lambda)$ . During the evolution of fluorescence techniques and methods various ways of resolving and dealing with heterogeneous fluorescence have been found [74]. In the particular case of time-resolved fluorescence the

decay associated spectra (DAS) are often used.

To calculate the DAS one combines steady-state and time-resolved data, obtaining as a result the relative contributions to the overall fluorescence of each lifetime component of a fluorescence decay, as a function of emission wavelength  $F_i(\lambda)$ . To create a DAS, using the TCSPC technique, fluorescence decays are measured for different emission wavelengths  $\lambda$ . From the time-resolved data one determines the fractional contributions of each decay component at a particular emission wavelength,  $f_i(\lambda)$ , using equation 3.12. The DAS for each  $i$  component of the fluorescence decay,  $F_i(\lambda)$ , can then be calculated according to

$$F_i(\lambda) = F(\lambda)f_i(\lambda) \quad (3.19)$$

where  $F(\lambda)$  is the overall steady-state fluorescence spectrum.

A DAS is the fluorescence emission spectra one would obtain if it were somehow possible to selectively detect photons from one emitting species (or state) and record, one at a time, each individual spectrum within the microheterogeneous fluorescent sample. In other words, the DAS represents the emission spectrum of a state (or species) with a particular decay lifetime. The capacity to resolve the lifetime of each individual state is therefore a crucial requisite to calculate these derived spectra [64, 75].

### 3.4 Protein fluorescence

Fluorescence techniques have recently become one of the fundamental methods for research in the field of protein studies. Fluorescence, due to its characteristic, allows the study of structural and dynamic properties of proteins that are linked directly to its biological functions, such as specific binding, biocatalysis or membrane transport [76].

To study protein molecules one must focus on processes between the fluo-

rophore and surrounding atoms than can affect the spectral, temporal and polarization characteristics of the emitted fluorescence. Extrinsic fluorophores can be linked to proteins in order to obtain such information, but these might disturb the biomolecule and therefore the choice of fluorescent tag should be carefully investigated. To avoid such inconvenient one can make use of the fluorescence of the protein itself.

From all the amino acids only three are aromatic and fluoresce, they are named phenylalanine, tyrosine (Tyr) and tryptophan (Trp). These amino acids are present in virtually all proteins, but their relative proportion in one given protein is small. This is very fortunate because if all amino acids of one protein were fluorescent interpreting the data would be extremely complex. Even so, many proteins have multiple fluorescent amino acids (as is the case of Barnase, a relatively small enzyme composed of 110 amino acids where three are Trp residues [77]) which adds significant complexity to the detected fluorescence.

The study of simpler systems, namely one Trp proteins, has significantly increased our knowledge of intrinsic protein fluorescence over the years. Technological advances such as the ability to create mutant proteins through sitedirected mutagenesis have allowed the study of simpler model proteins greatly contributing to the progress made in the past decade. However, even in simple engineered protein models there is significant complexity in the photophysical behaviour of the amino acid fluorophore, this is why intrinsic protein fluorescence is considered one of the most complex areas of biochemical fluorescence [65, 76].

The  $A\beta$  protein, subject of this thesis, is a small protein with high significance in Alzheimer's disease pathology. Due to their sensitivity, fluorescence techniques are suitable to study the aggregation process of the protein at a molecular level. From a photophysics point of view, the outstanding characteristic of this small protein is that it contains only one single Tyr amino acid and no Trp.

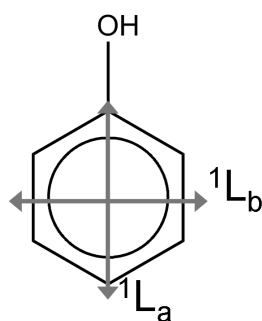


**Figure 3.4:** singlet-singlet electronic absorption transition moment orientation of phenol.

Trp is the fluorescent amino acid with the highest extinction coefficient and quantum yield, moreover Tyr usually transfer its excitation energy to Trp through resonance. This makes Tyr fluorescence studies very difficult in wildtype proteins that contain both Tyr and Trp. These two facts are part of the reason why Trp's fluorescence is the most studied making Trp the most important tool in intrinsic fluorescence studies [76].

The absence of Trp in  $A\beta$  and the presence of only one Tyr residue, makes this protein a very interesting subject and a natural model to study Tyr photophysics in proteins. In this thesis it is proposed that Tyr can be used as an intrinsic sensor for the oligomerisation of the wildtype  $A\beta$ , thus avoiding any interference with the natural state and biochemistry of the protein. Therefore, hereinafter the focus will become Tyr fluorescence.

### 3.4.1 Tyrosine fluorescence

Tyr's fluorescence is due to the phenol chromophore. Figure 3.4 illustrates the phenol's electronic absorption transition moments, in Platt's notation. These transitions are responsible for the two ultraviolet absorption bands of Tyr. Tyr's strong absorption with a maximum around 223 nm is due to the  $^1L_a$  transition and the lower energy transition, due to the  $^1L_b$ , peaks near 277 nm.

Fluorescence originates from the lowest vibrational level of the first singlet

electronic state as an unstructured wide band with its maximum near 303 nm for aqueous solutions of Tyr [78]. Hydrogen bonding red shifts both the absorption and fluorescence spectra [78–80]. Ionization of the hydroxyl group, resulting in the anion tyrosinate, leads to a large red shift in the fluorescence spectra placing the emission maximum near 340 nm [65, 78]. Excited state ionization can occur because the  $pK_a$  of the hydroxyl group of the phenol in the excited state is relatively low. If there are suitable proton acceptor molecules in Tyr’s surrounding ionization can occur during the excited state lifetime [81]. It is therefore conceivable that excited state proton transfer can occur for Tyr in proteins.

The excited state decay kinetics of Tyr in solution displays a mono exponential behaviour. In figure 3.5 can be seen the experimental data retrieved from a TCSPC measurement of a  $50\mu\text{M}$  Tyr solution in HEPES at  $37^\circ\text{C}$ , performed on the IBH Fluorocube system as previously described in Chapter 3 (page 30). The data can be successfully fitted to a mono-exponential decay and MEM analysis confirms such simple decay kinetics as can be seen in figure 3.6.

The inclusion of Tyr in a peptide chain significantly increases the complexity of its excited state decay kinetics which becomes becomes multi-exponential or even non-exponential. The simple addition of the amide groups to Tyr structure to create the N-acetyltyrosinamide (NAYA) (figure 3.7) introduces changes to Tyr’s phenol microenvironment that result in a multi-exponential decay. Unruh et al. [82] have also found such evidence and shown that in small peptides (a tripeptide and a pentapeptide) the complexity of Tyr decay increases and demonstrates non-exponential features.

Such complex behaviour of Tyr, and also of Trp and phenylalanine amino acids, is commonly interpreted in terms of the existence of rotamers. In the backbone of a protein the peptide bonds of the amino acid chain are relatively rigid, but rotations are possible around single bonds of the amino acid residues. The  $C_\alpha - C_\beta$  chemical bond in Tyr residue can rotate (figure 3.8) giving rise to existence of different side chain conformations called

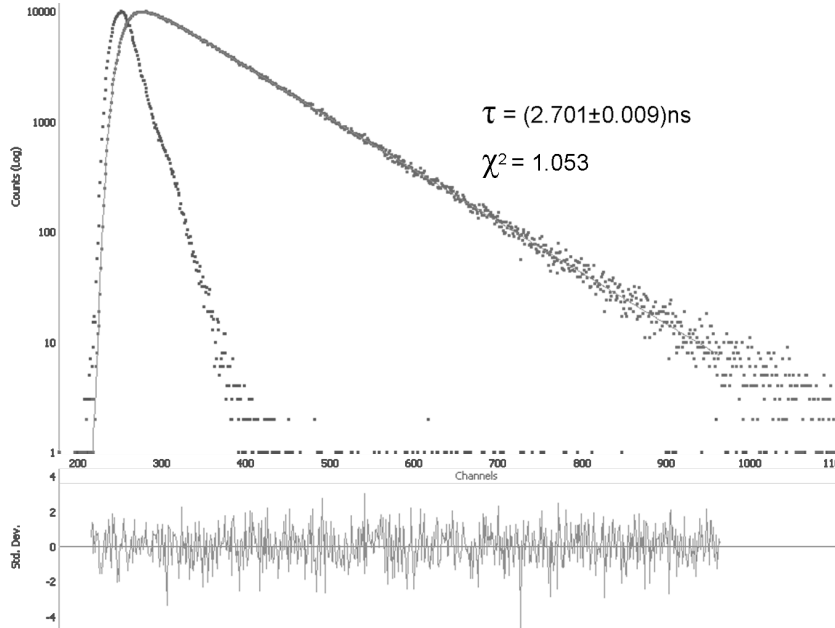


**Figure 3.5:** Tyr fluorescence decay (emission: 315 nm) fitted to a mono-exponential decay function. The fitted function can be seen as a light trace through the experimental data, Tyr decay data is shown as grey squares and prompt as black squares. Retrieved parameters for lifetime are presented with 3 standard deviations as error.

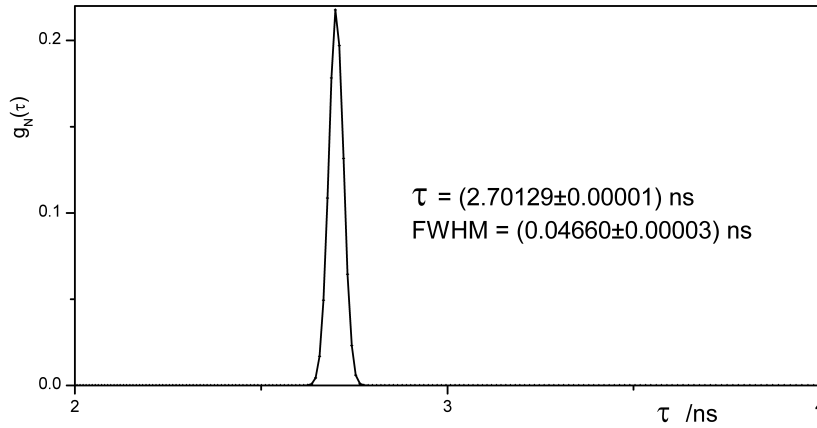


**Figure 3.6:** Lifetime distribution of Tyr fluorescence decay (emission: 315 nm) obtained with MEM. Lifetime and full width half maximum (FWHM) parameters presented with 3 standard deviations as error.

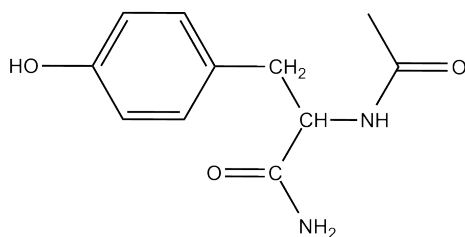


**Figure 3.7:** Chemical structure of NAYA.

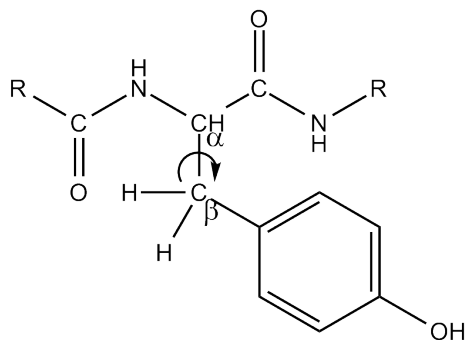


**Figure 3.8:** Tyrosine amino acid residue chemical structure in a peptide chain, showing the possible rotation around  $C_\alpha - C_\beta$  chemical bond. R residues represent the remaining peptide sequence.

rotamers. According to the common Tyr rotamer model rotation tends to cluster around three defined angles  $\chi_1 = 180^\circ, +60^\circ, -60^\circ$  [82–84]. In each rotameric conformation the phenol group is exposed to different environments and remains at different distances from potential quenchers, such as amide groups in the peptide chain [85–87]. As the fluorescence decay is determined by the local interactions between the phenol ring and its microenvironment each of the excited state rotamers has a characteristic fluorescence decay. If interconversion between rotamers is slow compared to the lifetime of the excited state, lifetime experiments can have enough resolution to distinguish the different decays arising from the different population of rotamers.

The ability to selectively excite the only Tyr present in  $A\beta$  makes this peptide a good candidate for lifetime measurements using its intrinsic fluorescence. Moreover, aggregation of single  $A\beta$  peptides should create changes in

the fluorophore's surroundings within Å scales therefore affecting Tyr's fluorescence decay kinetics. Hence the proposition that Tyr lifetime response could be used as non-invasive sensor of A $\beta$ 's aggregation that gave rise to this thesis.

# Chapter 4

## Tyrosine sensitivity to early stages of $A\beta_{40}$ aggregation

### 4.1 Introduction

In this chapter is addressed the problem of invasiveness of the fluorescence sensing methods by making use of the  $A\beta$  intrinsic fluorescence. In the amyloid-related methods reported in the literature, the proteins are labelled with fluorescent probes whose alterations in fluorescence responses indirectly demonstrate amyloid aggregation. Clearly the requirement of fluorescent labelling is a serious drawback of these approaches, due to potential disturbance of the peptide behaviour, a common criticism of all fluorescent techniques that use extrinsic molecular probes as labels.

The lack of Trp and concomitant Tyr to Trp energy transfer, and the presence of only one Tyr in the  $A\beta$  peptide helps make Tyr fluorescence a truly native, non-invasive and interpretable sensor of  $A\beta$  aggregation, thus obviating the need to use an extrinsic fluorophore. Tyr fluorescence decay times, being responsive to environmental changes on the Å scale, enable the monitoring of interactions between individual biomolecules. Advantageously when compared to other techniques, this approach reveals crucial information on the initial stages of  $A\beta$  aggregation without disturbing it.

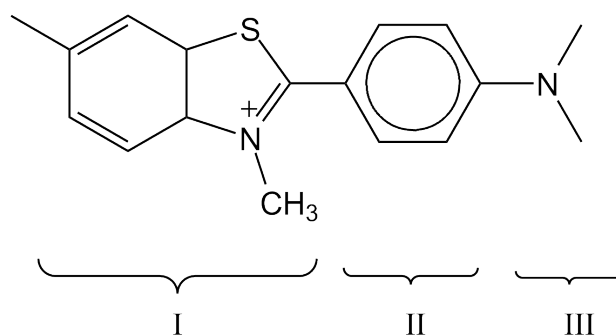


**Figure 4.1:** Thioflavin T chemical structure. The fragments identified as I, II and III are the benzthiazole ring, benzene ring and dimethylamino group respectively.

Here,  $A\beta$  aggregation is monitored using the fluorescence decay of its intrinsic fluorophore, Tyr. Simultaneously, aggregation is followed through the traditionally used method of Thioflavin T (ThT) fluorescence intensity. It is shown that alterations in the fluorescence decay of Tyr correlate with  $A\beta$  aggregation at an earlier stage than the ThT assay, revealing that Tyr is not only sensitive to aggregation but reports on its pre-fibrillar stages.

## 4.2 Thioflavin T

ThT is a dye used as a probe to indicate the presence of amyloid aggregates. In *in vitro* studies of fibril formation, the changes in ThT intensity, monitored through the traditional steady-state fluorescence method, report the appearance of fibrils.

ThT is composed of three fragments (figure 4.1): a benzthiazole ring, a benzene ring and a dimethylamino group. In the ground state the two ring structures of ThT are in an almost planar orientation. Upon excitation the rings rotate to the most stable excited state conformation, which has a low quantum yield. The intramolecular charge transfer results in the twisting of the rings to an angle of  $\approx 90^\circ$  [88]. The twisted intramolecular charge transfer state (TICT) is non fluorescent and this is the major reason for the

quenching of ThT fluorescence in solution.

ThT behaves as a molecular rotor, meaning that its ability to undergo torsional relaxation is determined by its microenvironment viscosity or rigidity and, consequently, so is the rate of formation of the TICT state [88]. It is thought that binding of ThT to amyloid fibrils stabilises the planar (fluorescent) form of the molecule and promotes steric hindrance on the internal rotation of the benzthiazole and aminobenzene rings relative to each other resulting in the increase of ThT's quantum yield.

It is not known exactly how ThT binds amyloid fibrils, but studies have shown that the longer axis of the molecule is parallel to the long axis of the fibrils [89,90]. It is in this direction that run the channels created by the  $\beta$ -sheets characteristic of the amyloid fibrils. These facts lead to the belief that the channels are the binding sites of ThT, in which the molecule is constrained to remain in the planar fluorescent form, and in this way accounting for ThT specificity to amyloid fibrils. Therefore, the increase in ThT fluorescence quantum yield reports the binding of the molecule to  $\beta$ -sheet channels which are present in large ordered structures, such as protofibrillar aggregates and mature amyloid fibrils.

### 4.3 Methodology

A $\beta_{40}$ , ThT and buffer tablets were purchased from Sigma-Aldrich (Poole, UK). A solution of monomeric A $\beta_{40}$  was obtained by dissolution in hexafluoroisopropanol (HFIP) to a concentration of  $10^{-4}$ M, evaporating the solvent and then re-dissolving in a phosphate buffer (pH 7.0) containing ThT, sonicating for approximately 10 min. Final sample concentrations were:  $30\mu$ M A $\beta$  and  $15\mu$ M ThT.

Measurements were performed at the temperature of  $22^{\circ}$ C using a temperature controlled sample holder connected to a Neslab RTE-11 thermostat (Thermo Scientific, UK). The luminescence spectrometers PerkinElmer Lambda2 UV/VIS and PerkinElmer LS-50B were used for absorption and

fluorescence spectra measurements, respectively. ThT was excited at 450 nm and its fluorescence was measured in the range of 460-650 nm. The fluorescence decay of Tyr was recorded using the TCSPC technique on the IBH Fluorocube system as previously described in Chapter 3 (page 30).

## 4.4 Results and discussion

To test the hypothesis that the process of A $\beta$  aggregation is reflected not only by an increase in ThT intensity, but also by alterations in Tyr fluorescence decay, fluorescence spectra of ThT and decays of Tyr were recorded at increasing times after sample preparation ( $t_{exp}$ ) for up to three weeks.

Figure 4.2a shows increasing fluorescence intensity of ThT with time, consistent with the previously reported [91] sensitivity of this dye to the presence of amyloid fibrils. The spectral peak intensity versus time (figure 4.2b) represents the dynamics of A $\beta$  fibrillisation. The change in ThT fluorescence intensity shows significant increase with time, but during the first  $\approx 50$  h is small and comparable with the noise level (the slope of  $F_t/F_0$  versus time is  $(2.17 \pm 2.01) \times 10^{-3}h^{-1}$ , see figure 4.4), and is thus not a useful indicator of initial aggregation. This may be consistent with the aggregates being too small and/or disordered to effectively stabilize planar conformations of ThT. The similar low ThT fluorescence intensity during the first  $\approx 40$  h of aggregation was observed in the study of another aggregating peptide,  $\alpha$ -synuclein [91].

Fluorescence decays of Tyr were analysed using a three-exponential function as a decay model through the NLLS method. Mono- and two-exponential models were rejected on the basis of the goodness of fit criteria ( $\chi_r^2$  and distribution of residuals). Figures 4.3a and 4.3b show the recovered decay times  $\tau_i$  and their relative percentage contributions  $f_i$  (defined by equation 3.12 where n equals 3).

The three-exponential decay is consistent with a commonly accepted ro-

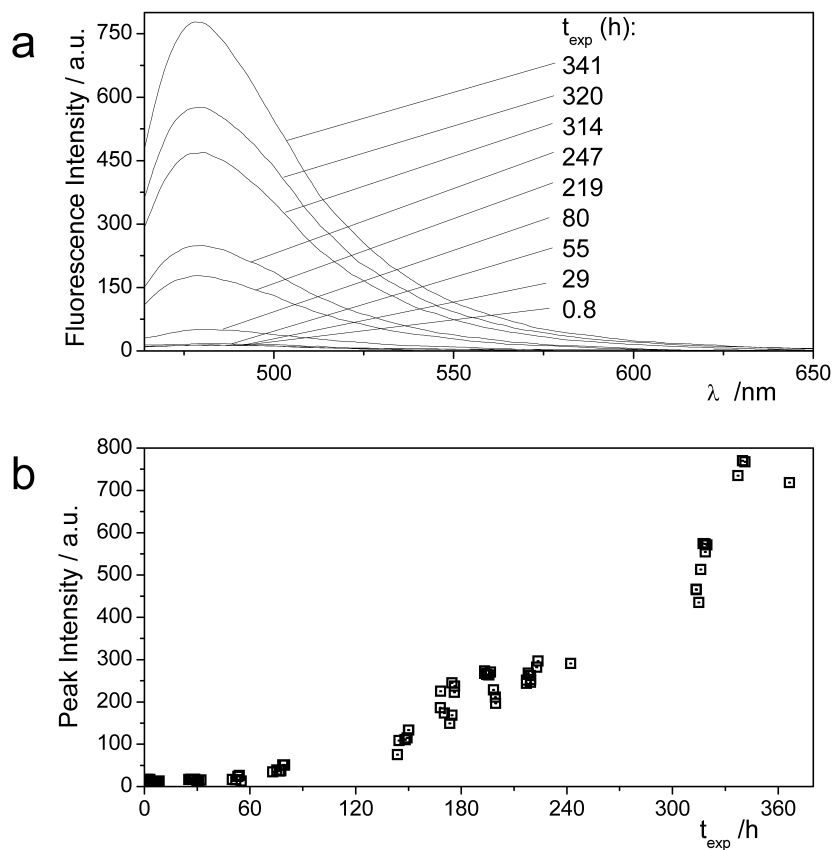


**Figure 4.2:** Emission spectra (a) and peak intensity (b) of ThT fluorescence at different stages of  $A\beta$  aggregation. The size of each point on the plot represents the experimental error (3 standard deviations).

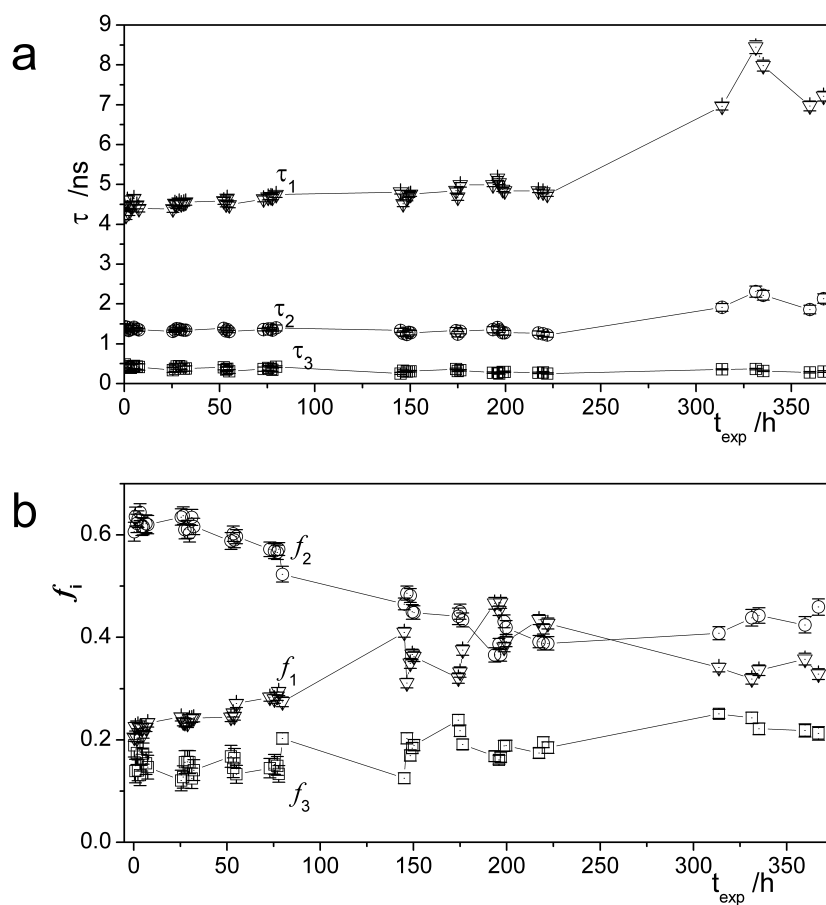


**Figure 4.3:** Tyr fluorescence decay time (a) and fluorescence intensity contributions (b) obtained from fitting Tyr decay to a three-exponential model.

tamer model of fluorescent amino acids in proteins. According to this model, Tyr can exist in three different rotameric forms, each characterized by its own fluorescence decay time determined by local interactions of the amino acid in a given conformation. If changes in the lifetimes and/or percentage contributions of rotamers are observed, it indirectly indicates conformational evolution of the protein in this case due to its aggregation.

In figure 4.3a one can observe that the longest ( $\tau_1$ ) and the middle ( $\tau_2$ ) decay times tend to increase slowly over a period of about 200 h of the experiment, while the shortest decay time ( $\tau_3$ ) remains constant. This weak effect could be caused by the gradual change of polarity due to solvent molecules being replaced by other A $\beta$  molecules during aggregation. The constant value of the third decay time lifetime ( $\tau_3$ ) suggests that rotamer conformation 3 is hidden inside the protein structure and does not respond to environmental changes.

The fluorescence contributions of the three rotamers  $f_1$ ,  $f_2$  and  $f_3$  (figure 4.3b) show substantial changes from the very beginning of the process. The ratio of increasing  $f_1$  and decreasing  $f_2$  values can be used as a parameter indicator of early stages of aggregation, including the first  $\approx 50$  h. Figure 4.4 compares changes in the  $f_2/f_1$  ratio [slope  $(1.32 \pm 0.13) \times 10^{-3} h^{-1}$ ] with ThT intensities ratio  $F_t/F_0$ , where  $F_t$  is the peak fluorescence intensity at time  $t$  and  $F_0$  the initial peak fluorescence intensity. The linear fit of ThT data shows a larger slope than Tyr's  $f_2/f_1$  ratio. However there is a high uncertainty in this value and therefore no conclusions can be drawn from the ThT assay during the first 50 h. On the other hand the  $f_2/f_1$  ratio obtained from Tyr decay shows a clear trend since the beginning of the measurement. This serves to demonstrate the enhanced capacity of Tyr decay to detect early aggregation stages of single A $\beta$  peptides. The above observation also illustrates the advantages of fluorescence lifetime-based sensing over intensity-based approaches in complex biological media.

At longer times ( $t_{exp} > 200$  h), the recovered parameters for Tyr decay did not yield satisfactory statistical results. In figures 4.3a and 4.3b one

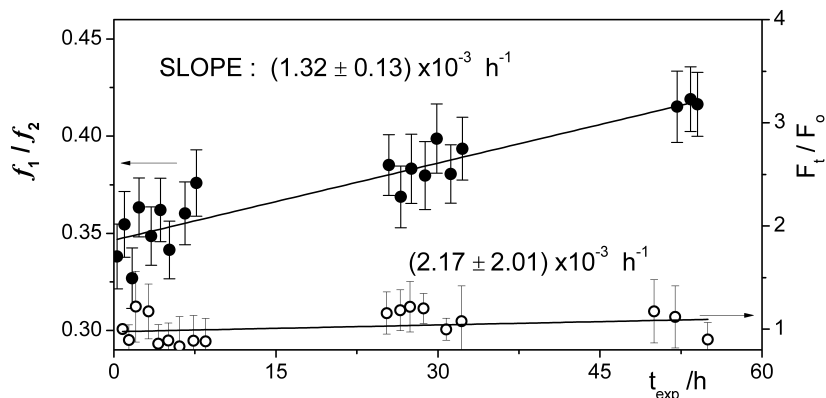


**Figure 4.4:** Ratio of the decay time contributions to the fluorescence intensity  $f_1/f_2$ , together with relative increase in ThT fluorescence  $F_t/F_0$ , detected during first 50 h of  $A\beta$  aggregation. Data fitted to linear regressions.

can see that the decay times  $\tau_i$  are no longer stable and changes in  $f_i$  values seem to reverse. This could be due to more complex excited-state kinetics and such observation encouraged the investigation of whether a three-exponential decay model adequately describes Tyr fluorescence responses during whole process of aggregation. For this purpose, a model free fluorescence decay time distribution analysis based on MEM was applied to a number of recorded decays. Instead of three sharp peaks expected for a three-exponential decay, four relatively broad distributions of decay times were detected (figure 4.5).

Three decay time bands centered at  $\approx 0.5, 1.5$  and  $4$  ns, correspond to the previously obtained rotamer discrete decay times. The presence of the fourth, and longest decay time band, could be caused by a specific mechanism resulting, e.g., from Tyr-Tyr interactions at close proximity within an aggregate. During the initial period of about 200 h, a three-exponential decay with a slow increase of the medium and longer ( $\approx 4$  ns) decay time, seems to be an acceptable description of the fluorescence phenomenon because the contributions of the long decay times ( $15 - 18$  ns) are relatively small. In the decay time distribution obtained at 314 h (see figure 4.5) the fourth component is no longer negligible and this explains the failure of the three-exponential decay model at later times and breakdown of the trend in

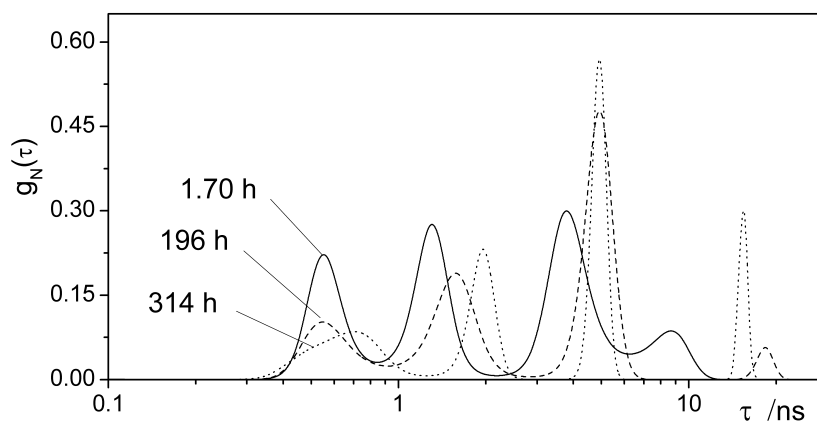


**Figure 4.5:** fluorescence lifetime distributions of Tyr decays detected after 1.7, 196 and 314 h of aggregation.

the parameters shown in figure 4.3.

## 4.5 Conclusions

In this chapter was demonstrated that time-resolved fluorescence measurements of Tyr in  $A\beta$  can be used as an early indicator of peptide aggregation in AD's research.

The approach has two key advantages above the traditional ThT intensity-based technique. It is completely non-invasive as it does not require an extrinsic fluorophore and uses pulses of light of very low intensity, thus there is minimal interference with the native  $A\beta$  and its biochemistry. Also very important, it reports on the critical early stages of aggregation, before the formation of  $\beta$ -sheet containing structures can be detected by ThT.

$A\beta$  is a special case of a single Tyr peptide, its use to monitor protein aggregation might prove advantageous in the search for analytes or factors accelerating, slowing down or reversing the progress of protein aggregation in neurodegenerative diseases in general. This could result in drug discoveries that might bring closer the prevention, control or even reversal of the aggregation that leads to AD.

# Chapter 5

## Examination of Tyrosine response to $A\beta_{40}$ oligomerisation

### 5.1 Introduction

In this chapter is shown how  $A\beta$ 's intrinsic fluorescence of Tyr can be used to monitor oligomer formation non-invasively starting from the early onset of single peptide-to-peptide interactions. This alternative approach eliminates the drawbacks of extrinsic fluorophore based methods, e.g. their potential to perturb both the native structure and the aggregation kinetics.

In the previous chapter was already demonstrated the sensitivity of Tyr lifetime measurements to aggregation at much earlier stages than widely reported ThT steady-state measurements. Here,  $A\beta$ 's intrinsic fluorophore Tyr is used to probe the earliest peptide-to-peptide stages of aggregation in the region often merely labeled as the fibrillisation time lag because of the negligible changes observed with the ThT assay. The distribution of three rotamer conformations of the single Tyr in  $A\beta$  tracks the aggregation across such time lag and beyond. Tyr lifetime responses are used as fingerprints of different stages of initial  $A\beta$  aggregation leading to the formation of oligomers.

A more detailed investigation of the role of the initial monomer peptide concentration and combined lifetime and spectral data are presented in order to better understand the underlying photophysics of Tyr fluorescence response.

## 5.2 Methodology

In order to better simulate the conditions present in the human body, namely in cerebrospinal fluid (37°C temperature and pH:7.3 [92]), the sample preparation method was slightly modified and optimised. From this point on all samples presented in this thesis were made according to the preparation method presented below, unless explicitly stated otherwise.

N-(2-Hydroxyethyl)piperazine-N'-(2-ethanesulfonic) acid (HEPES) buffer solution was used to prepared samples in which its concentration is 100mM and pH is 7.3. Once made, all samples were maintained at 37°C. When performing measurements the temperature was controlled by the use of a temperature-controlled sample holder connected to a Neslab RTE-11 thermostat (Thermo Scientific, UK). In all other occasions the samples were kept in a SalvisLab Incucenter incubator (SalvisLab Renggli AG, CH).

A $\beta_{40}$ , HFIP and HEPES were purchased from Sigma-Aldrich (Poole, UK). To monitor the early stages of aggregation it is important to start from a monomeric solution of peptides as the presence of preformed aggregates can influence the kinetics of the process. A monomer solution was achieved by treating the received A $\beta_{40}$  with HFIP [93]. Treatment consisted of dissolving A $\beta$  powder in pure HFIP to a concentration of 10<sup>-4</sup>M and sonicating for at least 10 minutes. The peptide containing solution was then aliquoted into Eppendorf LoBind microcentrifuge tubes and the alcohol allowed to evaporate. For thorough HFIP removal the resulting peptide films were dried under vacuum. The aliquots were then stored at -20°C.

To prepare a sample an aliquot was taken and allowed to thermally sta-

bilize at room temperature prior to opening. The peptide film was then re-suspended in HEPES (100mM; pH: 7.3) and sonicated for about 2 min at 37°C. The samples were prepared directly before the first measurement and all cuvettes and buffer solutions were in thermal equilibrium at the desired temperature before use.

A Perkin-Elmer LS-50 B luminescence spectrometer was used for fluorescence spectral measurements. Tyr fluorescence was collected in the range 300-360 nm. Fluorescence decays were recorded using the TCSPC technique on the IBH Fluorocube system as previously described in Chapter 3 (page 30).

The complex nature of protein aggregation makes the time between sample preparation and the experiment,  $t_{exp}$ , and the wavelength at which the decay is measured,  $\lambda$ , critical factors in determining the fluorescence decay. This implies the fluorescence decay being a parametrical function of  $t_{exp}$  and  $\lambda$ , i.e.,  $I(t, t_{exp}, \lambda)$ . Therefore two types of lifetime experiments were performed. To monitor the influence of the peptide aggregation on Tyr fluorescence decay, the decays  $I_{\lambda}(t, t_{exp})$  were measured with  $\lambda = 315$  nm at increasing times  $t_{exp}$  after sample preparation. In order to obtain the wavelength-dependent decays of Tyr, the decays  $I_{t_{exp}}(t, \lambda)$  at time  $t_{exp}$  were collected for different emission wavelengths  $\lambda$  between 300 and 330 nm with wavelengths steps of 3 nm.

A three-exponential decay model (defined by equation 3.11 where  $n$  equals 3) was chosen to fit the data on the basis of the best-fit  $\chi_r^2$  values and random distributions of weighted residuals obtained for the function when applied to all the decays. Fitting the data to mono- and two-exponential models recovered statistically unacceptable results. The index  $i$  refers to one of three rotamers and the pre-exponential components  $\alpha_i$  and corresponding lifetimes  $\tau_i$  are regarded as functions of  $t_{exp}$  and  $\lambda$ . The fractional contributions of each lifetime component  $f_i$  were calculated according to equation 3.12.

Fluorescence decays measured for the different emission wavelengths  $\lambda$  allowed determination of the wavelength dependent fractional contributions  $f_i(\lambda)$ . The DAS  $F_i(\lambda)$ , each representing the fluorescence spectrum of the relevant Tyr rotamer  $Y_i$ , were calculated from the fractional contributions  $f_i(\lambda)$  according to equation 3.19.

## 5.3 Results and discussion

The simplistic rotamer model, considered in the preceding chapter, implies a three-exponential fluorescence decay of Tyr with the recovered lifetimes reporting on the excited-state kinetics of individual rotamers. All decays of Tyr detected exhibit a three-exponential character confirmed by means of the  $\chi_r^2$  goodness of fit and the distribution of residuals criteria.

If the rotamer model is suited to interpret lifetime data then the recovered parameters are expected to reflect fluorescence processes which are dependent on molecular distance (like fluorescence quenching, proton/electron transfer, fluorescence resonance energy transfer, etc.) and thus are likely to accompany peptide aggregation.

### 5.3.1 Effect of initial monomer concentration

To investigate Tyr's performance as an intrinsic reporter of aggregation present naturally in the A $\beta$  peptide, its fluorescence decay was measured in samples of different peptide concentrations. As the fluorescence decay can be affected by the mutual interactions between A $\beta$  peptides, the monomer concentration in solution might influence the complex fluorescence response of Tyr.

Lifetime measurements were performed for 8 samples of increasing A $\beta$  concentrations, namely 5, 12, 20, 27, 35, 42, 50 and 57  $\mu$ M. The intention was to collect fluorescence decays prior to aggregation, however, it cannot be excluded that the aggregation in at least some of the samples started immediately after sample preparation, before or indeed progressed during the

measurement. In order to maintain the same experimental conditions in all the samples, the measurement of each sample was started exactly ten minutes after its preparation.

The retrieved lifetimes ( $\tau_i$ ) and fractional contributions ( $f_i$ ) as function of A $\beta$  concentration are shown in figures 5.1a and 5.1b, respectively. The lifetime values (figure 5.1a) do not change markedly with concentration of A $\beta$  peptide, but the percentage contributions of decay lifetimes (figure 5.1b) depend on the peptide concentration quite significantly.

The contribution  $f_1$  (associated to a rotamer hereinafter referred as  $Y_1$  with the characteristic lifetime  $\approx 3.4$  ns) remains constant, while the dependencies of  $f_2$  ( $Y_2$ ,  $\approx 1.1$  ns) and  $f_3$  ( $Y_3$ ,  $\approx 0.4$  ns) on concentration are non-monotonic. Up to the A $\beta$  concentration of  $\approx 30\mu\text{M}$  there is an increase in fractional contribution  $f_2$  and decrease in  $f_3$ , while for the higher A $\beta$  concentrations, these trends reverse. The effect of A $\beta$  concentration on the rotamers contributions to the total fluorescence becomes more clear on the plot in figure 5.1c, where the values of  $f_i[A\beta]$  (a parameter proportional to fluorescence intensities of the rotamers  $Y_i$ ), are plotted as the function of A $\beta$  total concentration,  $[A\beta]$ .

The curves in the plot on figure 5.1c represent the fluorescence intensities of each rotamer. Their changes with  $[A\beta]$  can be interpreted in terms of the changes in the relevant rotamers populations, providing their quantum yields remain unaffected by the concentration of the peptide. Constant values of quantum yields cannot be confirmed definitely, but are supported by stable values of lifetimes measured for different peptide concentrations. Accepting the stability of quantum yields leads to the conclusion that increasing the concentration of the peptide means, up to the concentration of about  $30\mu\text{M}$ , a proportional increase of the populations of the three rotamers, with dominating rotamer  $Y_2$ . For higher concentrations  $Y_2$  growth stops and the population of rotamer  $Y_3$  increases. Rotamer  $Y_1$  grows linearly with  $[A\beta]$ , which may be an indication of  $Y_1$  being less sensitive to the environment.

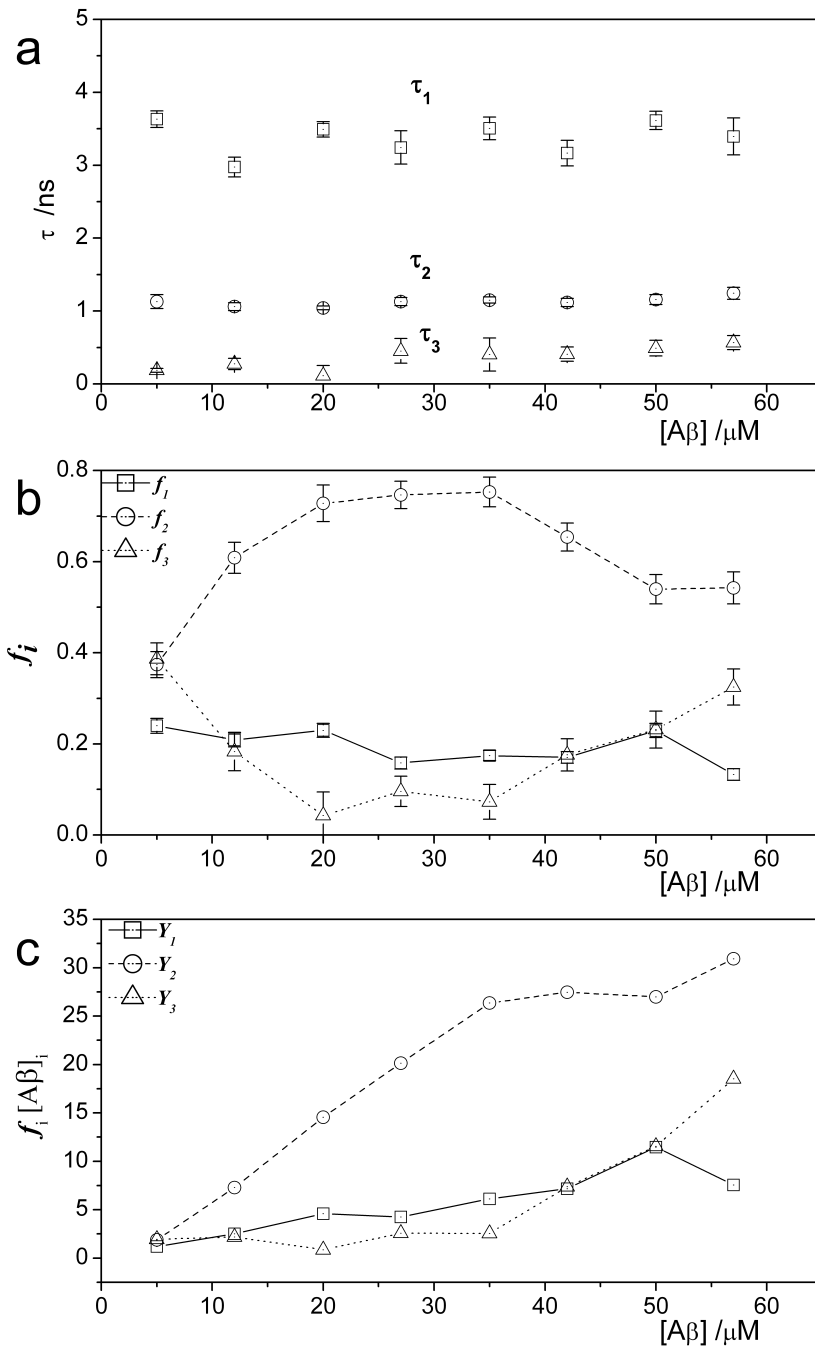


**Figure 5.1:** Parameters obtained from fitting Tyr fluorescence decay to a three-exponential decay model. a) Tyr fluorescence decay times; b) intensity fractional contributions; c) population of Tyr rotamers  $Y_1, Y_2, Y_3$ , as a function of initial A $\beta$  concentration. Experimental errors are 3 standard deviations.

The fact that A $\beta$ 's Tyr shows a high sensitivity to the effect of concentration, and therefore to the presence of neighboring A $\beta$  monomers, indicates indirectly that Tyr can be used as a non-invasive intrinsic sensor to study the A $\beta$  peptide and its process of aggregation into amyloid fibrils.

### 5.3.2 Evolution of fluorescence response with peptide aggregation

As it is expected that the aggregation process depends on the initial concentration of peptides, two samples of different initial monomer concentrations were investigated and their lifetime responses  $I(t, t_{exp}, 315nm)$  followed over the course of about two weeks. The first sample was of a low concentration of initial A $\beta$  monomers, 5 $\mu$ M, and the second of 50 $\mu$ M.

#### Low concentration sample

The retrieved lifetimes ( $\tau_i$ ) and fractional contributions ( $f_i$ ) as functions of experiment time (aggregation time) for the low concentration sample (LC) are shown in figures 5.2a and 5.2b, respectively. It can be seen that the lifetime values are stable during the course of the 210 h of the experiment. The fractional contributions of the decay lifetimes (figure 5.2b) show some, but not large, change throughout the experiment. No significant change in all the parameters suggests the LC is fairly stable and aggregation does not occur or occurs at a slow rate and is unnoticeable during the first 210 h.

This is confirmed by the ratio of  $f_1$  to  $f_2$  values, which can be used as an indicator of aggregation as has been shown in the previous chapter. It can be seen (figure 5.2c) that no significant changes in  $f_1/f_2$  occur, with its value scattered around the level of  $0.864 \pm 0.018$ .

To better understand the kinetics of Tyr fluorescence in the LC sample, its decays were then detected at different emission wavelengths. The sample

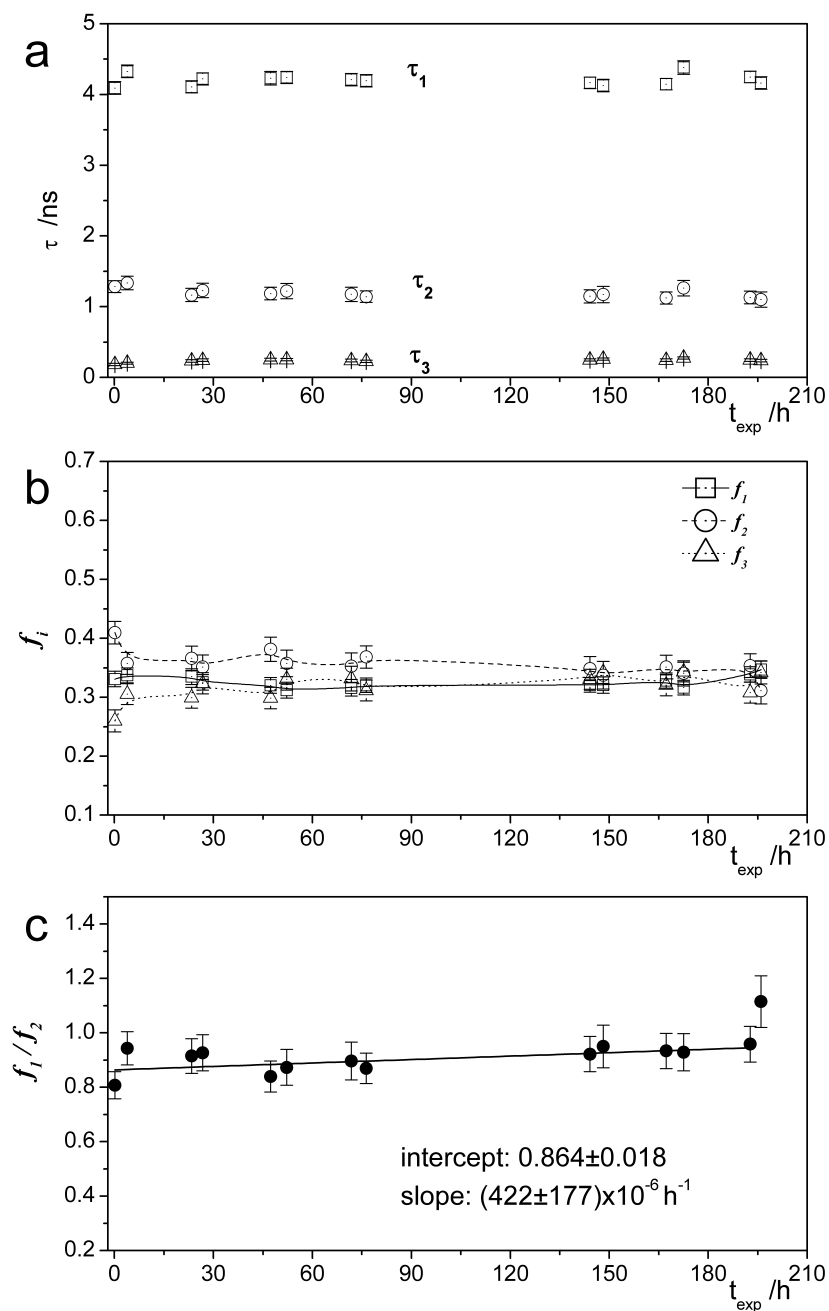


**Figure 5.2:** Parameters obtained from fitting Tyr decay in the LC sample to a three-exponential decay model. a) Tyr fluorescence decay times; b) fluorescence intensity fractional contributions; c) ratio between decay times fractional contributions  $f_1/f_2$ , data fitted to a linear regression. Experimental errors are 3 standard deviations.

was considered as stable at  $t_{exp} > 210$  h, as no further evolution in Tyr decay was observed. The parameters obtained from fitting the resulting data to a three-exponential decay model are shown in figures 5.3a (lifetimes) and 5.3b (fractional contributions).

Figure 5.3a shows a small but clear increase in the recovered lifetimes with the detection wavelength. This effect cannot be explained in terms of a simple three-rotamer model, in which each rotamer is represented by a fixed fluorescence lifetime. The observed changes in lifetimes could indicate that the rate of solvation of Tyr's phenol group following electronic excitation is comparable to the rate of fluorescence, thus lifetimes detected at longer  $\lambda$  are longer.

It is worth noting that the relative changes in these three lifetimes, i.e.

$$(\tau_i(324nm) - \tau_i(300nm))/\tau_i(300nm)$$

are 0.26, 0.80 and 1.91 ns for  $Y_1$ ,  $Y_2$  and  $Y_3$ , respectively. This suggests the relaxation times of the phenol groups in all three rotamers are long (nanoseconds instead of typical picoseconds) but are different for each rotamer due to their different local surroundings. Alternatively, the observed changes in fluorescence lifetimes can be caused by an actual more complex fluorescence kinetics than the three-exponential model considered in this analysis.

The time-domain results (figures 5.3a and 5.3b) were used with the steady-state emission spectrum of the sample to create the DAS,  $F_i(\lambda)$  (equation 3.19), representing the separate spectra of the three rotamers  $Y_1$ ,  $Y_2$  and  $Y_3$  (figure 5.3c). It can be observed that the individual spectra are almost identical indicating that all forms contribute a similar profile and intensity to the overall fluorescence. The relatively large differences in  $f_i$  values at short wavelengths, 300-305 nm, (see figure 5.3b) affect the DAS of  $Y_1$  and  $Y_2$  to a small extent. The fact that the DAS of the shorter-lived rotamer  $Y_3$  is slightly higher influenced can be rationalized by the possibility of scattered light affecting the measurements at such low wavelengths. Due to the virtual null lifetime of scattered light its effects are more noticeable in the shorter lifetime components of the decay.

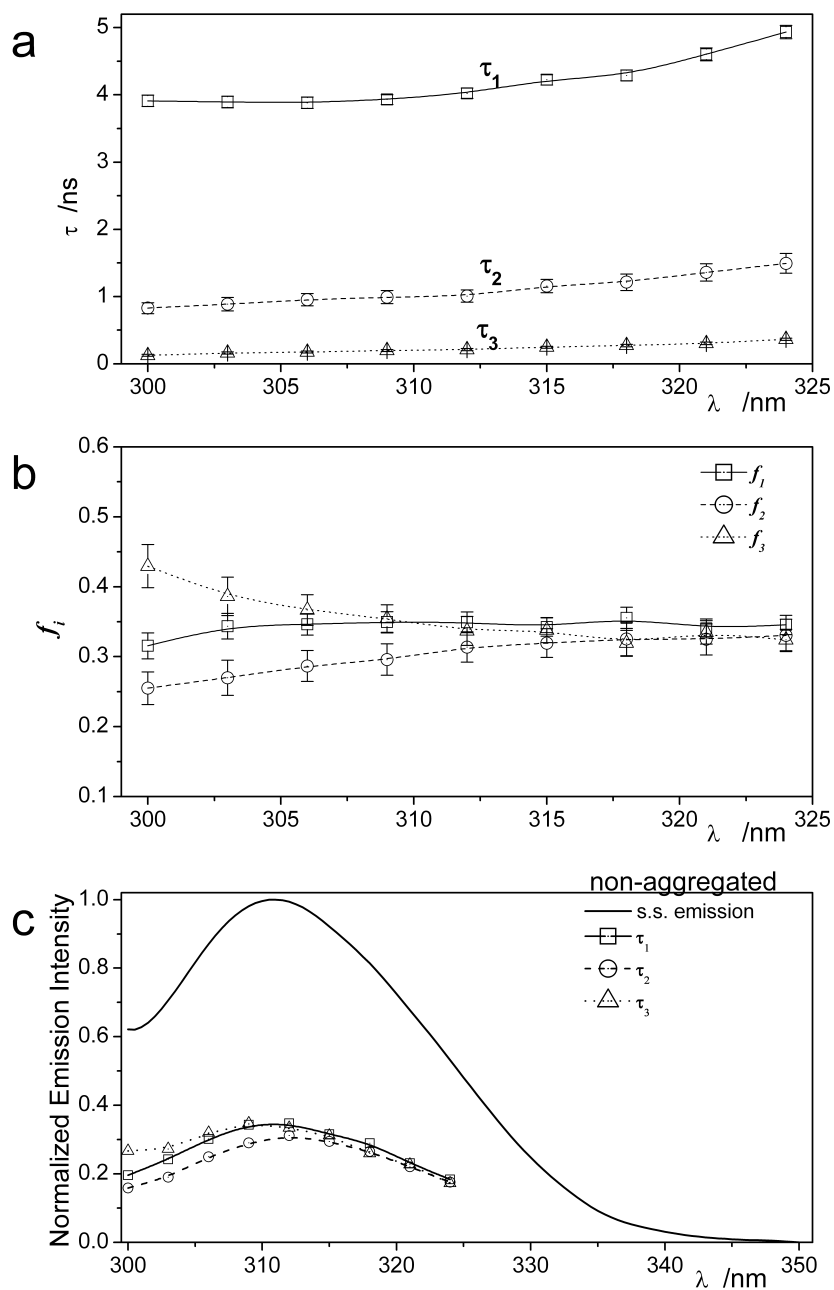


**Figure 5.3:** Parameters obtained from fitting Tyr decay in the LC sample to a three-exponential decay model. a) Tyr fluorescence decay times as a function of wavelength; b) fluorescence intensity fractional contributions; c) full line: emission spectra of A $\beta$ 's Tyr; dotted lines: Decay associated spectra for the three retrieved decay times. Experimental errors are 3 standard deviations.

If all rotamers exhibit the same quantum yields, the result in figure 5.3c would imply equal abundance of the three rotamers in the sample. However, due to substantially different lifetimes shown by the rotamers, different quantum yields seem to be more likely. Indeed, assuming that the rate of the radiative transition for Tyr is  $k_F = 1/\tau_o$  and the total rate of the non-radiative transitions (e.g. due to quenching mechanism) of the rotamer  $Y_i$  is  $k_{NRi}$ , the resulting lifetime  $\tau_i$  of the  $Y_i$  form is given by

$$\frac{1}{\tau_i} = \frac{1}{\tau_o} + k_{NRi} \quad (5.1)$$

and its quantum yield  $\eta_i$  is

$$\eta_i = \frac{k_F}{k_F + k_{NRi}} = \frac{\frac{1}{\tau_o}}{\frac{1}{\tau_o} + k_{NRi}} = \frac{\tau_i}{\tau_o} \quad (5.2)$$

As  $\tau_o$  is unknown, it is not possible to estimate the quantum yields of the rotamers, but their concentrations  $[Y_i]$  can be worked out. The total fluorescence emitted by the rotamer  $Y_i$ , namely  $\int F_i(\lambda)d\lambda$ , is proportional to the rotamer concentration  $[Y_i]$  and its quantum yield  $\eta_i$ . Thus

$$\int F_i(\lambda)d\lambda = \beta\eta_i[Y_i] \quad (5.3)$$

where  $\beta$  is the coefficient of proportionality. From equations 5.2 and 5.3 results

$$[Y_i] = \frac{\tau_o}{\beta} \frac{\int F_i(\lambda)d\lambda}{\tau_i} \quad (5.4)$$

As  $[Y] = \sum[Y_i]$ , it can be written that

$$[Y_i] = [Y] \frac{\tau_i^{-1} \int F_i(\lambda) d\lambda}{\sum_{j=1}^3 \tau_j^{-1} \int F_j(\lambda) d\lambda} \quad (5.5)$$

As the total concentration  $[Y]$  is known ( $5\mu\text{M}$ ), equation (5.5) can be used to estimate the concentrations of individual rotamers. For LC, they are  $0.22\mu\text{M}$  (4.45%),  $0.75\mu\text{M}$  (15.10%) and  $4.02\mu\text{M}$  (80.45%), for  $Y_1$ ,  $Y_2$ , and  $Y_3$ , respectively. The percentage contributions shown here represent the occurrence of Tyr rotamers in a solution of  $A\beta$  monomers.

### High concentration sample

The lifetimes and fractional contributions obtained for the high concentration sample HC of  $50\mu\text{M}$  are shown in figures 5.4a and 5.4b, respectively. The lifetimes show a very slow increase with experiment time while the changes in the fractional contributions are quite significant. Contrary to LC, all three  $f_i$  factors change with time which may indicate a new process, not observed in LC, likely the effect of the spontaneous aggregation of the  $A\beta$  peptides.

Note that the initial  $f_i$  values are very close to the result obtained for  $50\mu\text{M}$   $A\beta$  in the experiment performed to investigate the concentration effect (page 59) with dominating  $f_2$  contribution. As seen in figure 5.4b, for the later times  $f_2$  decrease is accompanied by increase of the  $f_1$  and  $f_3$  factors. This result is different from that observed for monomer solutions, leading to the proposition that it is too a signature of oligomerisation.

For HC the ratio  $f_1/f_2$  (figure 5.4c) increases by 100% during the first 15 hours. The initial quick change slows down gradually in the later stages. Such kinetics may reflect high "consumption" of monomers forming small oligomeric species at the beginning of aggregation. As oligomers get bigger and diffuse slower and monomers become sparser the initial rate of aggregation slows down. The rate of the process can be arbitrary characterised by fitting the  $f_1/f_2$  versus  $t_{exp}$  dependence to the exponential function

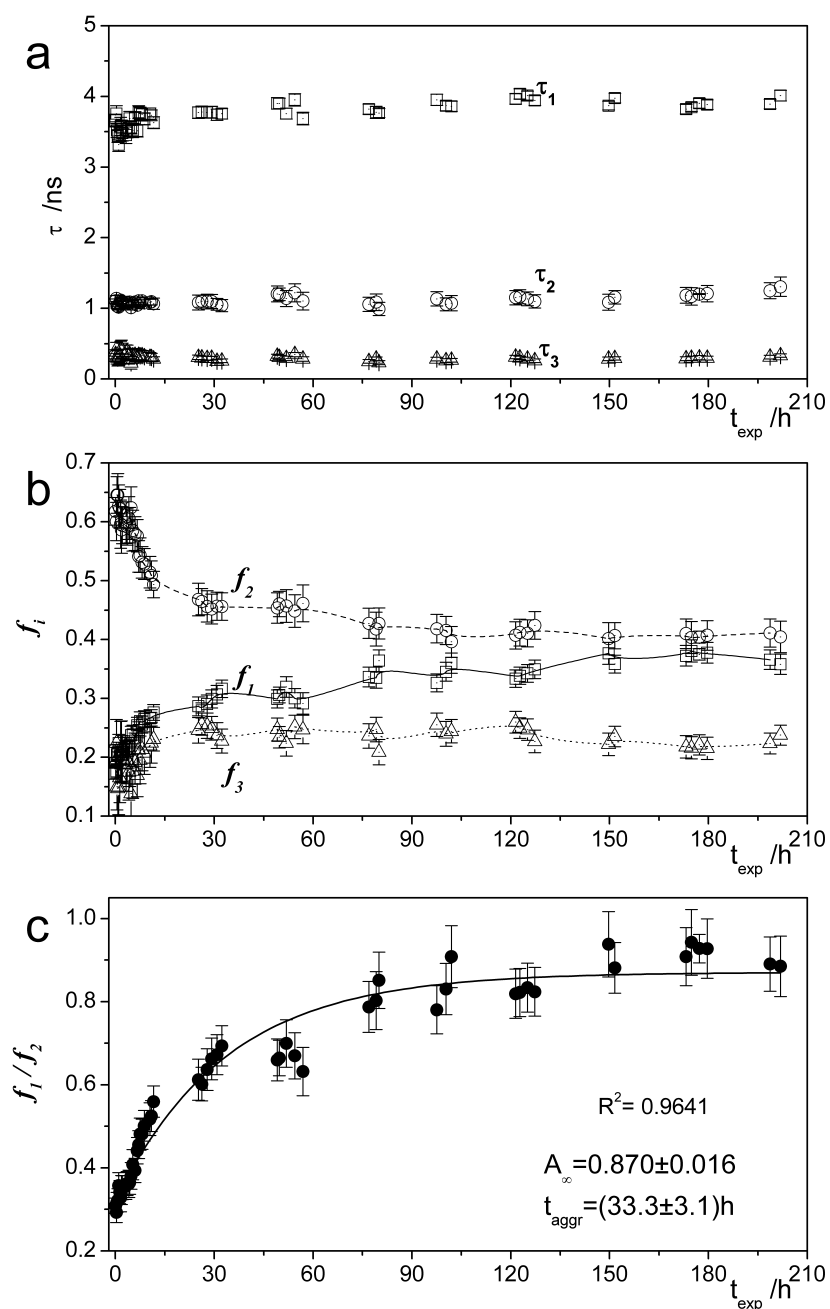


**Figure 5.4:** Parameters obtained from fitting Tyr decay in HC to a three-exponential decay model. a) Tyr fluorescence decay times ; b) fluorescence intensity fractional contributions; c) ratio between decay times fractional contributions  $f_1/f_2$ , data fitted according to equation 5.6. Experimental errors are 3 standard deviations.

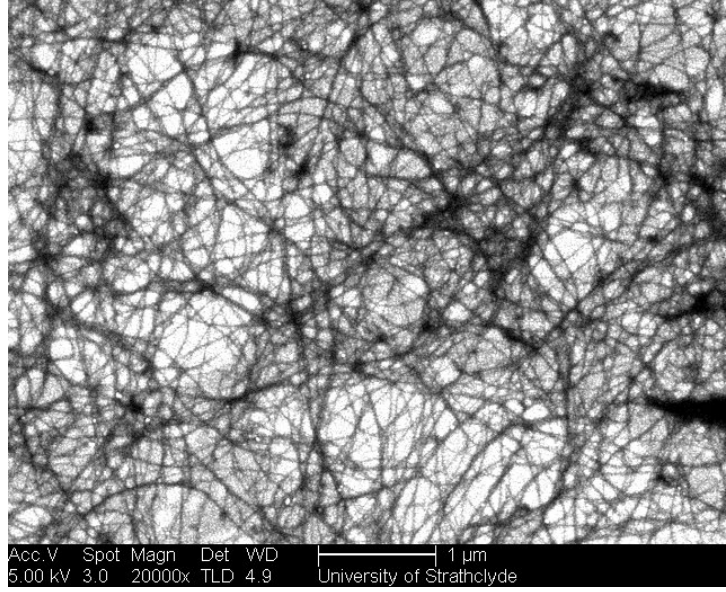


**Figure 5.5:** SEM image of sample HC (taken before lifetime measurements at different wavelengths were performed) confirming the existence of mature amyloid fibrils.

$$(f_1/f_2)(t_{exp}) = (A_0 - A_\infty)exp^{-t_{exp}/t_{aggr.}} + A_\infty \quad (5.6)$$

with  $A_0$  and  $A_\infty$  being technical parameters and  $t_{aggr.}$  a characteristic "aggregation time", which in this experiment achieved a value of  $(33.3 \pm 3.1)$  hours.

Fluorescence decays of HC were also measured at different emission wavelengths  $I(t, t_{exp} > 210h, \lambda)$ . As the retrieved fluorescence decay parameters for HC showed no further evolution for  $t_{exp} > 210$  h, it was regarded as a stable sample. Scanning electron microscope (SEM) images of the sample taken at this point in time, figure 5.5, confirm the existence of mature amyloid fibrils. Therefore, the sample was considered to be at equilibrium with  $A\beta$  aggregated into the final fibrillar structures. The fluorescence decays were again fitted to a three-exponential decay model and the retrieved parameters

are shown in figures 5.6a and 5.6b.

Figure 5.6a shows that the lifetimes increase substantially with an increase in the detection wavelength. This result could be explained, same as in the monomer, by the orientational relaxation of the phenol groups in the aggregated sample being slow and comparable to the fluorescence lifetimes. Again the relative changes in these three lifetimes, i.e.

$$(\tau_i(324nm) - \tau_i(300nm))/\tau_i(300nm)$$

are quite different for each rotamer, namely 0.64, 1.10 and 3.16 ns for  $Y_1$ ,  $Y_2$  and  $Y_3$ , respectively.

A comparison of the lifetime changes in the two presented samples (figures 5.3a and 5.6a) reveals that the effect is present in both, but is more pronounced in HC, the aggregated sample. Assuming validity of the three-exponential model of the kinetics, this effect suggests that the aggregation additionally slows down the relaxation of rotamers. This is consistent with the solvent present in the local environment of rotamers being removed and replaced by side chains of the adjacent, newly bound, peptide. Such replacement results in higher steric hindrance to the orientational relaxation of the rotamers and, therefore, the excited rotamers can remain as such for longer periods of time before eventually decaying to the more stable ground state.

The retrieved data were used to create the DAS shown in figure 5.6c. In the aggregated peptide the rotamer with the smallest lifetime,  $Y_3$ , is quenched as compared to the other two forms and appears to be red shifted in comparison with the non-aggregated sample. Also  $Y_2$ , the medium lifetime rotamer, shows a slight red-shifted emission ( $\approx 1nm$ ).

Using equation 5.5 for the HC data allows estimation of concentrations of the individual rotamers. Taking the total HC sample concentration of  $50\mu M$ ,  $Y_1$ ,  $Y_2$  and  $Y_3$  have the values  $3.62\mu M$  (7.25%),  $15.98\mu M$  (31.96%), and  $33.39\mu M$  (60.79%), respectively. Comparing these percentage contributions with the percentages obtained for LC, shows that the peptide aggregation is an additional factor, together with the bulk peptide concentration, which affects the selection of a rotameric form by individual Tyr.

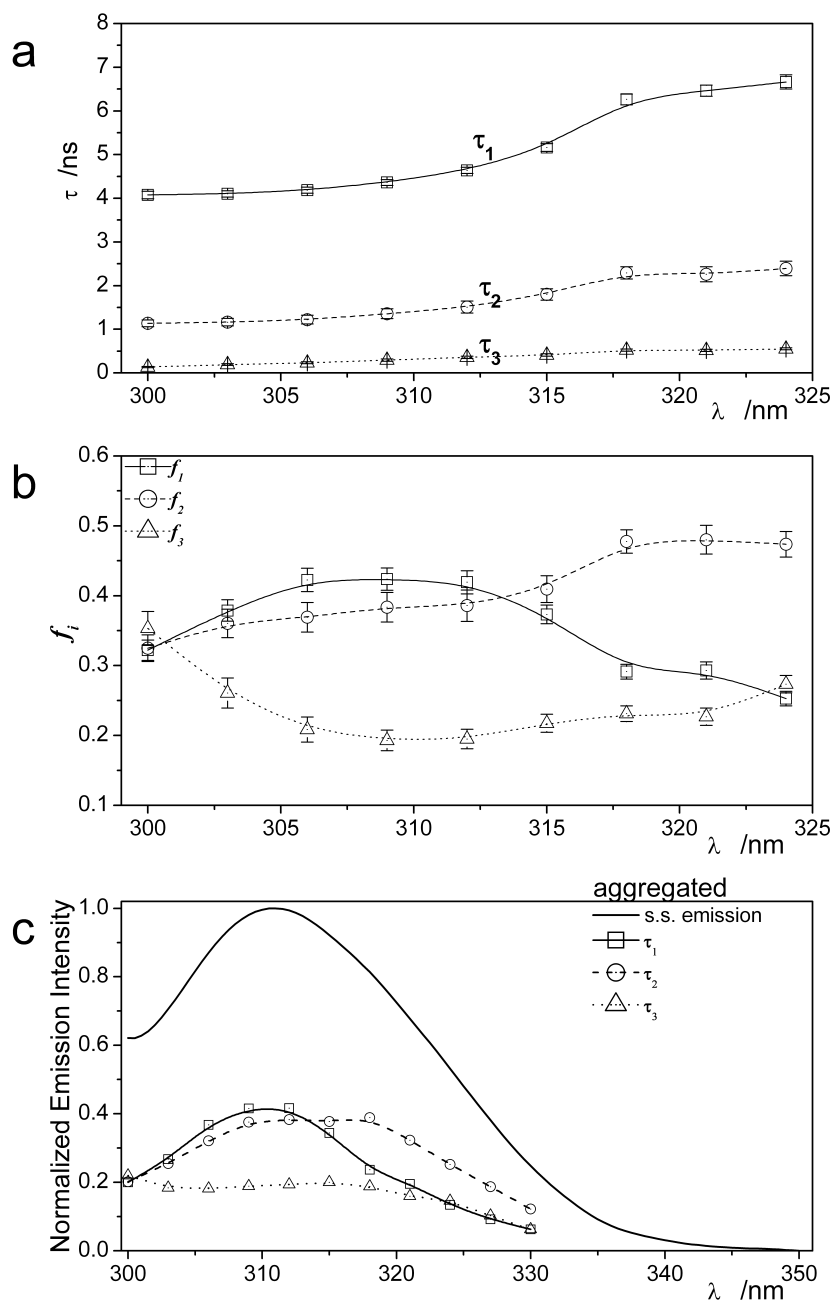


**Figure 5.6:** Parameters obtained from fitting Tyr decay in the HC sample to a three-exponential decay model. a) Tyr fluorescence decay times versus wavelength ; b) fluorescence intensity fractional contributions; c) full line: emission spectra of A $\beta$ 's Tyr; dotted lines: Decay associated spectra for the three retrieved decay times. Experimental errors are 3 standard deviations.

	rotamer	$\lambda_{max}$ (nm)	$\tau$ (ns) @300nm	$[Y_i]$ (%)
A $\beta$ monomers	Y <sub>1</sub>	311	3.9	4.45
	Y <sub>2</sub>	312	0.8	15.10
	Y <sub>3</sub>	310	0.1	80.45
A $\beta$ aggregates	Y <sub>1</sub>	310	4.1	7.25
	Y <sub>2</sub>	313	1.1	31.96
	Y <sub>3</sub>	314	0.1	60.79

**Table 5.1:** Peak positions of fluorescence spectra, fluorescence lifetimes and relative concentrations of Tyr rotamers in monomer solution and fully aggregated A $\beta$  solutions.

## 5.4 Conclusions

The finding that intrinsic fluorescence of Tyr in A $\beta$  peptide can be useful for monitoring very early stages of single A $\beta$  peptide-to-peptide aggregation reported in Chapter 3 has been further confirmed and extended. The presented results could be of fundamental importance in the research on the mechanisms of neurodegenerative diseases, because no other experimental technique enables detection of binding of single peptides non-invasively.

Using this sensing approach it was demonstrated, that the initial peptide concentration influences what rotameric conformations are taken by individual peptides (figure 5.1c), and determines the rate of their aggregation (figures 5.2c and 5.4c). At low A $\beta$  concentrations (5 $\mu$ M), the aggregation is negligible, while at higher concentrations (50 $\mu$ M) the rate of aggregation can be described by an exponential change in the  $f_1/f_2$  ratio as a function of time. In the particular conditions of such sample the characteristic aggregation time was of  $\approx$  33 hours.

A three-rotamer model can be effectively used to interpret main fluorescence properties of both the monomer solution and the fully aggregated A $\beta$  peptides. The rotamers parameters estimated from the steady-state and lifetime data are collected in table 5.1. A comparison between the numbers characterising monomers and aggregated forms shows that the parameters most sensitive to aggregation are relative concentrations of individual ro-

tamers. Therefore fitting the  $A\beta$  lifetime data to a three-exponential model and estimating the relative concentrations of rotamers can be helpful in assessing the state of aggregation.

On the other hand, the gradual increase in lifetimes with emission wavelength observed for the both monomer and aggregated samples indicates that the actual  $A\beta$  excited-state kinetics is complex and a more advanced modeling of Tyr photophysics can help to reveal in full the information on  $A\beta$  aggregation offered by intrinsic fluorescence.

# Chapter 6

## Discrete and continuous lifetime analysis of Tyrosine fluorescence decay during $A\beta_{40}$ and $A\beta_{42}$ oligomerisation

### 6.1 Introduction

In this chapter is investigated the aggregation of  $A\beta_{40}$  and  $A\beta_{42}$  peptides using Tyr fluorescence decay as a sensor to compare the early stages of oligomer formation of the different peptides. The decays are analysed using two different approaches: first using discrete lifetimes through the NLLS method, as in the previous chapters, fitting the decays to a three-exponential model; second, using the MEM to recover lifetime distributions without any *a priori* assumptions regarding the decay kinetics and its components.

MEM allows to ascertain how realistically the exponential model describes Tyr photophysics in  $A\beta$  during aggregation and reveals more information on the peptides behaviour. Because of the variety of the potential factors determining Tyr fluorescence it is possible that its emission decay does not have in fact a discrete exponential character. In such case, the continuous

lifetime distributions would better represent the observed fluorescent decays.

For obtaining a more comprehensive view, the molecular dynamics (MD) simulations of the  $A\beta_{40}$  and  $A\beta_{42}$  peptides aggregation are also presented. In a collaboration with Dr. Karina Kubiak-Ossowska (Department of Chemical and Process Engineering, University of Strathclyde). MD simulations were performed in the explicit water. The simulations give theoretical insights into peptide dynamics in water environment, the conformational adjustments, the aggregation process and the structure and stability of the oligomers. The analysis of both Tyr fluorescence data and MD simulations shows a link between the observed photophysics of Tyr and the conformations of  $A\beta$  peptides during the aggregation process. The MD simulations support the lifetime data here presented and therefore the relevant results are briefly included in this chapter.

## 6.2 Methodology

Amyloid samples were prepared according to the methodology presented in Chapter 5 (page 55). To monitor the influence of the peptide aggregation on Tyr fluorescence decay, the measurements were performed collecting 315nm emission at increasing times  $t_{exp}$  after sample preparation using the TCSPC technique on the IBH Fluorocube system as previously described in Chapter 3 (page 30).

## 6.3 Results and Discussion

### 6.3.1 Three-exponential model

It was demonstrated in the previous chapter that the changes in Tyr lifetime data observed at different times after sample preparation support the hypothesis that conformational changes in the  $A\beta_{40}$  peptides occur due to their spontaneous aggregation. The lifetimes and fractional contributions

presented in Chapter 5 for the HC sample of  $50\mu\text{M}$   $\text{A}\beta_{40}$  (Figures 5.4a and 5.4b, page 66) will be used in this chapter for comparison with  $\text{A}\beta_{42}$  aggregation process.

In summary, Tyr decay in  $\text{A}\beta_{40}$  displays the following characteristics: lifetimes display a small increase with the experiment time  $t_{exp}$  while changes in the fractional contributions are significant,  $f_2$  decreases accompanied by an increase in  $f_1$  and  $f_3$ . The results suggest that when the aggregation progresses, the preferences of Tyr to stay in a particular rotameric form evolve in such a way that the population of the rotamer  $Y_2$  decreases in favour of the rotamers  $Y_1$  and  $Y_3$ . The  $f_1/f_2$  ratio, used as an indicator of aggregation, was fitted according to equation (5.6) revealing a characteristic "aggregation time"  $t_{aggr.}$  of  $(33.3 \pm 3.1)\text{h}$ .

The  $\text{A}\beta_{42}$  peptide differs from  $\text{A}\beta_{40}$  only at the C-terminus where two additional apolar amino acids (isoleucine and alanine) are present at the end of the sequence. The hydrophobic C-terminal sequence seems to play a determinant role in the spontaneous aggregation of the peptides and it has been shown [29–31] that  $\text{A}\beta_{42}$  peptides aggregate into amyloid fibrils more rapidly than  $\text{A}\beta_{40}$ .

The parameters obtained for the three-exponential model NLLS analysis of Tyr's decay in  $\text{A}\beta_{42}$  are presented in figure 6.1. The data is superimposed with the parameters retrieved for the  $\text{A}\beta_{40}$  experiment for an easier comparison, except for the case of the factorial contributions (figure 6.1b), where the vast amounts of data would become confusing.

It is clear that all lifetimes (figure 6.1a) obtained for the  $\text{A}\beta_{42}$  are higher than the lifetimes retrieved for the  $\text{A}\beta_{40}$ . This may suggest a slightly different microenvironment surrounding Tyr in the two peptides, effect that could be caused by the increased hydrophobicity of the C-terminal sequence in the  $\text{A}\beta_{42}$ . The difference in hydrophobicity could result in a different peptide conformation for the two peptides, and in  $\text{A}\beta_{42}$  Tyr might be more effectively shielded from interactions with solvent molecules.

The factorial contributions (figure 6.1b) of the decay lifetimes for  $\text{A}\beta_{42}$

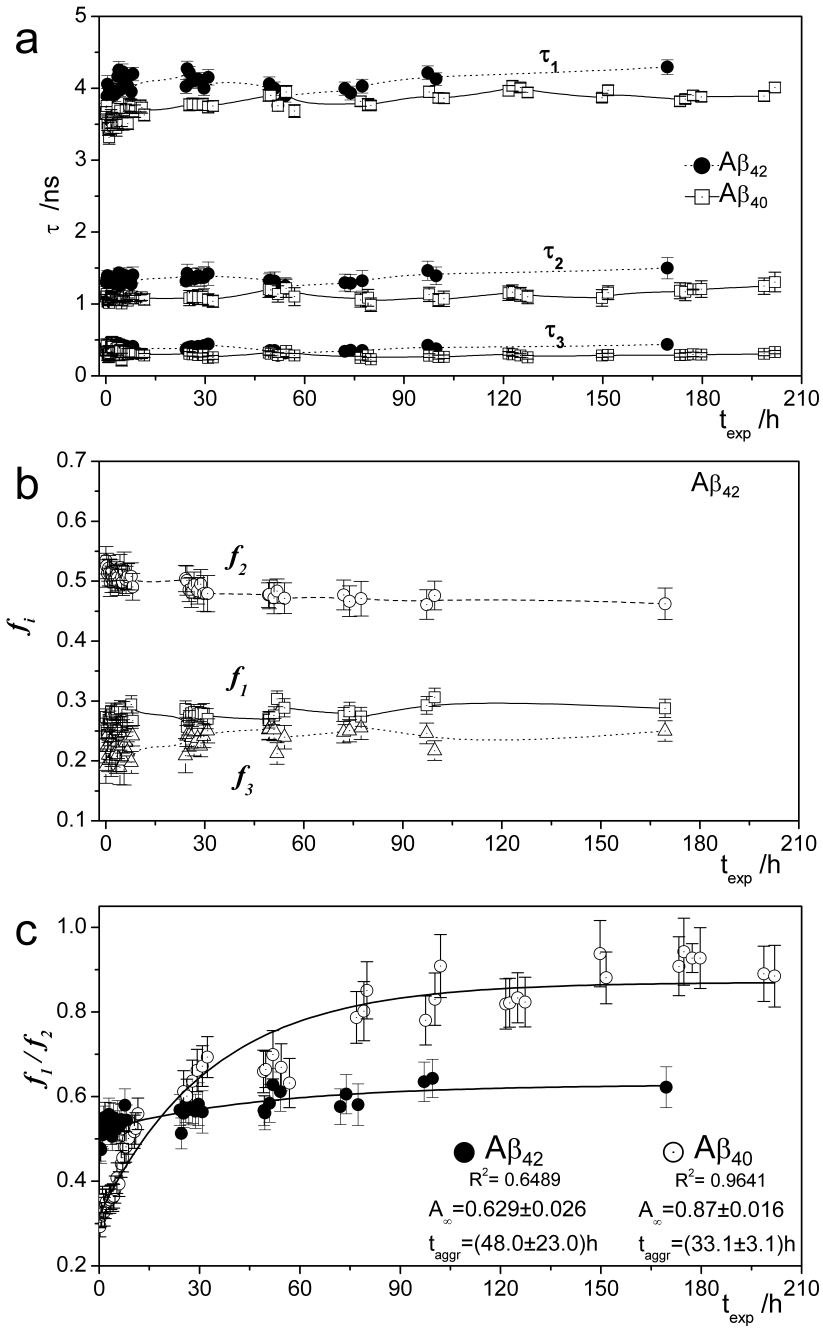


**Figure 6.1:** Parameters obtained from fitting Tyr decay to a three-exponential decay model. a) fluorescence decay times; b) fluorescence intensity fractional contributions; c)  $f_1/f_2$  ratio, data fitted according to equation (5.6). Experimental errors are 3 standard deviations.

display substantially smaller changes in the first 30 hours of experiment, when compared to the case of  $A\beta_{40}$ . The effect is more clearly seen through the  $f_1/f_2$  ratio presented in figure 6.1c. Assuming that the changes in lifetimes exhibited by Tyr during aggregation are a measure of the stage of aggregation, then the potential explanation of this difference could be the rate of oligomerisation for  $A\beta_{42}$  being much faster than for  $A\beta_{40}$ . In such hypothesis, the initial quick change in the fluorescence decay would be too fast to be efficiently detected for  $A\beta_{42}$  within the timescale of the traditional lifetime experiments. The ratio values increase only slightly to then stabilise in a profile that resembles the final stages of  $A\beta_{40}$  kinetics. This may indeed suggest that most of the peptide had oligomerised rapidly after preparation of the monomeric solution. Fitting the ratio parameter for  $A\beta_{42}$  with equation (5.6), as done for  $A\beta_{40}$ , does not produce a good fit due to the lack of the initial rise, and paradoxically shows a longer characteristic aggregation time.

It should be observed, though, that Tyr fluorescence is primarily determined by its local environment and therefore the lifetimes and contributions of rotamers are only an indirect indication of the stages of aggregation. It was mentioned above that the increased lifetime values of Tyr in  $A\beta_{42}$  could be a result of reduced solvent access. If that is the case then the environment sensed by Tyr in both peptides would be different and the discrepancy between the initial values of the lifetime component contributions  $f_i$  could be a result of such environmental divergence. In this case, the lower values obtained for  $A\beta_{42}$   $f_1/f_2$  could be a result, not of faster oligomerisation, but of reduced solvent access to Tyr in the  $A\beta_{42}$  monomers. The solvent shielding effect of aggregation would then be smaller and the change in Tyr surrounding microenvironment therefore less significant. This would result in a much smaller influence in Tyr decay throughout the aggregation resulting in less significant changes in  $f_1/f_2$ . Opposed to such situation, in  $A\beta_{40}$  Tyr has a higher initial exposure to solvent and the formation of oligomers and consequent reduced solvent exposure of Tyr has a more dramatic effect. This

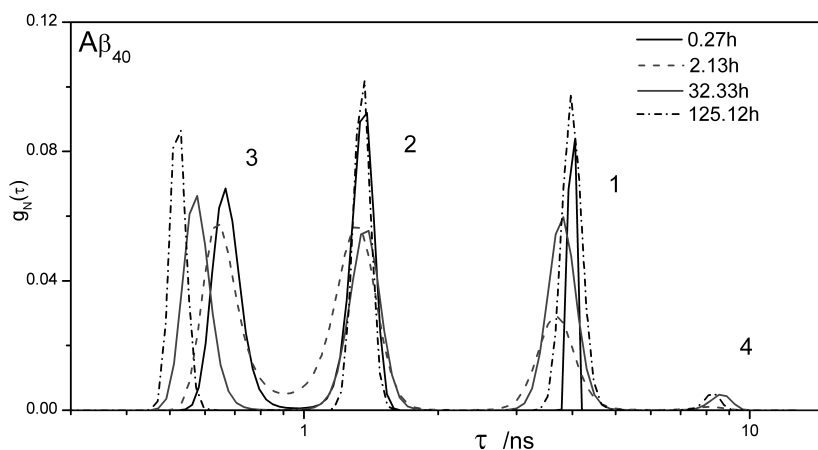


**Figure 6.2:** Representative normalized lifetime distributions  $g_N(\tau)$  obtained with MEM for  $A\beta_{40}$

alternative explanation implies that Tyr in  $A\beta_{42}$  is not as good a sensor of oligomerisation as in the  $A\beta_{40}$  peptide, precisely because it is more protected from solvent interactions.

### 6.3.2 Model-free lifetime distributions

As up to this point, the exponential model still adequately fits to the experimental data as proven by both goodness-of-fit criteria, the  $\chi_r^2$  and the distribution of residuals. However, the findings presented in the previous chapter indicated that the three-exponential model might be too simplistic to represent the true nature of Tyr decay in the  $A\beta_{40}$  peptide. The MEM is able of analysing decays that are intrinsically complex and can not be reduced to multi-exponential model decay functions, and thus provides a more realistic description of fluorescence decay kinetics. In this section the MEM analysis of Tyr decay, in both  $A\beta_{40}$  and  $A\beta_{42}$  peptides, is presented.

In figure 6.2 are shown four representative lifetime distribution obtained with MEM for the  $A\beta_{40}$  peptide during its aggregation process. It can be seen that, in fact, the distributions do not display three but four peaks meaning that Tyr decay has not three but four components. The relatively small

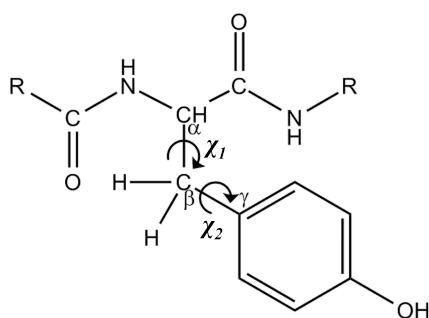


**Figure 6.3:** Structure of tyrosine residue showing the possible rotations around  $C_\alpha - C_\beta$  ( $\chi_1$ ) and  $C_\beta - C_\gamma$  ( $\chi_2$ ) chemical bonds.

contribution of the "new" fourth lifetime component explains why the three-exponential model yields statistically acceptable results.

The rotational freedom of Tyr around the  $C_\alpha - C_\beta$  and  $C_\beta - C_\gamma$  chemical bonds (figure 6.3) creates a surface landscape of potential energy  $V(\chi_1, \chi_2)$  with potential wells that define the conformations of the Tyr molecule and therefore gives rise to its rotamers. The common rotamer model referenced previously only takes into account the rotations around  $\chi_1$  and that might be the cause that reduces the existence of Tyr to three rotameric forms. The four decay components found with MEM analysis clearly suggest the existence of four well defined minima in the  $V(\chi_1, \chi_2)$  landscape and therefore of four rotameric forms of Tyr in the  $A\beta_{40}$  peptide.

The peaks lifetime and contributions to the overall fluorescence decay obtained through MEM are presented in figure 6.4a and figure 6.4b, respectively, as functions of experiment time  $t_{exp}$ . The peak lifetimes are stable through the aggregation of the peptide, with the exception of a couple of data points in the case of the longest lifetime  $\tau_4$  (whose relevant Tyr rotamer will be hereinafter referred as  $Y_4$ ). Such exceptions are probably a consequence of noise in the data overpowering the weak contribution of the  $Y_4$  rotamer to the overall fluorescence. In the initial lifetime distribution only three peaks compose the output, the fourth component contribution might be non-existent or purely too weak for MEM to consider it as a feature of the

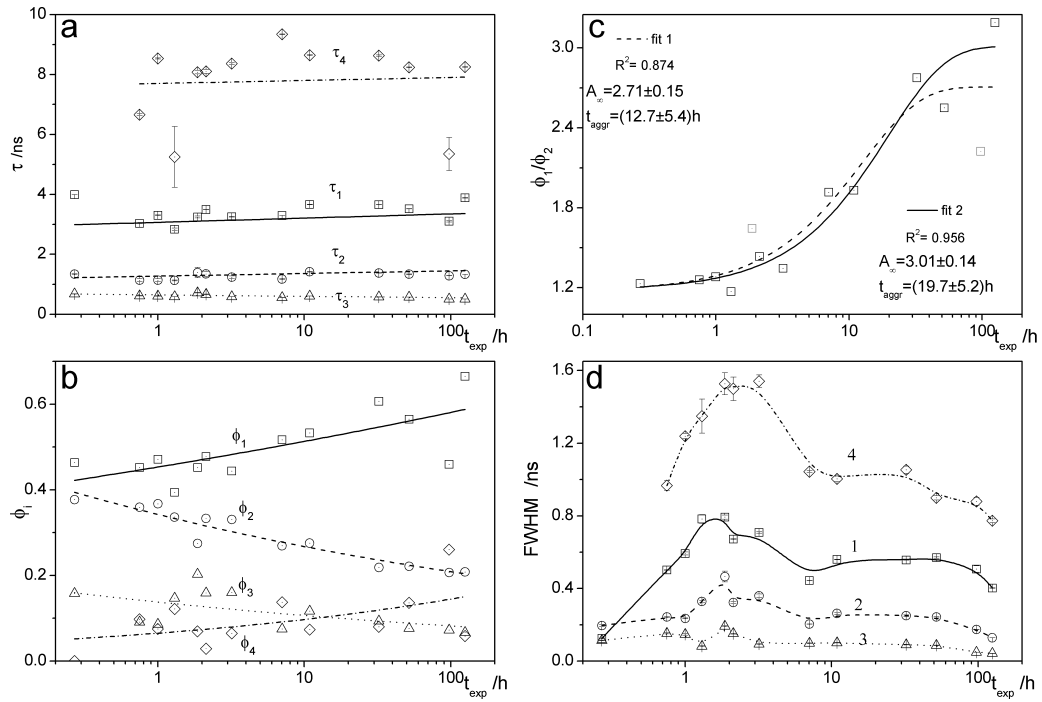


**Figure 6.4:** Parameters from Tyr lifetime distributions for  $A\beta_{40}$  plotted in a logarithmic scale. a) peak fluorescence decay times; b) fluorescence intensity fractional contributions  $\phi_i$ ; c) ratio between  $\phi_1$  and  $\phi_2$ , data fitted according to equation (5.6); d) Full width at half maximum. Error bars equal 3 standard deviations.

decay kinetics. Either way the best representation of the decay is therefore the simpler construction of three decay components.

As in the NLLS, the contributions of each rotamer to the overall fluorescence decay,  $\phi_i$ , change with sample aging, i.e., with the oligomer formation. The contributions of  $\phi_1$  ( $Y_1, \approx 3.4$  ns) and  $\phi_2$  ( $Y_2, \approx 1.3$  ns) still seem to be the most sensitive to aggregation while the contributions  $\phi_3$  and  $\phi_4$  show only small changes. The lines in figure 6.4b are meant as a guideline for the eye.

In analogy to the analysis done to the NLLS data, one can take the ratio between the contributions of peaks 1 and 2 ( $\phi_1/\phi_2$ ) as an indicator of aggregation. This is shown in figure 6.4c, note the logarithmic time scales. Fitting the data to equation (5.6) as done for the NLLS results, produces a statistically unacceptable fit (fit 1) due to the outlier data points. Fitting the ratio after removal of the two outlier data points (fit 2) yields an acceptable fit that reveals a characteristic aggregation time of  $(19.7 \pm 5.2)$ h, a much smaller value than the  $(33.3 \pm 3.1)$ h obtained from the NLLS analysis based on the three-exponential model. The discrepancy comes probably from the three-exponential model being only a simplification of the actual Tyr decay kinetics.

The full width at half maximum (FWHM) values of the four peaks recovered for Tyr decay in of  $A\beta_{40}$  are plotted in figure 6.4d as functions of experiment time  $t_{exp}$ . The characteristics of the the FWHM provide unique information on the aggregation process. The value of FWHM for each rotamer is a characteristic feature related to the profile of the potential well that restrains said rotamer. Wider potential wells allow higher freedom and thus a larger distributions of possible lifetimes can be expected resulting in bigger FWHM for the relevant peak.

The non-monotonic changes in the FWHM may be caused by a complex aggregation process. The characteristic lifetime, and its FWHM, of a given Tyr rotamer might depend on whether it is a part of the  $A\beta$  monomer, dimer, trimer, etc., and the initial increase in the FWHM of each rotamer

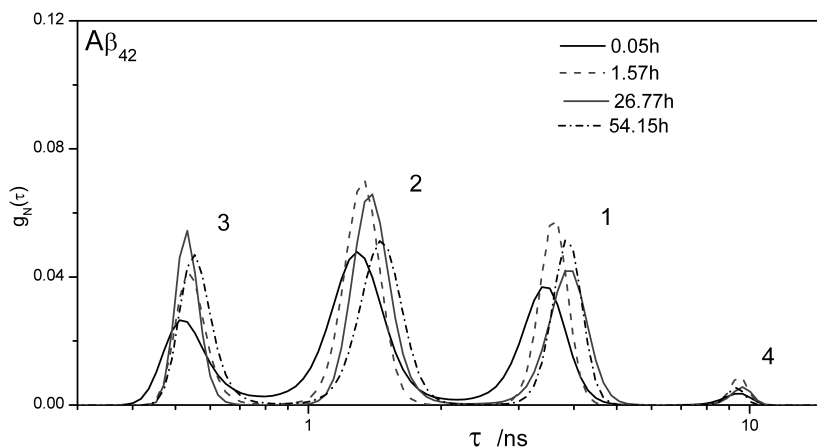


**Figure 6.5:** Representative normalized lifetime distributions  $g_N(\tau)$  obtained with MEM for  $A\beta_{42}$

lifetime distribution peak could be caused by increasing variety of  $A\beta_{40}$  structures. At the later stages of aggregation, the structures are becoming not only bigger and more rigid, but also more homogeneous and therefore the variety of different species in which one particular rotamer exists becomes smaller and with it the FWHM of the relevant lifetime distribution becomes narrower.

Representative lifetime distributions for the  $A\beta_{42}$  sample at different times after its preparation can be seen in figure 6.5. The peak lifetimes (figure 6.6a) are similar to those found for  $A\beta_{40}$  to the exception of the fourth lifetime peak  $Y_4$  whose value is approximately 1 ns higher. The higher lifetime of  $Y_4$  is likely to cause the fact that the lifetimes retrieved from the NNLS fit of  $A\beta_{42}$  are longer than those of  $A\beta_{40}$  (figure 6.1a). In the attempt of fitting the decay to the more reductive three-exponential model the NLLS method spreads the influence of  $Y_4$  across all three exponential components, in different proportions. The fact that all Tyr lifetimes found through the NLLS analysis are higher for  $A\beta_{42}$  than the lifetimes obtained with the same method for  $A\beta_{40}$  can thus be explained.

The higher value for  $Y_4$  in  $A\beta_{42}$  might, nonetheless, still be a consequence

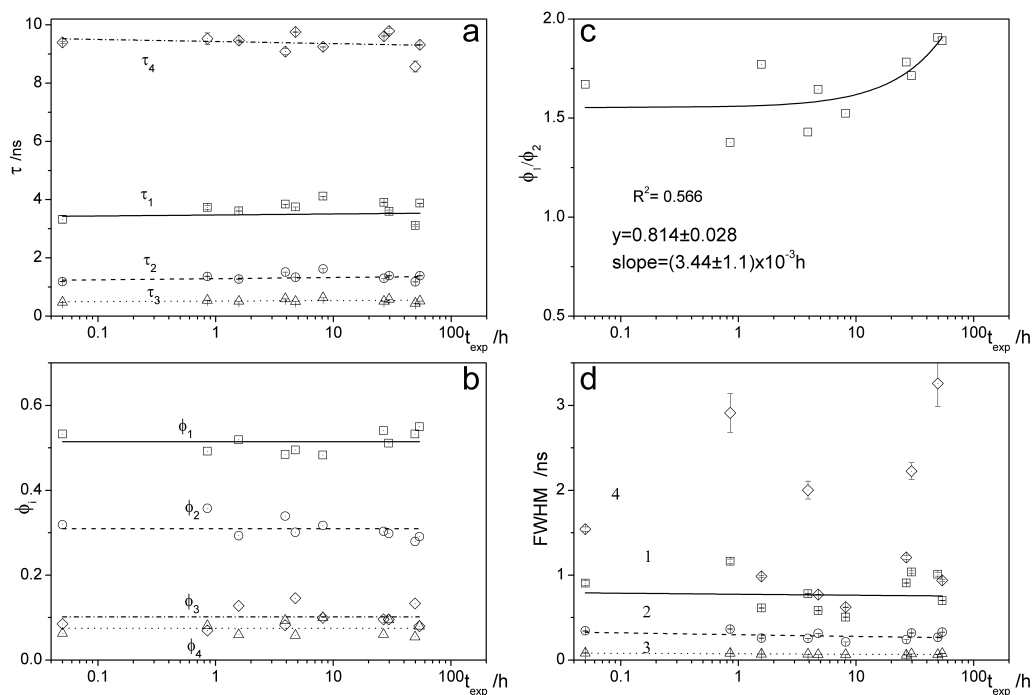


**Figure 6.6:** Parameters from Tyr lifetime distributions for  $A\beta_{42}$  plotted in a logarithmic scale. a) peak fluorescence decay times; b) fluorescence intensity fractional contributions  $\phi_i$ ; c) ratio between  $\phi_1$  and  $\phi_2$ , data fitted according to a linear regression; d) Full width at half maximum. Error bars equal 3 standard deviations.

of solvent protection but not all rotamers are better shielded from the solvent in this peptide, as NLLS lead to believe.

In figure 6.6b can be seen the  $\phi_i$  contributions of each peak. The data does not display dramatic changes as found for  $A\beta_{40}$ , there only appears to be a very slight increase in  $\phi_1$  and drop in  $\phi_2$ . The small variance of the  $\tau_i$  and  $\phi_i$  parameters throughout sample aging supports either of the hypothesis raised by the NLLS analysis: the formation of small oligomers cannot be observed due to the fast rate of  $A\beta_{42}$ 's oligomerisation; or Tyr surrounding microenvironment does not change significantly enough during oligomerisation to result in a substantial change its fluorescence response, because it is more protected or buried in the  $A\beta_{42}$  peptides 3 dimensional structure.

Whichever might be true, the common feature in both analysis is that Tyr fluorescence in  $A\beta_{42}$  seems to be less sensitive to the intermolecular phenomenon of aggregation. As a consequence the  $\phi_1/\phi_2$  ratio (figure 6.6c) varies only slightly over the entire experiment time. Fitting the data to a linear regression yields a slope of  $(3.44 \pm 1.07) \times 10^{-3}$  h, which demonstrates the small magnitude of the variation.

In part d of figure 6.6 are shown the FWHM of the four peaks. The values for peaks 1, 2 and 3 also do not show significant trends suggesting yet again a stable system. Regarding peak 4 there is a big scattering of the data and no obvious conclusion can be drawn.

## Discussion on NLLS and MEM

The results obtained with MEM show relatively sharp peaks revealing that fluorescence of Tyr in  $A\beta$  has a reasonable exponential character. This indicates that Tyr must be rather constricted in all its rotameric forms. Such behaviour indicates the existence of distinct and well defined potential wells in the  $V(\chi_1, \chi_2)$  landscape.

Although fitting the decay throughout aggregation with a NLLS fit to a three-exponential model results in good fit criteria, it does not represent the

true nature of Tyr decay. MEM revealed that the three-exponential model was found to be a good representation of Tyr decay in the beginning of the aggregation process, i.e., after sample preparation (figure 6.4), however, when oligomers start becoming dominant the bulk Tyr response changes. Nonetheless, fitting it to a discrete three-exponential model still yields fits with good  $\chi_r^2$  and residuals. Although the three-exponential model might no more realistically describe the photophysical behaviour of Tyr it is still valid as a sensing tool to describe the process of oligomer formation. Fitting the data throughout the whole aggregation experiment with a three-exponential model proves to be a simple, quick and useful way to obtain kinetic information about the oligomerisation process and compare it between different systems, as was attempted in this chapter with the different varieties of A $\beta$ .

The information obtained through MEM lifetime distributions and NLLS discrete lifetimes both point in the same direction. For the A $\beta_{40}$  solution both methods reveal that the system changes according to an exponential growth function. The rates obtained through both methods are different with MEM revealing that the process might be faster than the NLLS data suggests. As MEM is believed to depict more realistically Tyr photophysics and the NLLS fit to the three-exponential model to be a more reductive simplification, the oligomerisation rate of  $(19.7 \pm 5.2)$ h retrieved from MEM should be itself the more accurate result.

It had been reported previously that A $\beta_{42}$  peptide fibrillation occurs faster than the fibril formation of the A $\beta_{40}$  variant. The data presented here suggests that this trend might also present in the early stages of aggregation. The comparison between the  $f_1/f_2$  ratios (figure 6.1c) seems to indicate that the oligomerisation also occurs at a faster rate for the A $\beta_{42}$  peptide.

NLLS and MEM analysis methods equally demonstrate there is small variance in the A $\beta_{42}$  Tyr decays during the peptide's aggregation. Such effect might be caused by the process of oligomerisation occurring too fast to be effectively detected, as suggested above, or on the other hand that

$A\beta_{42}$ 's Tyr fluorescence response to oligomerisation is too weak to reveal useful information. The former could be caused by Tyr in  $A\beta_{42}$  being more buried in the peptide's structure and the changes in its microenvironment due to the intermolecular process of aggregation between peptides are not being substantial enough to create a discernible effect in its decay photophysics. Both hypothesis cannot be totally discarded.

### 6.3.3 Molecular dynamic simulations

To allow further interpretation of the fluorescence lifetime data and find their relationship with the performance of aggregation, 100 ns long molecular trajectories were obtained for  $9A\beta_{40}$  and  $9A\beta_{42}$  systems in MD simulations.

After the 100 ns of simulation the  $A\beta_{40}$  molecular system was composed of one oligomer made of eight peptides and one monomer (figure 6.7), and the  $A\beta_{42}$  system contained one oligomer composed of seven peptides and two peptides in the monomeric form (figure 6.8). From the figures it can be seen that the  $A\beta_{42}$  oligomer is very tightly bonded and twisted and does not form a relatively linear structure as the  $A\beta_{40}$ .

Comparison between the two systems reveals that the structural changes depend on the peptide length. The C-terminal  $\alpha$ -helix of the more hydrophobic  $A\beta_{42}$  peptide unfolds more than in the case of less hydrophobic  $A\beta_{40}$  peptide. For  $A\beta_{42}$  the range of conformational changes seems to depend on the oligomerisation state, monomeric peptides are unfolded slightly less than the oligomerised ones meaning that the C-terminal  $\alpha$ -helix is maintained better in the monomers than oligomers. This might indicate that the C-terminal hydrophobic  $\alpha$ -helix serves as an oligomerisation seed. Due to the lack of this part of the sequence it can be speculated that the  $A\beta_{40}$  oligomer will be bound more weakly than the  $A\beta_{42}$  one, and indeed such a difference is observed in the simulations.

Examination of the final structure and the interactions within the oligomer suggests that the more hydrophobic  $A\beta_{42}$  peptide creates a more tightly

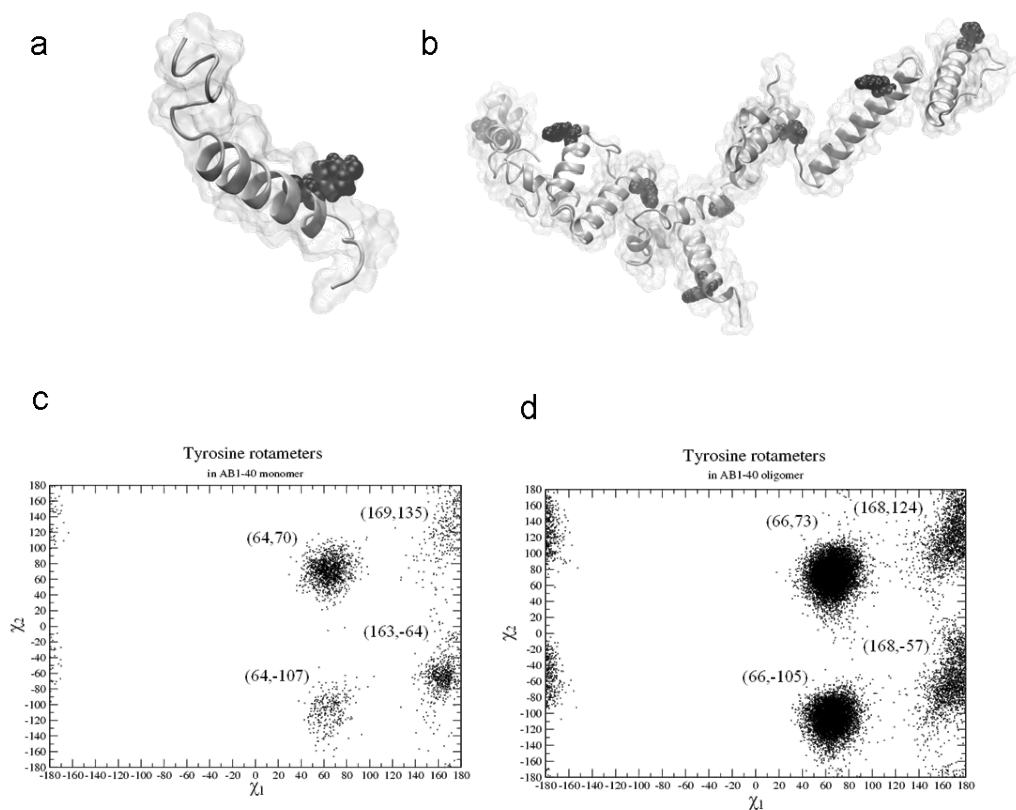


**Figure 6.7:** Final structures in the  $9A\beta_{40}$  system: a) monomer, b) oligomer. The Tyr residue is indicated as a VdW sphere, the peptide secondary structure is shown as a cartoon and its surface as a ghost surface. Plot of  $\chi_1$  versus  $\chi_2$  angles of Tyr showing the rotamers observed: c) in the monomer, d) in the oligomer. The average values of angles calculated after removing the most outlying points are indicated in parenthesis.

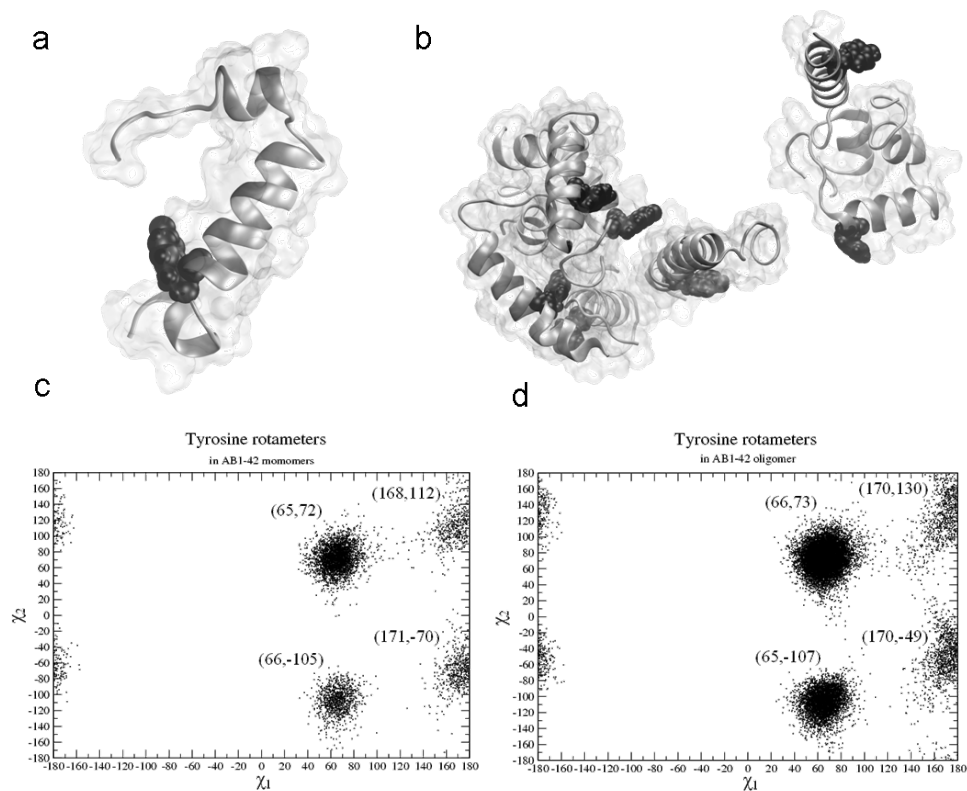


**Figure 6.8:** Final structures in the 9Aβ<sub>42</sub> system: a) monomer, b) oligomer. The Tyr residue is indicated as a VdW sphere, the peptide secondary structure is shown as a cartoon and its surface as a ghost surface. Plot of  $\chi_1$  versus  $\chi_2$  angles of Tyr showing the rotamers observed: c) in the monomer, d) in the oligomer. The average values of angles calculated after removing the most outlying points are indicated in parenthesis.

bonded and more stable oligomer than the shorter and less hydrophobic  $A\beta_{40}$  peptide. In both oligomers the most involved region in the peptide-peptide interactions is the C-terminal  $\alpha$ -helix with residues from 28 to 40(42). This agrees with the idea of hydrophobic driven oligomerisation with strong trend to bury the C-terminal part of the sequence that strongly unfolds in the polar environment and serves as a oligomerisation seed. The hydrophobic interactions have been shown to be important in the stability of  $A\beta$  peptide protofilaments [94] and aggregates [95] as well as for the peptide adsorption on various surfaces [96–98]. The structural changes dependence with the oligomerisation state here observed were found in a relatively small population. To make general conclusions further simulations are required.

It is worth to mention that independently on the system the Tyr residues are usually accessible to the solvent. While Tyr is not directly involved in the peptide-peptide interactions within the oligomer it can be partially buried at its interface. In figures 6.7 and 6.8 are shown the plots of  $\chi_1$  versus  $\chi_2$  angles for the Tyr residue in monomer (c) and oligomer (d) for  $A\beta_{40}$  and  $A\beta_{42}$ , respectively. It can be seen that Tyr exclusively populates four areas within the space defined by  $\chi_1$  and  $\chi_2$ . The average angle values are indicated in the plots. This data shows that Tyr exists in four distinct rotational structures, i.e., as four rotameric forms. The four populations of rotamers are well separated which supports the MEM findings discussed in the previous section. The distribution of Tyr rotamers found here identifies the existence of four well defined minima, or potential wells, in the potential energy landscape  $V(\chi_1, \chi_2)$  and justifies the existence of four peaks in the lifetime distributions.

## 6.4 Conclusions

Tyr sensitivity to peptide-peptide interactions makes it a good sensor for monitoring the critical early stages of  $A\beta$  aggregation. Using  $A\beta$ 's intrinsic

fluorescence as a sensing tool can bring advantages in the AD research because it allows monitoring of the oligomerisation process where toxic species are being created.

In this chapter the NLLS fitting to discrete lifetime models of Tyr decay was used to compare the oligomerisation of two distinct forms of  $A\beta$ , namely  $A\beta_{40}$  and  $A\beta_{42}$ . The simplicity of the discrete lifetime approach and NLLS method makes it a good tool to easily analyse a system and compare different experimental situations regardless of the photophysics of the sensor Tyr. For example it can be used to directly compare the kinetics of oligomerisation of samples in different conditions, e.g. with additives. This could help find factors that slow down or disrupt the oligomerisation of the peptides in its early stages and consequently slow down or disrupt the formation of cytotoxic oligomers linked with AD onset. The use of this sensing technique *in vitro* to search for such analytes is within reach of many research teams around the world. Finding such factors will have clear implications for AD therapeutics in particular and perhaps for all amyloidoses in general.

MEM on the other hand is a more complex and time consuming analysis. Lifetime distributions can be useful if the objective is obtaining information on the photophysics of Tyr and understand its behaviour in a more fundamental view instead of using the method in a pure sensor approach. If the interest is in studying the sensor and not just the oligomerisation kinetics, then using a discrete lifetime method might be too reductive and information can be lost as has been shown here. Therefore, if one wants to study the photophysical behaviour of Tyr in the  $A\beta$  peptide, and how aggregation can affect Tyr photophysics, MEM would be recommended as an additional analysis tool.

The MEM method revealed that Tyr photophysics is more complex than a simple three-exponential model. MEM results show that Tyr decay demonstrates a reasonable exponential character but is a composition of four decays

and not three. This observation is further supported by the MD simulations. Recently Hernandez, et al. [99] have calculated potential energy landscapes for Tyr in hydrated media and have found four minima in  $V(\chi_1, \chi_2)$ , supporting the findings here reported regarding the existence of four stable rotameric forms of Tyr instead of the commonly accepted model of three rotamers.

The possibility that Tyr decay could be more complex than the three-exponential model used to describe it, hypothesis mentioned in the previous chapter and brought to light due to the observed behaviour of Tyr decay with increasing wavelength of detection, is here confirmed. The existence of four components in Tyr decay can justify the behaviour observed in the wavelength dependent experiments. More studies in such direction would contribute to understand better the photophysical behaviour of Tyr in the A $\beta$  peptide and perhaps also in other proteins. Due to Tyr decay complexity, MEM would be an important tool in such investigations.

# Chapter 7

## Oligomerisation of dye-labelled $A\beta_{40}$

### 7.1 Introduction

In this chapter Tyr is used as an intrinsic sensor to monitor oligomer formation non-invasively from the early onset of single peptide-to-peptide interactions in samples with added extrinsic fluorophores. Tyr decay is analysed using the NLLS method in a purely sensor approach.

Two probes, the small coumarin derivative 7-diethylaminocoumarin-3-carbonyl (DEAC) and the larger Hilyte Fluor 488 (HLF), are here used to study the influence of covalently bound fluorophores in the kinetics of oligomerisation. The fluorescent tags are covalently bound to the N-terminal of  $A\beta_{40}$  peptides. Additionally, the extrinsic associating probe ThT is also shown to have an effect on the kinetic profile of oligomer formation.

### 7.2 Methodology

$A\beta_{40}$  tagged with DEAC ( $A\beta_{40}$ -DEAC) and  $A\beta_{40}$  tagged with HLF ( $A\beta_{40}$ -HLF) were purchased from AnaSpec (Fremont, USA). The ratio of tagged- $A\beta_{40}$  to untagged  $A\beta_{40}$  was of 1:26 for all samples. All samples were prepared

according to the methodology presented in Chapter 5 (page 55). To prepare the  $A\beta_{40}$ -HLF sample with ThT (ThT/ $A\beta_{40}$ -HLF) all preparation conditions were maintained and ThT was added when producing the sample at a ratio of 1 ThT molecule to 2  $A\beta_{40}$  total peptides, i.e., producing a final ThT concentration of  $25\mu\text{M}$ .

To monitor the influence of the peptide aggregation on Tyr fluorescence decay, the measurements were performed collecting 315 nm emission at increasing times  $t_{exp}$  after sample preparation using the TCSPC technique on the IBH Fluorocube system as previously described in Chapter 3 (page 30). A Perkin-Elmer LS-50 B luminescence spectrometer was used for fluorescence spectral measurements, ThT was excited at 450 nm.

### 7.3 Results and Discussion

The three-exponential decay model of Tyr fluorescence will be considered in this chapter and a NLLS analysis is made of Tyr's decay. All detected decays fitted to the model exhibited acceptable statistical criteria, namely  $\chi_r^2$  and distribution of residuals.

As has been shown in the previous chapter, the three-rotamer model is simplistic, however the three-exponential decay model can be effectively used to interpret the main fluorescence properties of Tyr during the process of amyloid oligomerisation and thus be used in a sensor approach to perform comparisons between samples in different conditions. The HC sample ( $50\mu\text{M}$   $A\beta_{40}$ ) discussed in Chapter 5 will again (as in Chapter 6) be used as a reference. For a quick summary of Tyr decay characteristic behaviour please refer to page 74 or page 66 for the larger discussion and figures.

In figure 7.1 is represented the structure of the small coumarin derivative 7-diethylaminocoumarin-3-carbonyl (DEAC) dye and in figure 7.2 the larger dye Hilyte Fluor 488 (HLF) is represented.

The dye molecules were covalently bound through their carbonyl group

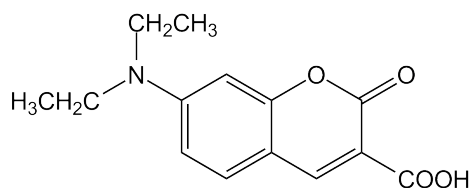


**Figure 7.1:** Chemical structure of DEAC molecule.

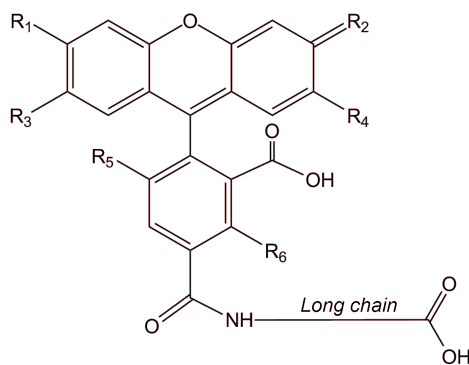


**Figure 7.2:** Chemical structure of HLF molecule.  $R_i$  are substituents.

to the last amino acid residue of  $A\beta_{40}$ 's N-terminal.

### 7.3.1 DEAC labelled $A\beta_{40}$

DEAC is a relatively small dye compared to HLF but still has dimensions larger than most of the 20 amino acids. The absorption and emission spectra of DEAC bound to  $A\beta_{40}$  are shown in figure 7.3a.

$A\beta_{40}$ -DEAC emission spectrum is well separated from Tyr emission. From the absorption spectrum it was estimated that resonance energy transfer between DEAC and Tyr is not expected to be efficient. The intended final purpose of the experiments with labelled  $A\beta_{40}$  peptides was to perform FRET measurements between DEAC and HLF in the labelled peptides. For this the ratio between labelled and unlabelled peptides was kept low, both DEAC and HLF sample were prepared so that only 1 in 26 peptides were labelled. The FRET experiments proved to be unsuccessful due to complex donor decay photophysics and will not be presented. It will be demonstrated in this chapter that even at low ratios of labelled to unlabelled peptides the fluo-

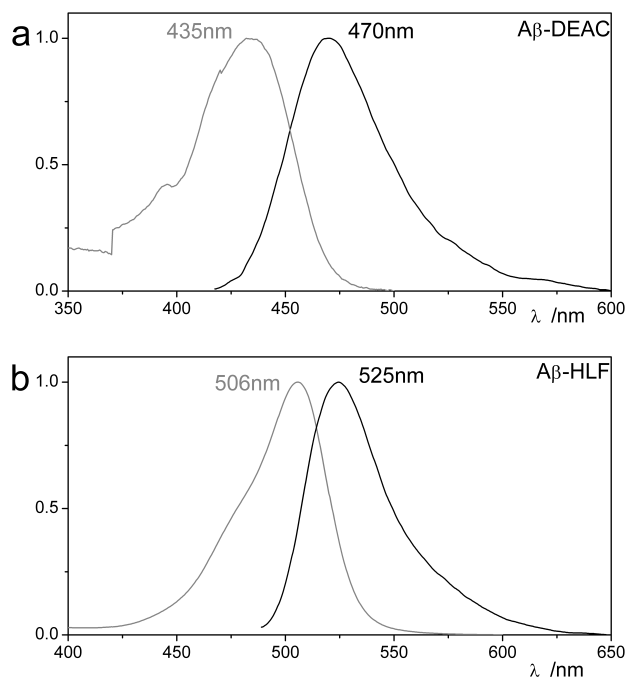


**Figure 7.3:** Absorption spectrum (grey) and fluorescence emission spectrum (black) of fluorescent labels bound to  $A\beta_{40}$ , a)  $A\beta_{40}$ -DEAC and b)  $A\beta_{40}$ -HLF.

rescent tags have an influence the mechanism of aggregation and, therefore, even if possible the information given by the energy transfer experiments would contain artifacts in its depiction of the process of aggregation.

The fact that in the final samples 96% of the molecules were unlabelled means that Tyr fluorescence signal arises mainly from undisturbed peptides. This allows the samples containing tagged peptides to be compared with the previous data obtained for unlabelled  $A\beta_{40}$  peptides (figure 5.4, page 66).

The retrieved lifetimes  $\tau_i$  and fractional contributions  $f_i$  as functions of experiment time, or aggregation time, for the  $A\beta_{40}$ -DEAC sample are shown in figures 7.4a and 7.4b, respectively. The lifetimes display a slow increase with time, particularly  $\tau_1$  and  $\tau_2$ . Such behaviour has also been noted in all other experiments presented previously in this thesis. However, in the case of the unlabelled  $A\beta_{40}$  (figure 5.4a, page 66) the effect is clearer in the first hours becoming more subtle afterwards while in the  $A\beta_{40}$ -DEAC such dependence seems to be extended over a longer period of time.

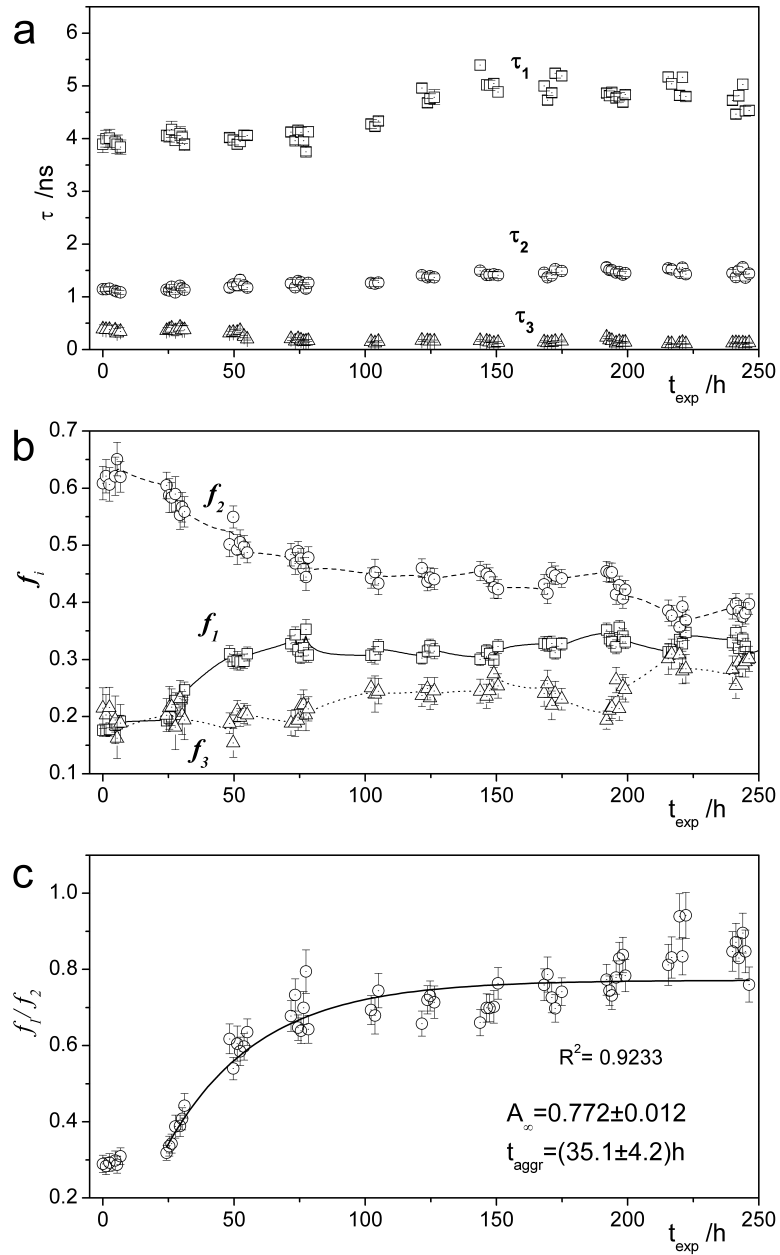


**Figure 7.4:** Parameters obtained from fitting Tyr decay in A $\beta$ <sub>40</sub>-DEAC to a three-exponential model. a) fluorescence decay time; b) fluorescence intensity fractional contributions. c) ratio between decay times fractional contributions  $f_1/f_2$  data fitted according to equation (5.6). Experimental errors are 3 standard deviations.

The significant changes in the fractional contributions  $f_i$  for the unlabelled  $A\beta_{40}$  (figure 5.4b, page 66) are also present in the  $\beta_{40}$ -DEAC sample (figure 7.4b). The trends in both samples are very similar to the exception of the initial experimental period. Such similarities and initial difference can also be seen and compared through the ratio  $f_1/f_2$  shown in figure figure 7.4c for  $A\beta_{40}$ -DEAC.

In the case of the unlabelled  $A\beta_{40}$  sample the  $f_i$  parameters are monotonic functions in time. The behaviour of  $f_i$  for the  $A\beta_{40}$ -DEAC sample is slightly different (figure 7.4b). In the initial hours the changes in the  $f_i$  parameters are small and within the associated error. One can say, therefore, that during the first  $\approx 7$ h Tyr responses seem to be stable, within their errors. This can also be seen in figure 7.4c where the values of the ratio appear constant.

What is found here with the  $A\beta_{40}$ -DEAC sample is that the initial coalescence of monomers must occur at a smaller rate thus justifying the differences between the two samples in the initial period. After  $\approx 7$ h the trends of the  $f_i$  parameters follow similar profiles to those found for the unlabelled  $A\beta_{40}$  sample.

In figure 7.4c is presented the  $f_1/f_2$  ratio. The values were fitted according to the equation (5.6) as was done for the unlabelled sample. The fit was restrained to the range of values after the first 7 h, due to the above mentioned behaviour of  $f_i$ . The fitting was performed in order to access how the increasing exponential function models the "exponential stage" of  $A\beta_{40}$ -DEAC oligomerisation kinetics and to compare its behaviour with the unlabelled amyloid kinetics of oligomerisation.

One can observe that the limiting values  $A_\infty$  are not identical, but are similar, in both situations:  $0.870 \pm 0.016$  for the unlabelled sample and  $0.772 \pm 0.012$  for  $A\beta_{40}$ -DEAC. These results suggest that in both situations Tyr senses a similar final equilibrium of monomers/high order oligomers/fibrils is achieved. The characteristic "aggregation time"  $t_{aggr.}$  for the sample with DEAC labelled  $A\beta_{40}$  peptides reached a value of  $\approx 35$  h. The retrieved value is, within error, identical to the characteristic "aggregation time" for the un-

labelled peptides ( $\approx 33$  h). Seemingly, the initial coalescence of monomers (at  $t_{exp} < 7$ h) takes place at a slower pace but the phase of exponential growth is identical.

The data suggests that binding DEAC to the N-terminal of  $A\beta_{40}$  decreases the number of effective encounters between peptides therefore effectively slowing the coalescence of monomers to form oligomeric species. An effective encounter can be described as a collision between peptides in which the peptides remain together resulting in an aggregation event. At first view many factors could cause the decrease of effective encounters between peptides, for example, such interference could be due to steric effects or perhaps the attached DEAC molecule disturbs the polarization of neighbouring groups reducing electrostatic interactions between peptides such as the ability to form hydrogen bonds.

Even though only approximately 4% of the peptides are tagged with DEAC such amount seems to be sufficient to promote a number of unsuccessful events that sabotage the start of the oligomerisation process. However, even with a delayed start, the aggregation still seems to proceed and the formation of more complex oligomers achieved. The DEAC label seems to have only a small influence on the oligomerisation and the progress of aggregation is similar to that of the unlabelled  $A\beta_{40}$  peptides.

### 7.3.2 HLF labelled $A\beta_{40}$

The absorption and emission spectra of HLF bound to  $A\beta_{40}$  are shown in figure 7.3b. The dye's emission and absorption spectra in  $A\beta_{40}$ -HLF are clearly separated from Tyr's emission and absorption. As for the case of  $A\beta_{40}$ -DEAC, resonance energy transfer between HLF and Tyr was estimated to be inefficient.  $A\beta_{40}$ -HLF samples were also prepared to yield 96% of unlabelled peptides, i.e., only 1 in 26  $A\beta_{40}$  peptides were HLF labelled.

Retrieved lifetimes  $\tau_i$  and fractional contributions  $f_i$  for  $A\beta_{40}$ -HLF are

shown in figures 7.5a and 7.5b, respectively. The lifetimes display an initial decrease followed by the expected increase of values after  $\approx 50$  h. The changes in the fractional contributions  $f_i$  are again similar to those found for the unlabelled  $A\beta_{40}$ . However, the initial stages of the experiment show significant differences. The retrieved  $f_i$  for  $A\beta_{40}$ -HLF are non-monotonic functions in time (figure 7.5b). In the initial hours there is an increase in  $f_2$  and a corresponding decrease in  $f_3$ . With the progress of oligomerisation  $f_2$  and  $f_3$  reach limit values after which they start to invert trends in an exponential fashion.

This non-monotonic behaviour is, however, not a new finding. Such response of the  $f_i$  parameters was already detected in the concentration depend experiments discussed in Chapter 5 (page 59). This suggests that the initial increase in  $f_2$  and decrease of  $f_3$  could be a signature behaviour of the very beginning of the oligomerisation process where the first peptide-to-peptide interactions occur leading to the creation of the first oligomers, such as dimmers. It can be seen that the values obtained for initial stages of the  $A\beta_{40}$ -DEAC resemble the values for  $A\beta_{40}$ -HLF after approximately 30 h of experiment time. These facts together support the idea that the presence of  $A\beta_{40}$ -HLF peptides in the sample slows down the progress of oligomerisation and this effect is more pronounced in this case than for the sample with DEAC labelled peptides. Therefore, the bigger HLF tag seemingly reduces the rate of oligomerisation even more substantially.

The  $f_1/f_2$  ratio for  $A\beta_{40}$ -HLF can be seen in figure 7.5c. The values were fitted according to the equation (5.6) as was done for the previous samples. The fit was restrained to the range of values after the first  $\approx 50$  h, due to the non-monotonic behaviour of  $f_i$ . The characteristic "aggregation time"  $t_{aggr.}$  for  $A\beta_{40}$ -HLF as value of  $(66.1 \pm 8.5)$  h, a value that is higher than the characteristic "aggregation time" for the unlabelled  $A\beta_{40}$  and  $A\beta_{40}$ -DEAC.

The binding of HLF to the N-terminal of the  $A\beta_{40}$  seems to further decrease the number of effective encounters between peptides therefore effectively slowing the coalescence of monomers to form oligomeric species even

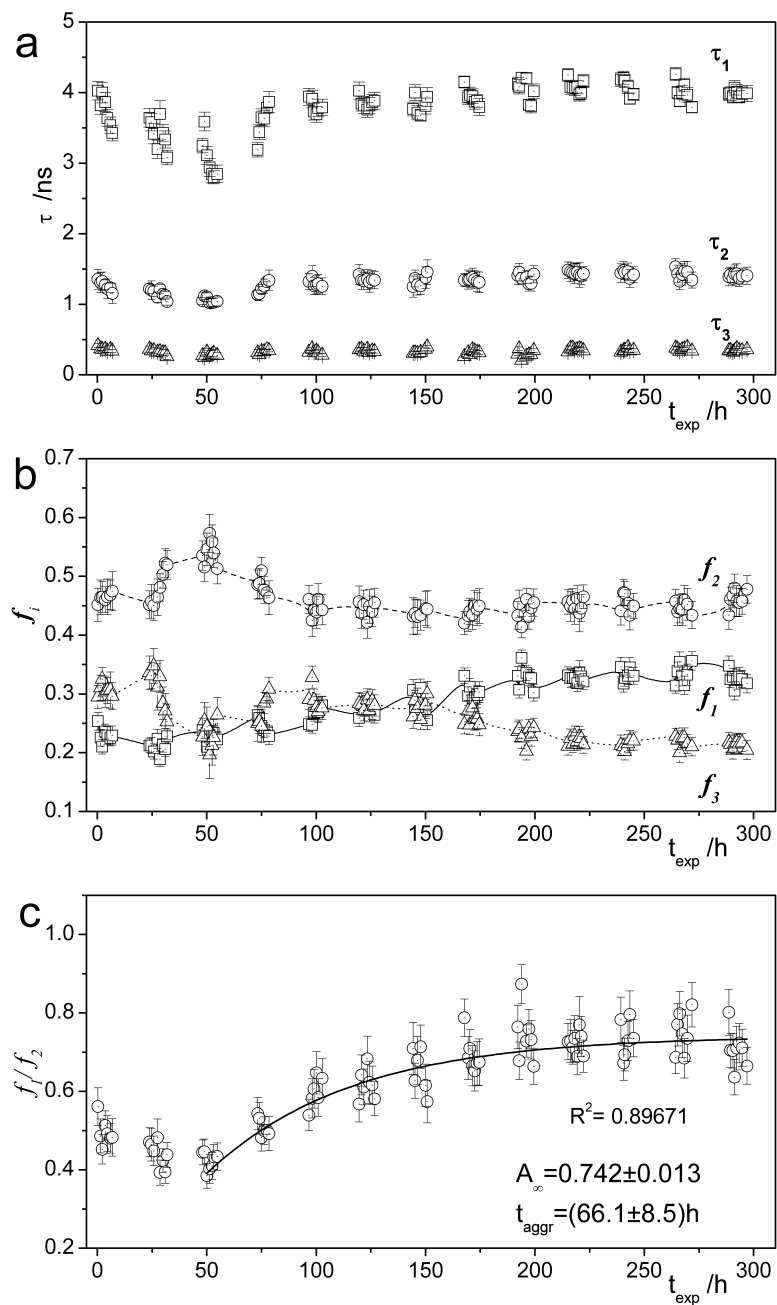


**Figure 7.5:** Parameters obtained from fitting Tyr decay in A $\beta$ <sub>40</sub>-HLF to a three-exponential model. a) fluorescence decay time; b) fluorescence intensity fractional contributions. c) ratio between decay times fractional contributions  $f_1/f_2$  data fitted according to equation (5.6). Experimental errors are 3 standard deviations.

more than the DEAC tag. This leads one to consider that the size of the label molecule might be the parameter with highest influence, or potential for disturbance, on the early oligomerisation of the  $A\beta_{40}$  peptides.

The limiting value  $A_\infty$  is slightly lower in the  $A\beta_{40}$ -HLF case ( $0.742 \pm 0.013$ ) when compared to the unlabelled and DEAC labelled  $A\beta_{40}$  samples. As with both previously presented samples, also  $A\beta_{40}$ -HLF seems to evolve towards higher order oligomers through similar kinetic profiles but with different time constants. However, being the equilibrium value  $A_\infty$  obtained for the  $f_1/f_2$  ratio lower than expected, the possibility of the equilibrium stage of this sample being different can be considered.

An explanation for such observation could be that HLF creates steric hindrance to such level that it does not permit the aggregation of peptides into more complex higher order oligomers. To understand this hypothesis an analogy can be drawn with the building of a brick tower: the bricks ( $A\beta_{40}$  peptides) are stacked one on top of the other, when a brick of different dimension ( $A\beta_{40}$ -HLF) is inserted into the construction it creates a break in the pattern and hinders the stability of the tower (high order oligomer). Further bricks might perhaps still be stacked but the structural integrity of the tower is compromised and eventually it will collapse due to lack of stability.

Tyr fluorescence response is sensitive to events occurring in its close surroundings, such as peptide-to-peptide binding, and is most likely not sensitive to changes happening at large distances. While one can use Tyr to monitor the formation of small oligomers, the coalescence of oligomers into higher order oligomers or/and fibrils will not produce significant changes in the bulk Tyr response. Therefore, to test the above formulated hypothesis using Tyr lifetime responses is not sufficient or adequate and a ThT assay can prove useful at this point. To test the hypothesis, the same  $A\beta_{40}$ -HLF experiment was performed with added ThT in order to track the formation of  $\beta$ -sheets and fibrils.

### 7.3.3 HLF labelled $A\beta_{40}$ + ThT

For the  $A\beta_{40}$ -HLF sample with ThT (ThT/ $A\beta_{40}$ -HLF) the 1:2 ratio (ThT to total  $A\beta_{40}$ ) was used in order to compare the results with the previous ThT data presented in Chapter 4 (page 49).

Tyr fluorescence decay evolution was still monitored through the TCSPC technique as previously and the results are shown in figure 7.6. Steady state measurements were performed to follow ThT emission during the process of aggregation, the intensity values at peak emission are presented in figure 7.7 as hollow circles.

When analysing Tyr decay in the ThT/ $A\beta_{40}$ -HLF sample remarkable differences are seen in its behaviour with aggregation time. The presence of ThT seems to significantly alter the kinetic profile of oligomerisation (figure 7.6). Regarding the fractional contributions  $f_i$ , figure 7.6b, the signature behaviour is still present but the process evolves at different rates than those found for the sample without ThT. The initial phase lasts for  $\approx 50$  h for  $A\beta_{40}$ -HLF, while for ThT/ $A\beta_{40}$ -HLF the maximum (minimum) values of  $f_2$  ( $f_3$ ) are reached within the first day of measurements. It seems that the presence of ThT speeds up the initial coalescence of monomers into simple oligomeric species, approximately reducing by half the time of this initial step in the oligomerisation profile.

There are also changes in the "second stage" of the oligomerisation process, where  $f_2$  and  $f_3$  invert trends and  $f_1$  starts to grow. While for all other samples the changes evolve in an exponential fashion, in ThT/ $A\beta_{40}$ -HLF the  $f_i$  evolution presents more similarities with a linear behaviour. In the previously experiment with ThT and  $A\beta_{40}$  (page 49) which is being used here as reference, it is also visible that the  $f_i$  dependence with experimental time presents a linear behaviour instead of the exponential one found for all other  $A\beta_{40}$  samples after  $f_2$  ( $f_3$ ) achieve their maximum (minimum).

The differences in the kinetic profile of oligomerisation are also patent in the  $f_1/f_2$  ratio, figure 7.6c. To find the equilibrium value of  $f_1/f_2$  a linear regression was performed at the end values (after 216 h). The intercept of

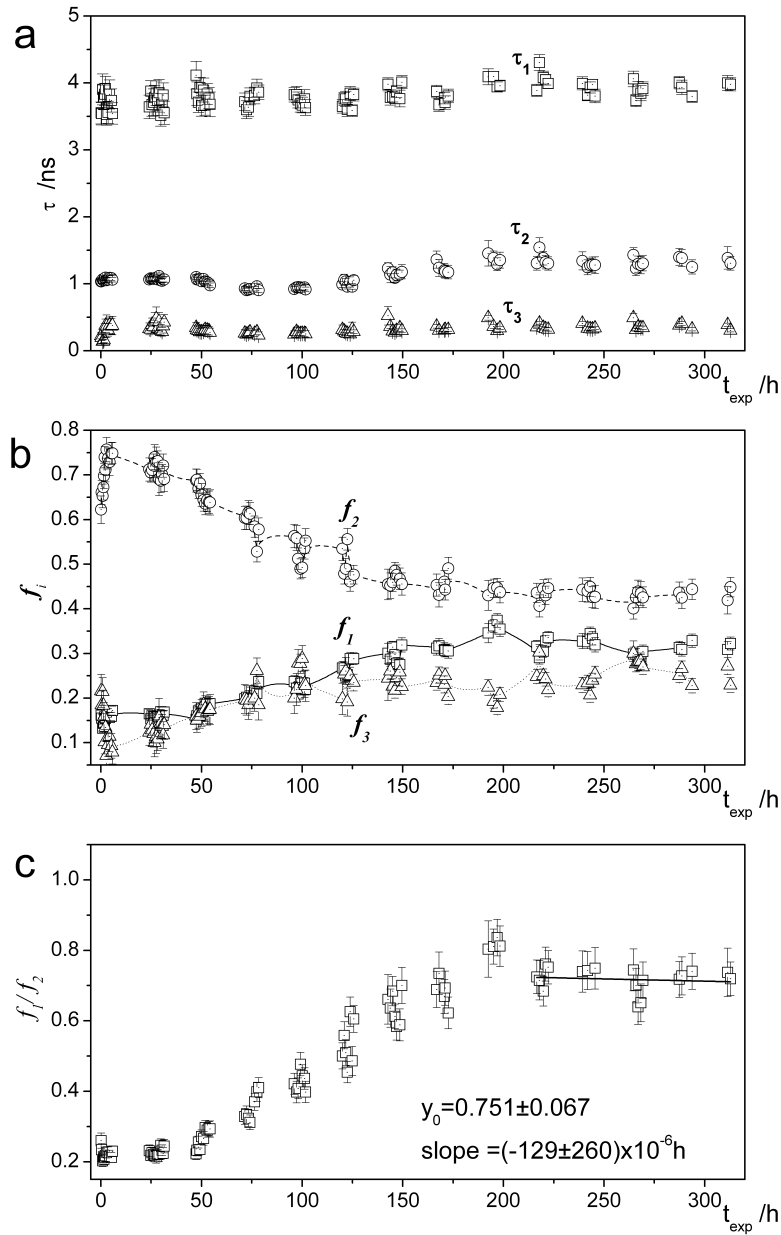


**Figure 7.6:** Parameters obtained from fitting Tyr decay in ThT/A $\beta_{40}$ -HLF to a three-exponential model. a) fluorescence decay time; b) fluorescence intensity fractional contributions. c) ratio between decay times fractional contributions  $f_1/f_2$ , data fitted to a linear regression. Experimental errors are 3 standard deviations.

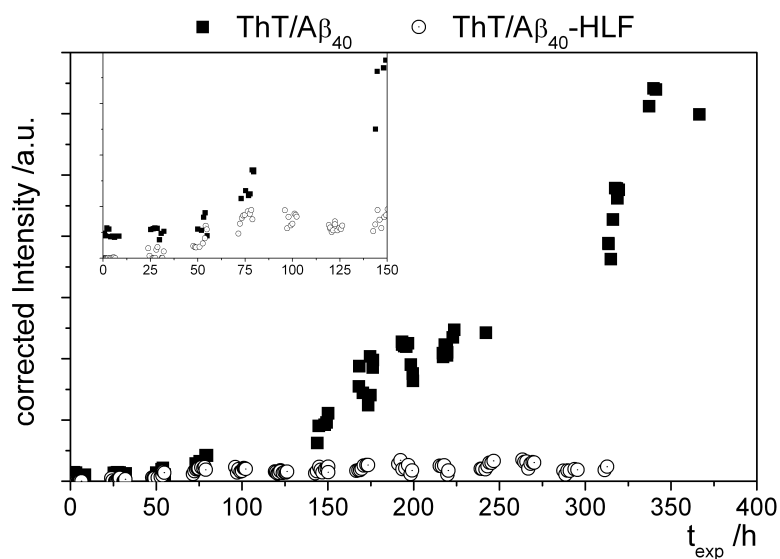


**Figure 7.7:** Peak intensity of ThT fluorescence at different stages of  $A\beta_{40}$  aggregation. Hollow circles: ThT/ $A\beta_{40}$ -HLF; Full squares: ThT/ $A\beta_{40}$  (data presented in figure 4.2, page 49).

the fit is placed at  $0.751 \pm 0.067$ , the value corresponds well with  $A_\infty$  for  $A\beta_{40}$ -HLF. The slope of the fit and its associated error,  $-(129 \pm 260) \times 10^{-6}$  h, reveal that at these times  $f_1/f_2$  values are merely scattered around the average value of 0.75. The good agreement between both  $A_\infty$  values suggests a similar final equilibrium position for both samples with and without ThT. As so it is reasonable to infer about the  $A\beta_{40}$ -HLF final equilibrium through the ThT data for the ThT/ $A\beta_{40}$ -HLF sample.

ThT intensity values at peak emission for ThT/ $A\beta_{40}$ -HLF are presented as hollow circles in figure 7.7. The full squares represent the data for the  $A\beta_{40}$  sample, of  $35 \mu\text{M}$  with a ThT/ $A\beta_{40}$  ratio of 1:2, which was initially presented in Chapter 4. The intensity values in the plot have been corrected to eliminate the effect of concentration on the emission intensity and therefore allow direct comparison between the two samples.

Observing figure 7.7 the differences between the samples final stage are striking. Below the first 100 h the samples behave in a similar fashion,

this can be better seen in the inset plot. Both samples display increasing values of ThT intensity which, due to ThT's specificity, signifies that complex structures with  $\beta$ -sheet content begin to appear. The changes in intensity are very small symbolizing that such structures are still a small fraction of the total composition of the sample.

For the  $A\beta_{40}$  sample, ThT intensity continues to increase in a characteristic fashion until the end of the aggregation process,  $\approx 350$  h after sample preparation. For ThT/ $A\beta_{40}$ -HLF such behaviour is not present. ThT intensity stops increasing and stagnates at a very low value compared to  $A\beta_{40}$ . Approximately 100 h after sample preparation no further increase in ThT is measured leading to the conclusion that the formation of structures with  $\beta$ -sheets is hindered by the presence of the labelled  $A\beta_{40}$ -HLF peptides in the sample. HLF seems to alter the oligomers stability to a level that does not allow the formation of a significant number of  $\beta$ -sheets and complex structures.

Such behaviour seems to confirm the hypothesis that HLF interferes significantly only with the process of oligomerisation but also with fibrillisation.  $A\beta_{40}$ -HLF peptides slow down the initial stages oligomerisation where single peptides bind together effectively to form small oligomers as shown by Tyr data (figure 7.6). Moreover, the presence of the  $A\beta_{40}$ -HLF peptides seems to hinder the formation of complex higher order oligomers with organized structure containing the  $\beta$ -sheet motif. Additionally, it seems that the lower value of  $A_{\infty}$  found for the equilibrium of  $A\beta_{40}$ -HLF (figure 7.6c) might be a signature of such effect.

Alternatively, the low values of ThT intensity obtained through the experimental time might be the result of quenching phenomena. In such case, the fact that ThT's intensity does not increase in the typical sigmoidal fashion does not directly mean that there are no  $\beta$ -sheets containing complex structures. The absence of increasing ThT fluorescence would merely be an effect of such quenching mechanisms and thus the lack of signal is artificial and not related to the absence of fibrils as suggested above. Performing CD

or infrared spectroscopy to monitor conformational changes and formation of  $\beta$ -sheets throughout the sample aging should prove useful to help exclude or confirm this alternative hypothesis.

## 7.4 Conclusions

In this chapter was demonstrated how intrinsic fluorescence of Tyr in  $A\beta_{40}$  can be useful for monitoring the early stages of oligomerisation. The "method" was used to study the influence of fluorescent labels on the early stages of  $A\beta_{40}$  oligomer formation.

Using Tyr as a sensor allowed the comparison of the kinetic profiles of oligomerisation of different  $A\beta_{40}$  samples. Using a three-exponential decay model function and the NLLS method of fitting, the change in the  $f_1/f_2$  ratio was retrieved and fitted allowing the comparison of the characteristic "aggregation times"  $t_{aggr.}$  for  $A\beta_{40}$  samples containing peptides with covalently bound probes. In the case of the sample with DEAC labelled peptides the  $t_{aggr.}$  was found to be of  $\approx 35$  h and for the sample with HLF labelled peptides  $t_{aggr.}$  achieved a value of  $\approx 66$  h. It was previously shown in Chapter 5 that for a sample of unlabelled  $A\beta_{40}$  the characteristic  $t_{aggr.}$  was  $\approx 33$  h.

As an explanation for the founds effects, the hypothesis that the size of the attached fluorescent molecule disturbs the interactions between  $A\beta_{40}$  peptides that lead to the formation of oligomeric species is proposed. It was demonstrated that even the small DEAC molecule covalently bound to the  $A\beta_{40}$  peptide influences the kinetics of oligomerisation effectively slowing down the formation of oligomers. The data also suggest that the bigger HLF molecule seems to disturb the oligomerisation process to a higher extent slowing down significantly the initial coalescence of monomers. Moreover the ThT data shows that HLF also might disrupt the formation of  $\beta$ -sheets structures and prevent the constitution of highly organized higher order species.

ThT, an extrinsic associating probe, has been shown to also influence the kinetic profile of oligomerisation. ThT promoted the initial stages of peptide

coalescence to form simple oligomeric species. However, the dye seems to alter the exponential character of the oligomerisation kinetics reducing it to a more linear dependence. Such linear behaviour was also patent in results shown previously in Chapter 4.

In this chapter it has been shown how the use extrinsic fluorophores can influence the oligomerisation process of  $A\beta_{40}$  peptides even at low label/ $A\beta_{40}$  ratios. In the amyloid field of studies many research groups focus on finding ways to monitor oligomerisation and prevent the formation of small oligomeric species. Awareness of label influences on the very beginning on the aggregation process is crucial to correctly interpret the data.

Here was not only shown that the experimental technique, or "method", used throughout this thesis in a sensor approach enables detection of binding of single peptides non-invasively but also, it was demonstrated how it can be effectively used to study the early stages of oligomerisation. The potential of using the "method" in the search for factors that influence the early stages of oligomerisation was exhibited. It is viable that this approach can be very useful in the search to discover how to halt the formation of simple oligomers, which could be of fundamental importance in the research on the mechanisms of neurodegenerative diseases and even lead to more effective therapeutics not only for AD but all amyloidoses.

# Chapter 8

## Conclusions

The findings presented in this thesis support the use of Tyr fluorescence as a non-invasive sensor for the oligomerisation of the  $A\beta$  protein.

It has been shown that Tyr fluorescence responds to  $A\beta$  aggregation earlier than the dye ThT, demonstrating that Tyr is sensitive to aggregation stages previous to the formation of  $\beta$ -sheets containing structures. This supports the idea that Tyr reports on the intermolecular phenomenon of aggregation at the level of single peptide-to-peptide binding.

The study of Tyr fluorescence behaviour in samples of different  $A\beta$  concentrations revealed that oligomerisation has characteristics of a nucleation dependent process. At low levels of monomer concentrations oligomer formation does not seem to occur and the oligomerisation rate has been shown to be concentration dependent.

The above mentioned experiments also revealed a non-monotonic response of Tyr to aggregation and the information gathered about Tyr behaviour can be used as reference for studies of oligomerisation kinetics. This has been, in fact, practiced and demonstrated when studying the effect of extrinsic fluorophores on  $A\beta_{40}$  oligomerisation.

It has been shown that covalently bound extrinsic fluorophores have significant influence on the oligomerisation kinetics and might even disrupt

the formation of  $\beta$ -sheets and complex higher order structures. It has been also found that the widely used ThT dye induces significant changes in the oligomerisation kinetic profile.

These findings demonstrate that extrinsic fluorophores produce artifacts, which does not mean that extrinsic fluorophores should not be used at all in the study of oligomers, but it serves to bring awareness to the kind of influences the foreign molecules might produce.

The study of Tyr fluorescence decay at different detection wavelengths introduced questions about the fidelity of the discrete three-exponential model used to deconstruct Tyr decay in  $A\beta$ . Using a model-free analysis, it has been shown that  $A\beta$ 's Tyr decay has in fact an exponential character but would be more accurately represented by a four-exponential model.

In monomeric  $A\beta$  the contribution of the fourth larger lifetime is small and a three-exponential model can be used to represent Tyr photophysics. With the progress of aggregation the contribution of the fourth peak grows bigger and even though a three-exponential model can still be used at these stages to interpret the data successfully, the photophysical behaviour of Tyr is no longer accurately described by it.

The lifetime distributions obtained display relatively narrow peaks. These must result from well defined potential wells where Tyr can exist in the form of different conformations, or rotamers. Trapped in the potential wells the rotamers have restricted movement resulting in a small range of possible interactions with their environment and thus a small dispersion of the possible decay lifetimes for each rotamer.

This finding obtained with MEM analysis of Tyr decay has been supported by MD simulations which revealed that Tyr in  $A\beta$  can exist in four well defined positions, breaking with the commonly used model of three rotameric forms of Tyr in proteins.

Recently Hernandez, et al. [99] have calculated potential energy landscapes for the three fluorescent amino acids in hydrated media and have found four minima in  $V(\chi_1, \chi_2)$  for Tyr, thus supporting the findings pre-

sented in this thesis regarding the existence of four stable rotameric forms of Tyr instead of the commonly accepted model of three rotamers.

Tyr proves to be a good sensor for studies of A $\beta$  oligomerisation. Experiments can be performed by researchers using this method almost in a "black-box" approach. The insight Tyr brings as a "neutral" reporter of the oligomerisation process opens new doors. This new "method" can be used to test and investigate how to slow down or prevent all together the formation of the cytotoxic oligomers.

The adoption of this "method" by research teams around the world, or the simple application of the idea here presented to other systems, would be the ultimate goal of the work developed and here presented.

In the quest to characterize Tyr response to the phenomenon of aggregation various features of Tyr photophysics where unveiled. The existence of four stable rotameric forms breaks with the common rotamer model for amino acid fluorescence. The shifts observed with increasing the emission wavelength detection suggest that there could be more complexity in Tyr decay that surely is worth exploring.

No longer in the realm of monitoring aggregation, further studies on purely the photophysical behaviour of Tyr can prove very interesting. As future work, studying the excited state kinetics of Tyr with MEM as a function of emission wavelength, in systems of increasing complexity is an exciting challenge. There is still much to know about Tyr decay kinetics and this thesis brought to light features of Tyr decay that are currently unexplained and therefore should be investigated.

## Bibliography

- [1] J. B. Martin, “Molecular basis of the neurodegenerative disorders,” *the New England Journal of Medicine*, vol. 340, no. 25, pp. 1970–1980, 1999.
- [2] D. M. Walsh and D. J. Selkoe, “A beta oligomers: a decade of discovery.,” *Journal of neurochemistry*, vol. 101, pp. 1172–84, June 2007.
- [3] K. N. Dahlgren, A. M. Manelli, W. B. Stine, L. K. Baker, G. A. Krafft, and M. J. LaDu, “Oligomeric and fibrillar species of amyloid-beta peptides differentially affect neuronal viability.,” *The Journal of biological chemistry*, vol. 277, pp. 32046–53, Aug. 2002.
- [4] M. Stefani and C. M. Dobson, “Protein aggregation and aggregate toxicity: new insights into protein folding, misfolding diseases and biological evolution.,” *Journal of molecular medicine (Berlin, Germany)*, vol. 81, pp. 678–99, Nov. 2003.
- [5] D. L. Nelson and M. M. Cox, *Lehninger principles of biochemistry*. New York: W.H. Freeman and Company, 5th ed., 2008.
- [6] A. M. Lesk, *Introduction to protein science: architecture, function and genomics*. New York: Oxford University Press, 2004.
- [7] C. Brandén and J. Tooze, *Introduction to protein structure*. New York: Garland Publishing, Inc., 2nd ed., 1999.
- [8] R. H. Pain, *Mechanisms of protein folding*. Oxford: Oxford University Press, 2nd ed., 2000.
- [9] U. Schubert, L. C. Antón, J. Gibbs, C. C. Norbury, J. W. Yewdell, and J. R. Bennink, “Rapid degradation of a large fraction of newly synthesized proteins by proteasomes.,” *Nature*, vol. 404, pp. 770–4, Apr. 2000.
- [10] J. D. Sipe and A. S. Cohen, “Review: history of the amyloid fibril.,” *Journal of structural biology*, vol. 130, pp. 88–98, June 2000.

- [11] W. J. Lennarz and M. D. Lane, *Encyclopedia of biological chemistry*. Amsterdam: Elsevier, 2004.
- [12] J. L. Jiménez, E. J. Nettleton, M. Bouchard, C. V. Robinson, C. M. Dobson, and H. R. Saibil, “The protofilament structure of insulin amyloid fibrils,” *Proceedings of the National Academy of Sciences of the United States of America*, vol. 99, pp. 9196–201, July 2002.
- [13] R. Nelson, M. R. Sawaya, M. Balbirnie, A. O. Madsen, C. Riek, R. Grothe, and D. Eisenberg, “Structure of the cross-beta spine of amyloid-like fibrils,” *Nature*, vol. 435, pp. 773–8, June 2005.
- [14] S. Kumar and J. B. Udgaonkar, “Mechanisms of amyloid fibril formation by proteins,” *Current Science*, vol. 98, no. 5, pp. 639–656, 2010.
- [15] S. K. Maji, L. Wang, J. Greenwald, and R. Riek, “Structure-activity relationship of amyloid fibrils,” *FEBS letters*, vol. 583, pp. 2610–7, Aug. 2009.
- [16] V. Nimmrich, C. Grimm, A. Draguhn, S. Barghorn, A. Lehmann, H. Schoemaker, H. Hillen, G. Gross, U. Ebert, and C. Bruehl, “Amyloid beta oligomers (A beta(1-42) globulomer) suppress spontaneous synaptic activity by inhibition of P/Q-type calcium currents,” *The Journal of neuroscience : the official journal of the Society for Neuroscience*, vol. 28, pp. 788–97, Jan. 2008.
- [17] M. Kawahara and Y. Kuroda, “Molecular mechanism of neurodegeneration induced by Alzheimer’s beta -amyloid protein : Channel formation and disruption of calcium homeostasis,” *Brain Research*, vol. 53, no. 4, pp. 389 –397, 2000.
- [18] M. Sakono and T. Zako, “Amyloid oligomers: formation and toxicity of Abeta oligomers,” *The FEBS journal*, vol. 277, pp. 1348–58, Mar. 2010.

- [19] M. B. Graeber, S. Kösel, R. Egensperger, R. B. Banati, U. Müller, K. Bise, P. Hoff, H. J. Möller, K. Fujisawa, and P. Mehraein, “Rediscovery of the case described by Alois Alzheimer in 1911: historical, histological and molecular genetic analysis.,” *Neurogenetics*, vol. 1, pp. 73–80, May 1997.
- [20] J. Hardy and D. J. Selkoe, “The amyloid hypothesis of Alzheimer’s disease: progress and problems on the road to therapeutics.,” *Science (New York, N.Y.)*, vol. 297, pp. 353–6, July 2002.
- [21] S. R. Robinson and G. M. Bishop, “The search for an amyloid solution,” *Science*, vol. 298, pp. 961–964, 2002.
- [22] J. Hardy, “The amyloid hypothesis for Alzheimer’s disease: a critical reappraisal.,” *Journal of neurochemistry*, vol. 110, pp. 1129–34, Aug. 2009.
- [23] D. J. Selkoe, “Translating cell biology into therapeutic advances in Alzheimer’s disease,” *Nature*, vol. 399, pp. 23–31, 1999.
- [24] M.-P. Marzolo and G. Bu, “Lipoprotein receptors and cholesterol in APP trafficking and proteolytic processing, implications for Alzheimer’s disease.,” *Seminars in cell & developmental biology*, vol. 20, pp. 191–200, Apr. 2009.
- [25] M. Gralle and S. T. Ferreira, “Structure and functions of the human amyloid precursor protein: the whole is more than the sum of its parts.,” *Progress in neurobiology*, vol. 82, pp. 11–32, May 2007.
- [26] J. Koolman and K.-H. Roehm, *Color Atlas of Biochemistry*. Stuttgart: Georg Thieme Verlag, 2nd ed., 2005.
- [27] H. Zheng and E. H. Koo, “The amyloid precursor protein: beyond amyloid.,” *Molecular neurodegeneration*, vol. 1, p. 5, Jan. 2006.

- [28] D. J. Selkoe, "Cell biology of protein misfolding: The examples of Alzheimer's and Parkinson's diseases," *Nature Cell Biology*, vol. 6, pp. 1054–1061, Nov. 2004.
- [29] Y. Yan and C. Wang, "Abeta42 is more rigid than Abeta40 at the C terminus: implications for Abeta aggregation and toxicity.," *Journal of molecular biology*, vol. 364, pp. 853–62, Dec. 2006.
- [30] J. T. Jarrett, E. P. Berger, and P. T. Lansbury, "The carboxy terminus of the .beta. amyloid protein is critical for the seeding of amyloid formation: Implications for the pathogenesis of Alzheimer's disease,," *Biochemistry*, vol. 32, pp. 4693–4697, May 1993.
- [31] O. M. El-Agnaf, D. S. Mahil, B. P. Patel, and B. M. Austen, "Oligomerization and toxicity of beta-amyloid-42 implicated in Alzheimer's disease.," *Biochemical and biophysical research communications*, vol. 273, pp. 1003–7, July 2000.
- [32] F. T. Senguen, T. M. Doran, E. A. Anderson, and B. L. Nilsson, "Clarifying the influence of core amino acid hydrophobicity, secondary structure propensity, and molecular volume on amyloid- $\beta$  16-22 self-assembly.," *Molecular bioSystems*, vol. 7, pp. 497–510, Feb. 2011.
- [33] M. Cheon, I. Chang, S. Mohanty, L. M. Luheshi, C. M. Dobson, M. Vendruscolo, and G. Favrin, "Structural reorganisation and potential toxicity of oligomeric species formed during the assembly of amyloid fibrils.," *PLoS computational biology*, vol. 3, pp. 1727–38, Sept. 2007.
- [34] T. R. Serio, "Nucleated Conformational Conversion and the Replication of Conformational Information by a Prion Determinant," *Science*, vol. 289, pp. 1317–1321, Aug. 2000.
- [35] J. C. Rochet and P. T. Lansbury, "Amyloid fibrillogenesis: themes and variations.," *Current opinion in structural biology*, vol. 10, pp. 60–8, Mar. 2000.

- [36] V. Koppaka and P. H. Axelsen, “Accelerated accumulation of amyloid beta proteins on oxidatively damaged lipid membranes.,” *Biochemistry*, vol. 39, pp. 10011–6, Aug. 2000.
- [37] A. Kakio, S. I. Nishimoto, K. Yanagisawa, Y. Kozutsumi, and K. Matsuzaki, “Cholesterol-dependent formation of GM1 ganglioside-bound amyloid beta-protein, an endogenous seed for Alzheimer amyloid.,” *The Journal of biological chemistry*, vol. 276, pp. 24985–90, July 2001.
- [38] M. Bokvist, F. Lindström, A. Watts, and G. Gröbner, “Two Types of Alzheimer’s  $\beta$ -Amyloid (140) Peptide Membrane Interactions: Aggregation Preventing Transmembrane Anchoring Versus Accelerated Surface Fibril Formation,” *Journal of Molecular Biology*, vol. 335, pp. 1039–1049, Jan. 2004.
- [39] N. Carulla, M. Zhou, M. Arimon, M. Gairí, E. Giralt, C. V. Robinson, and C. M. Dobson, “Experimental characterization of disordered and ordered aggregates populated during the process of amyloid fibril formation.,” *Proceedings of the National Academy of Sciences of the United States of America*, vol. 106, pp. 7828–33, May 2009.
- [40] C.-C. Lee, A. Nayak, A. Sethuraman, G. Belfort, and G. J. McRae, “A three-stage kinetic model of amyloid fibrillation.,” *Biophysical journal*, vol. 92, pp. 3448–58, May 2007.
- [41] B. O’Nuallain, S. Shivaprasad, I. Kheterpal, and R. Wetzel, “Thermodynamics of A beta(1-40) amyloid fibril elongation.,” *Biochemistry*, vol. 44, pp. 12709–18, Sept. 2005.
- [42] B. Bandyopadhyay, G. Li, H. Yin, and J. Kuret, “Tau aggregation and toxicity in a cell culture model of tauopathy.,” *The Journal of biological chemistry*, vol. 282, pp. 16454–64, June 2007.
- [43] R. Khurana, C. Ionescu-Zanetti, M. Pope, J. Li, L. Nielson, M. Ramírez-Alvarado, L. Regan, A. L. Fink, and S. A. Carter, “A general model for

- amyloid fibril assembly based on morphological studies using atomic force microscopy.," *Biophysical journal*, vol. 85, pp. 1135–44, Aug. 2003.
- [44] N. Benseny-Cases, M. Cocera, and J. Cladera, "Conversion of non-fibrillar  $\beta$ -sheet oligomers into amyloid fibrils in Alzheimers disease amyloid peptide aggregation.pdf," *Biochemical and biophysical research communications*, vol. 361, pp. 916–921, 2007.
- [45] A. E. Langkilde and B. Vestergaard, "Methods for structural characterization of prefibrillar intermediates and amyloid fibrils.," *FEBS letters*, vol. 583, pp. 2600–9, Aug. 2009.
- [46] J. Meinhardt, C. Sachse, P. Hortschansky, N. Grigorieff, and M. Fändrich, "Abeta(1-40) fibril polymorphism implies diverse interaction patterns in amyloid fibrils.," *Journal of molecular biology*, vol. 386, pp. 869–77, Feb. 2009.
- [47] H. A. Lashuel, D. Hartley, B. M. Petre, T. Walz, P. T. L. Jr, J. Turner, J. C. King, T. A. Lachlan-cope, and P. D. Jones, "Amyloid pores from pathogenic mutations," *Nature*, vol. 418, no. July, p. 291, 2002.
- [48] I. Maezawa, H.-S. Hong, H.-C. Wu, S. K. Battina, S. Rana, T. Iwamoto, G. A. Radke, E. Pettersson, G. M. Martin, D. H. Hua, and L.-W. Jin, "A novel tricyclic pyrone compound ameliorates cell death associated with intracellular amyloid-beta oligomeric complexes.," *Journal of neurochemistry*, vol. 98, pp. 57–67, July 2006.
- [49] S. Linse, C. Cabaleiro-Lago, W.-F. Xue, I. Lynch, S. Lindman, E. Thulin, S. E. Radford, and K. A. Dawson, "Nucleation of protein fibrillation by nanoparticles.," *Proceedings of the National Academy of Sciences of the United States of America*, vol. 104, pp. 8691–6, May 2007.
- [50] H. Wille, M. Shanmugam, M. Murugesu, J. Ollesch, G. Stubbs, J. R. Long, J. G. Safar, and S. B. Prusiner, "Surface charge of polyoxometa-

- lates modulates polymerization of the scrapie prion protein.," *Proceedings of the National Academy of Sciences of the United States of America*, vol. 106, pp. 3740–5, Mar. 2009.
- [51] H. D. T. Mertens and D. I. Svergun, "Structural characterization of proteins and complexes using small-angle X-ray solution scattering.," *Journal of structural biology*, vol. 172, pp. 128–41, Oct. 2010.
- [52] P. Bernadó, Y. Pérez, J. Blobel, J. Fernández-Recio, D. I. Svergun, and M. Pons, "Structural characterization of unphosphorylated STAT5a oligomerization equilibrium in solution by small-angle X-ray scattering.," *Protein science : a publication of the Protein Society*, vol. 18, pp. 716–26, Apr. 2009.
- [53] P. Bernadó, E. Mylonas, M. V. Petoukhov, M. Blackledge, and D. I. Svergun, "Structural characterization of flexible proteins using small-angle X-ray scattering.," *Journal of the American Chemical Society*, vol. 129, pp. 5656–64, May 2007.
- [54] P. Sikorski, E. D. Atkins, and L. C. Serpell, "Structure and Texture of Fibrous Crystals Formed by Alzheimer's A $\beta$ (1125) Peptide Fragment," *Structure*, vol. 11, pp. 915–926, Aug. 2003.
- [55] A. Olofsson, M. Lindhagen-Persson, E. A. Sauer-Eriksson, and A. Ohman, "Amide solvent protection analysis demonstrates that amyloid- $\beta$ (140) and amyloid- $\beta$ (142) form different fibrillar structures under identical conditions," *Biochem. J.*, vol. 404, pp. 63–70, 2007.
- [56] S. Tomaselli, V. Esposito, P. Vangone, N. A. J. van Nuland, A. M. J. J. Bonvin, R. Guerrini, T. Tancredi, P. A. Temussi, and D. Picone, "The alpha-to-beta conformational transition of Alzheimer's A $\beta$ (1-42) peptide in aqueous media is reversible: a step by step conformational analysis suggests the location of beta conformation seeding.," *Chem-biochem : a European journal of chemical biology*, vol. 7, pp. 257–67, Feb. 2006.

- [57] S. Nath, J. Meuvis, J. Hendrix, S. A. Carl, and Y. Engelborghs, “Early aggregation steps in alpha-synuclein as measured by FCS and FRET: evidence for a contagious conformational change.,” *Biophysical journal*, vol. 98, pp. 1302–11, Apr. 2010.
- [58] J. Kim and M. Lee, “Observation of multi-step conformation switching in beta-amyloid peptide aggregation by fluorescence resonance energy transfer.,” *Biochemical and biophysical research communications*, vol. 316, pp. 393–7, Apr. 2004.
- [59] A. Kitamura and H. Kubota, “Amyloid oligomers: dynamics and toxicity in the cytosol and nucleus.,” *The FEBS journal*, vol. 277, pp. 1369–79, Mar. 2010.
- [60] M. Lindgren and P. Hammarström, “Amyloid oligomers: spectroscopic characterization of amyloidogenic protein states.,” *The FEBS journal*, vol. 277, pp. 1380–8, Mar. 2010.
- [61] D. Allsop, L. Swanson, S. Moore, Y. Davies, A. York, O. M. El-Agnaf, and I. Soutar, “Fluorescence anisotropy: a method for early detection of Alzheimer beta-peptide (Abeta) aggregation.,” *Biochemical and biophysical research communications*, vol. 285, pp. 58–63, July 2001.
- [62] S. Thirunavukkuarasu, E. A. Jares-Erijman, and T. M. Jovin, “Multiparametric fluorescence detection of early stages in the amyloid protein aggregation of pyrene-labeled alpha-synuclein.,” *Journal of molecular biology*, vol. 378, pp. 1064–73, May 2008.
- [63] J. R. Lakowicz, *Topics in fluorescence spectroscopy. Volume 6: Protein Fluorescence*. New York: Kluwer Academic / Plenum Publishers, 2000.
- [64] B. Valeur, *Molecular Fluorescence: Principles and Applications*. Weinheim: Wiley-VCH Verlag GmbH, 2001.
- [65] J. R. Lakowicz, *Principles of Fluorescence Spectroscopy*. Singapore: Springer Science+Business Media, LLC, 3rd ed., 2006.

- [66] P. Atkins and R. Friedman, *Molecular quantum mechanics*. New York: Oxford University Press Inc., 4th ed., 2005.
- [67] W. Becker, *Advanced Time-Correlated Single Photon Counting Techniques*. Berlin: Springer-Verlag, 2005.
- [68] D. J. S. Birch and R. E. Imhof, “Time-domain fluorescence spectroscopy using time-correlated single-photon counting. In J. Lakowicz (Ed.), Topics in fluorescence spectroscopy. Volume 1: Techniques,” in *Topics in fluorescence spectroscopy. Volume 1: Techniques* (J. R. Lakowicz, ed.), New York: Plenum press, 1991.
- [69] C. D. McGuinness, K. Sagoo, D. McLoskey, and D. J. S. Birch, “A new sub-nanosecond LED at 280 nm: application to protein fluorescence,” *Measurement Science and Technology*, vol. 15, pp. L19–L22, Nov. 2004.
- [70] A. K. Livesey and J. C. Brochon, “Analyzing the distribution of decay constants in pulse-fluorimetry using the maximum entropy method,” *Biophysical journal*, vol. 52, pp. 693–706, Nov. 1987.
- [71] D. V. O’Connor and D. Phillips, *Time-correlated Single Photon Counting*. London: Academic Press Inc. Ltd., 1984.
- [72] E. T. Jaynes, “Information Theory and Statistical Mechanics,” *The Physical Review*, vol. 106, pp. 620–630, May 1957.
- [73] J. C. Brochon, “Maximum Entropy Method of Data Analysis in Time-Resolved Spectroscopy,” *Numerical Computer Methods*, vol. 240, no. 240, pp. 262–311, 1994.
- [74] K. J. Willis, A. G. Szabo, J. Drew, M. Zuker, and J. M. Ridge-way, “Resolution of heterogeneous fluorescence into component decay-associated excitation spectra. Application to subtilisins.,” *Biophysical journal*, vol. 57, pp. 183–9, Feb. 1990.

- [75] J. R. Knutson, D. G. Walbridge, and L. Brand, "Decay-associated fluorescence spectra and the heterogeneous emission of alcohol dehydrogenase.," *Biochemistry*, vol. 21, pp. 4671–9, Sept. 1982.
- [76] A. P. Demchenko, "Fluorescence and Dynamics in Proteins. In J. Lakowicz (Ed.), Topics in fluorescence spectroscopy. Volume 3: Biochemical Applications," in *Topics in fluorescence spectroscopy. Volume 3: Biochemical Applications* (J. R. Lakowicz, ed.), New York: Plenum press, 1992.
- [77] Y. Engelborghs and A. Fersht, "Barnase: Fluorescence analysis of a three tryptophan protein. In J. Lakowicz (Ed.), Topics in fluorescence spectroscopy. Volume 6: Protein Fluorescence," in *Topics in fluorescence spectroscopy. Volume 6: Protein Fluorescence* (J. R. Lakowicz, ed.), New York: Kluwer Academic / Plenum Publishers, 2000.
- [78] J. B. A. Ross, W. R. Laws, K. Rousslang, and H. R. Wyssbrod, *Tyrosine fluorescence and phosphorescence from proteins and polypeptides. In J. Lakowicz (Ed.), Topics in fluorescence spectroscopy. Volume 3: Biochemical Applications.* New York: Plenum press, 1992.
- [79] D. A. Chignell and W. B. Gratzer, "Solvent effects on aromatic chromophores and their relation to ultraviolet difference spectra of proteins," *The Journal of Physical Chemistry*, vol. 72, pp. 2934–2941, Aug. 1968.
- [80] J. K. Lee, R. T. Ross, S. Thampi, and S. Leurgans, "Resolution of the properties of hydrogen-bonded tyrosine using a trilinear model of fluorescence," *The Journal of Physical Chemistry*, vol. 96, pp. 9158–9162, Nov. 1992.
- [81] D. M. Rayner, D. T. Krajcarski, and A. G. Szabo, "Excited state acid-base equilibrium of tyrosine," *Canadian Journal of Chemistry*, vol. 56, no. 9, pp. 1238–1245, 1978.

- [82] J. R. Unruh, M. R. Liyanage, and C. K. Johnson, "Tyrosyl rotamer interconversion rates and the fluorescence decays of N-acetyltyrosinamide and short tyrosyl peptides.," *The journal of physical chemistry. B*, vol. 111, pp. 5494–502, May 2007.
- [83] W. R. Laws, J. B. Ross, H. R. Wyssbrod, J. M. Beechem, L. Brand, and J. C. Sutherland, "Time-resolved fluorescence and  $^1\text{H}$  NMR studies of tyrosine and tyrosine analogues: correlation of NMR-determined rotamer populations and fluorescence kinetics.," *Biochemistry*, vol. 25, pp. 599–607, Mar. 1986.
- [84] J. B. Ross, W. R. Laws, A. Buku, J. C. Sutherland, and H. R. Wyssbrod, "Time-resolved fluorescence and  $^1\text{H}$  NMR studies of tyrosyl residues in oxytocin and small peptides: correlation of NMR-determined conformations of tyrosyl residues and fluorescence decay kinetics.," *Biochemistry*, vol. 25, pp. 607–12, Mar. 1986.
- [85] W. Wiczak, "Mechanism of fluorescence quenching of tyrosine derivatives by amide group," *Chemical Physics Letters*, vol. 341, pp. 99–106, June 2001.
- [86] P. L. Muiño and P. R. Callis, "Solvent effects on the fluorescence quenching of tryptophan by amides via electron transfer. Experimental and computational studies.," *The journal of physical chemistry. B*, vol. 113, pp. 2572–7, Mar. 2009.
- [87] M. Noronha, J. C. Lima, P. Lamosa, H. Santos, C. Maycock, R. Ventura, and A. L. Maçanita, "Intramolecular Fluorescence Quenching of Tyrosine by the Peptide  $\alpha$ -Carbonyl Group Revisited," *The Journal of Physical Chemistry A*, vol. 108, pp. 2155–2166, Mar. 2004.
- [88] V. I. Stsiapura, A. A. Maskevich, V. A. Kuzmitsky, V. N. Uversky, I. M. Kuznetsova, and K. K. Turoverov, "Thioflavin T as a Molecular Rotor: Fluorescent Properties of Thioflavin T in Solvents with Different Viscosity.," *The journal of physical chemistry. B*, Nov. 2008.

- [89] M. R. H. Krebs, E. H. C. Bromley, and A. M. Donald, “The binding of thioflavin-T to amyloid fibrils: localisation and implications.,” *Journal of structural biology*, vol. 149, pp. 30–7, Jan. 2005.
- [90] C. Rodríguez-Rodríguez, A. Rimola, L. Rodríguez-Santiago, P. Ugliengo, A. Alvarez-Larena, H. Gutiérrez-de Terán, M. Sodupe, and P. González-Duarte, “Crystal structure of thioflavin-T and its binding to amyloid fibrils: insights at the molecular level.,” *Chemical communications (Cambridge, England)*, vol. 46, pp. 1156–8, Feb. 2010.
- [91] L. A. Munishkina and A. L. Fink, “Fluorescence as a method to reveal structures and membrane-interactions of amyloidogenic proteins.,” *Biochimica et biophysica acta*, vol. 1768, pp. 1862–85, Aug. 2007.
- [92] D. N. Irani, *Cerebrospinal fluid in clinical practice*. Philadelphia: Saunders, Elsevier, 2009.
- [93] W. B. Stine, K. N. Dahlgren, G. A. Krafft, and M. J. LaDu, “In vitro characterization of conditions for amyloid-beta peptide oligomerization and fibrillogenesis.,” *The Journal of biological chemistry*, vol. 278, pp. 11612–22, Mar. 2003.
- [94] N.-V. Buchete, R. Tycko, and G. Hummer, “Molecular dynamics simulations of Alzheimers  $\beta$ -amyloid protofilaments.pdf,” *Journal of molecular biology*, vol. 353, pp. 804–821, 2005.
- [95] C. Lee and S. Ham, “Characterizing Amyloid-Beta protein misfolding from Molecular Dynamics Simulations with explicit water,” *Journal of Computational Chemistry*, vol. 32, no. 2, pp. 349–355, 2010.
- [96] C. E. Giacomelli and W. Norde, “Influence of hydrophobic Teflon particles on the structure of amyloid beta-peptide.,” *Biomacromolecules*, vol. 4, no. 6, pp. 1719–26, 2003.

- [97] C. E. Giacomelli and W. Norde, “Conformational changes of the amyloid beta-peptide (1-40) adsorbed on solid surfaces.,” *Macromolecular bioscience*, vol. 5, pp. 401–7, May 2005.
- [98] S. Rocha, R. Krastev, A. F. Thünemann, M. C. Pereira, H. Möhwald, and G. Brezesinski, “Adsorption of amyloid beta-peptide at polymer surfaces: a neutron reflectivity study.,” *Chemphyschem : a European journal of chemical physics and physical chemistry*, vol. 6, pp. 2527–34, Dec. 2005.
- [99] B. Hernández, F. Pflüger, A. Adenier, S. G. Kruglik, and M. Ghomi, “Vibrational analysis of amino acids and short peptides in hydrated media. VIII. Amino acids with aromatic side chains: L-phenylalanine, L-tyrosine, and L-tryptophan.,” *The journal of physical chemistry. B*, vol. 114, pp. 15319–30, Nov. 2010.